ABSTRACT

Title of Document: **VEHICLE SHAPING FOR MINE BLAST DAMAGE REDUCTION**

Kevin Genson,
Master's of Science, 2006

Directed By: Dr. William Fourney, Chairman,
Aerospace Engineering Department

When a buried explosive is detonated beneath a target (such as a vehicle), the target is rapidly loaded by flying ejecta, high pressure gas, and shock waves. This paper explores how changes in the shape of the underside of a target affect the total impulse captured from the detonation of a buried charge. The effects of changes in target height and charge burial depth are also examined. Testing was conducted on dihedral target plates using 0.636 gram charges. These were buried in saturated sand at three depths, and shaped targets were placed at four heights above the surface. The impulse applied to the plate by the exploding charge was determined through analysis of high speed digital video recordings. Changing the geometry of the target reduced the impulse by up to 45%. Increasing standoff distance reduced impulse by up to 70%.

VEHICLE SHAPING FOR MINE BLAST DAMAGE REDUCTION

By

Kevin William Genson

Thesis submitted to the Faculty of the Graduate School of the
University of Maryland, College Park, in partial fulfillment
of the requirements for the degree of
Master's of Science
2006

Advisory Committee:
Dr. William Fourney, Chair
Dr. Jim Duncan
Dr. Henry Haslach
Mr. Leslie Taylor

Acknowledgements

I would like to thank the following individuals for their assistance in completing this research. Without them my research would have not been possible.

Dr. William Fourney, for your leadership, guidance, and patience. Meeting your expectations was a rewarding and educational challenge. I could not have asked for a better advisor.

Dr. Robert Bonenberger, Uli Leiste, Chi-Ming Wang, Alexander Tsarev, and all of the German students who worked at the Dynamic Effects Lab. Thank you for your support, your advice, and countless hours of entertainment.

Mr. Leslie C. Taylor, for sharing your experience and mentorship. Your insight into explosive effects, as well as your advice regarding my research, was invaluable.

Mr. Brian Beechener, my undergraduate assistant, for your dauntless work in completing many tests with the utmost in precision and efficiency.

Mr. Timothy Hennessey and the Office of Naval Research (Contract ONR N000140610335), for making this research possible and for providing me with the opportunity to make even larger explosions.

And lastly, my family for their love and support. Thank you Mom for your kind words and care, and the little bits of advice that always seem to fit right. Thank you Dad for your wisdom and insight, and for always having the right perspective on things. Mom, Dad, Laura; I love all of you.

Table of Contents

List of Figures

List of Tables

Chapter 1: Introduction & Background

Overview

This paper describes research conducted at the University of Maryland, College Park in the Dynamic Effects Lab of the A. James Clark School of Engineering. This was accomplished through the use of small-scale explosive testing and high speed digital photography.

The primary research goal was to examine the effect of variations in plate angle, standoff distance, and depth of burial on the impulse transmitted by a buried charge to a suspended target plate. The independent variables were target geometry (dihedral angle), depth of burial and standoff distance. The measured dependent variable was captured impulse.

Buried explosives in the form of mines or improvised explosive devices are a constant threat to vehicles. Light armored vehicles (LAV) are particularly susceptible to this form of attack due to their reduced protection when compared to heavier vehicles such as main battle tanks. Adding armor to a LAV is not always an option due to weight constraints, so alternate protection schemes must be explored.

This research involved small scale explosive testing. Full scale testing is extremely expensive, and requires the use of specialized facilities and technicians. Small scale testing is cheaper, simpler, and is easily repeated. The explosive charges used in this research consisted of 0.636 g charges, or 0.01% of the 10lb of explosive in a typical anti-vehicular mine.

1.1 Antivehicular (AV) Mines

Since World War II, more vehicles have been lost to land mines than all other threats combined [1]. Antivehicular (AV) mines are capable of disabling a heavy vehicle, or completely destroying a lighter vehicle. Mine survivability is one of the least understood aspects of vehicle survivability, and is typically defended against through the use of extra armor. The physics surrounding a buried landmine blast and the loading mechanisms that damage a vehicle are not well understood.

The most common form of antivehicular landmine is the blast mine, which uses a large amount of explosive to directly damage the target. Light or unprotected vehicles are particularly susceptible to blast mines. Figures 1.1 and 1.2 show the detonation and aftereffects of a 6.5kg TNT blast mine against an unprotected 5/4 ton truck. Heavily armored vehicles are less threatened by most blast mines, but can be damaged by shaped charges and penetrator mines. Shaped charges consist of an inverted hollow cone of ductile metal (typically copper) surrounded by a jacket of high explosive. The explosive is detonated in such a manner that it compresses the cone, forcing a hot jet of molten metal to spurt forward. This jet is capable of cutting through several inches of steel. Penetrator mines defeat armor by shooting a projectile into the target. Both shaped charges and penetrator mines are beyond the scope of this study.

Figure 1.1: Unprotected 5/4 Ton Truck Against a 6.5kg TNT Antitank Mine [1]

Figure 1.2: Unprotected 5/4 Truck After Mine Test [1]

1.2 Casualty Mechanisms

Vehicles must be designed to protect the crew from several casualty mechanisms. The greatest threat comes from blast overpressure, which causes severe damage to the lungs and as well as burns and secondary fires from the fireball. A floor rupture in the event of an explosion is considered a crew kill [1]. Fragments from the casing and secondary projectiles (Figure 1.3) have varying levels of lethality. Small fragments from antipersonnel mines are a moderate threat to crews, and can be defended against through light armor. Large, heavy fragments are very energetic and pose a severe threat. Shock loads transmitted through the floor can break bones, while deformation of the crew compartment can cause crushing injuries. Finally, gross vehicle movement in the form of a crash has also been found to be a source of injury.

Figure 1.3: Fragments and Ejecta Created After Mine Blast [1]

1.3 Physics of Mine Blasts

Detonation is the process of a pressure wave propagating through an explosive medium, causing a chemical reaction to initiate behind it. This reaction rapidly releases energy in the form of a shock wave and, more slowly, in the form of an expanding gas bubble. Initial pressures near the detonation products can be as high as 200,000 atmospheres and temperatures can be as high as 6000°C [1]. When the explosive is confined in soil, the result is three distinct phases as the explosive interacts with the soil, gas expands to the surface, and soil interacts with the vehicle. Figure 1.4 shows a time sequence of a full-scale mine explosion, with the detonation products expanding upward surrounded by a ring of ejected soil.

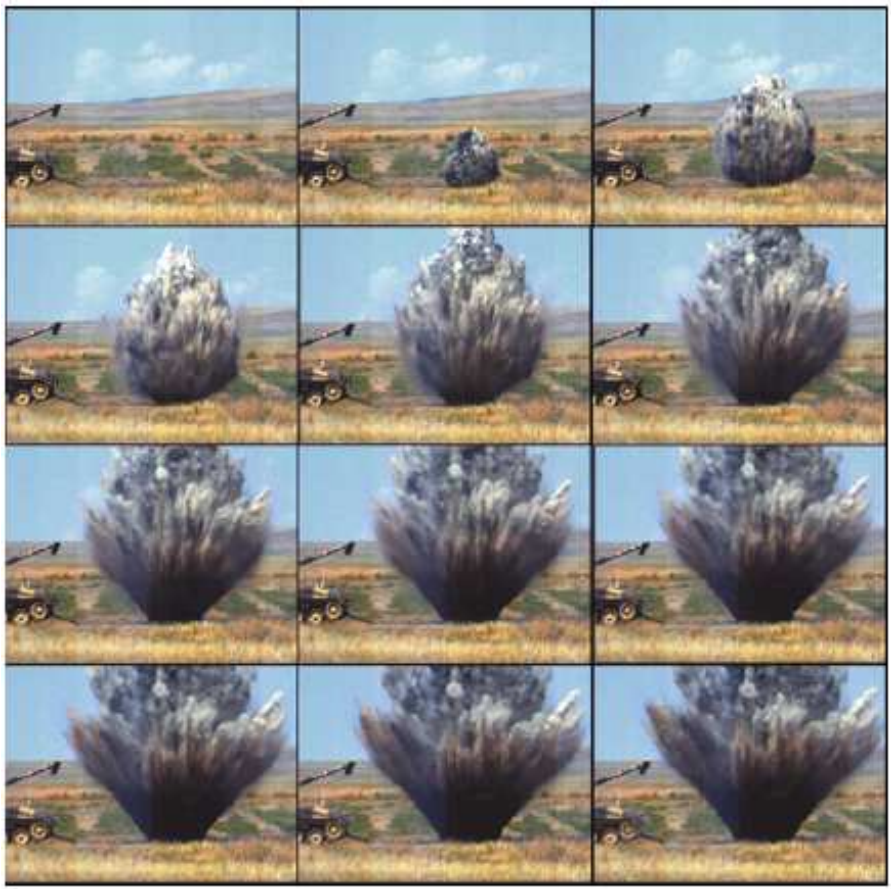

Figure 1.4: Time Sequence of Mine Explosion [1]

1.3.1 Early Interaction & Shock

When the detonation wave emerges from the explosive product in the form of a shock wave, it interacts with the surrounding soil [1]. The strength of the shock wave depends on the acoustic impedance match between the materials the wave travels through; if a shockwave travels from a high impedance material (such as soil or metal) to a low impedance material (such as gas), then most of the shock wave is reflected. When the shockwave from an explosive reaches the surface, a thin layer of soil is ejected upward as the shockwave transitions between the soil and air. The large impedance mismatch between soil and air generally means the explosive shock wave has little direct effect on the target unless the target is directly touching the soil [2]. If the target touches the soil, energy is transmitted into the target in the form of a stress wave [9].

1.3.2 Gas Expansion

The detonation products also produce mechanical work in the form of expanding gas. The mass of the explosive determines the amount of gas produced. Confinement by the soil causes the gas to expand primarily in the vertical direction [9]. As the detonation products expand they eject the soil plug at supersonic speeds and create a bow shock wave in the air. Figure 1.5 shows the distribution of detonation products as they begin to expand upward. It is theorized that the gas may have a high dynamic pressure which can cause localized deformation if flows are trapped by the geometry of the target. The expanding gas may be confined by the soil and target to create a “bubble” with a high pressure that acts on a large area of the target. It is theorized that the gas expansion phase produces significant global and

localized effects on the target. The direction and amount of the gas expansion is heavily dependent on the soil properties. Deeper burial depths, increased soil density, and higher moisture content will cause the gas flow to expand in a more vertical direction [1].

1.3.3 Soil Ejecta

The initial expansion of the detonation products causes the soil directly above the charge (the "plug" or soil plug) to rapidly move upward ahead of the expanding gas. The expanding gas also imparts energy into the surrounding soil, causing it to flow as an annulus of ejecta surrounding the expanding detonation products [9]. The properties of the soil, particularly saturation level and porosity, determine the amount of soil and the direction of soil flow [1]. Figure 1.5 shows the distribution of the detonation products and soil ejecta for a typical blast. Notice how the soil ejecta (the blue shaded region) rings the detonation products. This effect is more pronounced in the final frames of Figure 1.4. During testing, the portion of the ejecta ringing the gas will be referred to as the "soil annulus."

Figure 1.5: Detonation Products and Soil Ejecta [1]

1.4 Load Mechanism Components

The data seems to indicate that the interaction of the gas expansion and soil ejecta on the target plate results in a loading mechanism that can be divided into two components. The first is a concentrated, short duration load referred to as the impact load. This component is composed of the soil plug ejected ahead of the detonation products and overpressure effects from the high pressure of the gas pushing it. The second component is a dispersed, longer duration load referred to as the distributed load. This component appears to be a product of extended pressure from the expanding gas bubble and momentum transfer from the crater ejecta. The effects of a mine blast over time can be seen in Figure 1.6, which compares digital imagery taken from a small-scale buried mine test featuring a transparent target to a computer simulation of that test. It is postulated that the target is first impacted by the soil plug above the charge propelled by the initial expansion of the detonation products, and then subject to extended loading by the impact of ejecta and the gas bubble.

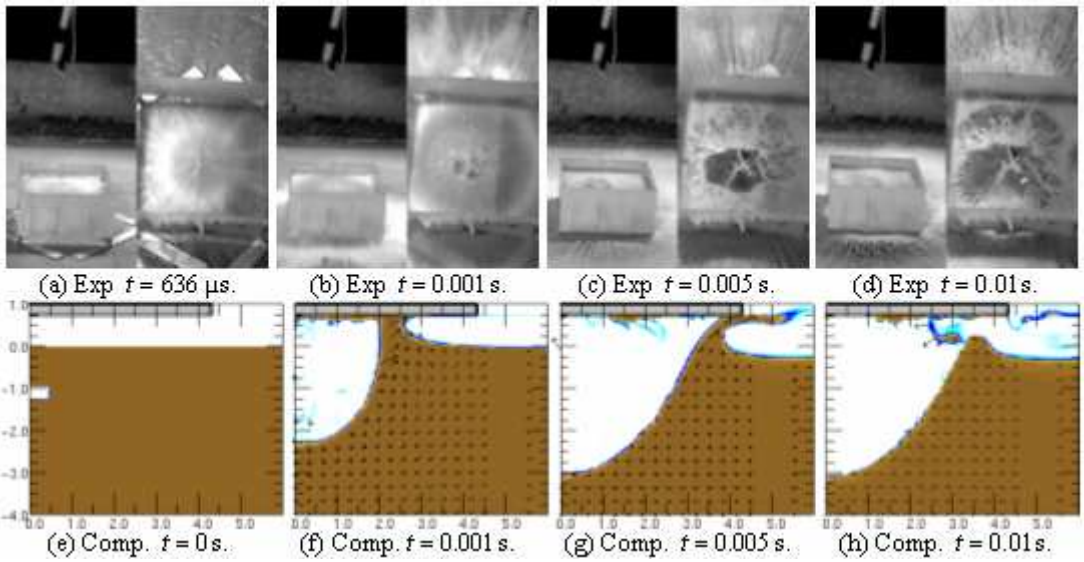

Figure 1.6: Small-Scale Mine Blast Test (Top) and Simulation (Bottom) [10]

1.4.1 Shock Load

One loading component comes from the shock wave emitted from the detonation products. The poor impedance match between the soil and air means this component is only present when the target is touching or extremely close to the surface. At further standoff distances the shock load has a minimal effect [3]. The relative magnitude of this component is unknown, but the duration is extremely short.

1.4.2 Impact Load

The data seems to indicate that the initial loading comes in the form of a high-speed "plug" of soil. The soil plug can have an initial velocity of up to 1.5 km/s for a full-size charge [2], and the initial impact of these products against a vehicle has the capacity to induce large loads in a very short period of time. It is suggested that changes in the flow field resulting from target geometry can create localized pressure spikes, particularly if the field stagnates inside reentrant corners [1]. The effects of dynamic pressure changes and impact of the soil plug can cause localized material failure and breach the vehicle, exposing the crew directly to the blast effects.

Figure 1.7 is a series of images from a small-scale test captured by a high speed camera. A 0.5g charge of Detasheet was buried to a depth of 0.69" and detonated, and the resulting explosion was recorded. The camera captured an image once every 44μs. Figure 1.7 shows the first frame before the explosion and then the 3 frames afterward.

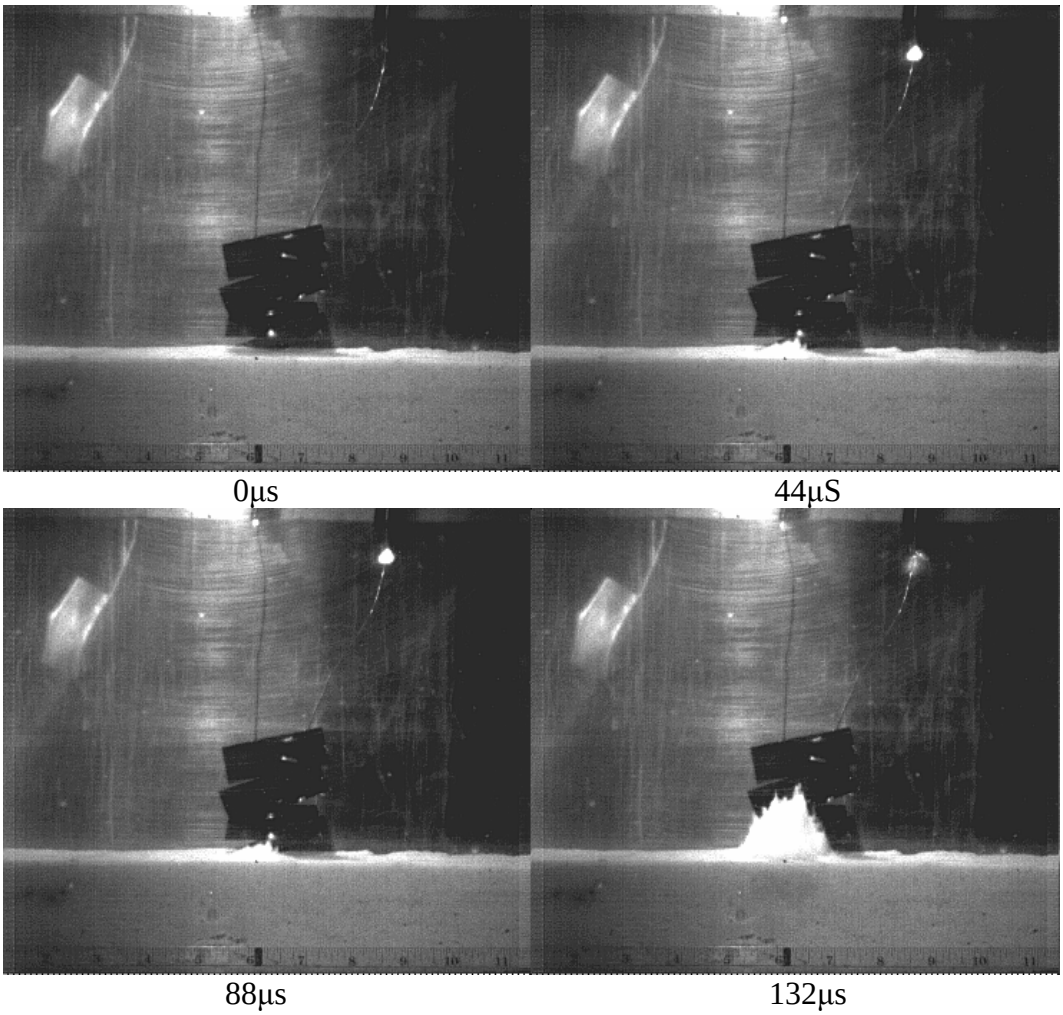

Figure 1.7: Initial Blast from 0.5g Charge at 0.69" Depth of Burial

The frames in Figure 1.7 show the soil directly above the charge (the soil plug) being projected upward a velocity of over 400 m/s. The soil directly over the charge has a supersonic vertical velocity, and in the presence of an air gap (meaning the shock load is mitigated) the soil plug is the first thing to strike against the target. The impact of the soil plug, acting as a concentrated load over a short period of time is called the impact load in this paper.

1.4.3 Distributed Load

The second loading component involves a load acting over a longer period of time and a greater area. If the detonation products are confined by the target plate and ejecta, they form an expanding gas bubble that places an extended pressure load on the target. As long as the bubble is confined it will continue to load the target, and may even "suck back" the target if the expanding bubble pressure falls below ambient. The ejecta from the crater impacts against the target, producing a direct momentum transfer. These effects act for a longer period of time after the detonation. Small-scale tests involving rigid flat plates suggest that loading by the soil annulus imparts 2/3 of the impulse transmitted to a target plate from a buried charge [3]. As seen in Figure 1.6 the soil and gas bubble act on the target for at least 5 ms; this is a significant period of time when dealing with small-scale explosive events. The distributed load acts over a much larger area than the impact load.

1.5 Parameter Investigaton

Target response is heavily dependent on several factors, including the standoff distance, depth of burial, conditions of the soil, and shape of the target. All four factors have a significant effect on the total impulse captured by a target from a buried charge.

1.5.1 Standoff Distance

The distance between the target and the surface is one of the primary factors in determining blast damage. If the target is in contact with the soil, the shock wave will be directly transmitted into the target as the impedance match between the soil and a solid (such as a steel tank track) is much closer than that between soil and air. Increasing the distance between the target and the soil causes direct shock wave effects to be negligible. Higher standoff distances allow for greater expansion of the gas bubble and soil annulus diameter [2]. While this increases the area over which the forces act, it decreases their intensity.

1.5.2 Depth of Burial

The depth of burial of an exploding charge has a significant influence on the nature of the loading mechanism against the target. At shallow burial depths, the loading mechanism is primarily from the detonation products rather than the soil. As the depth of burial increases, the detonation products are forced to move more soil out of the way. The deeper burial increases the mass and reduces the velocity of the soil plug. The impact of the soil plug against the target plate is also dispersed over a larger area.

Figure 1.8 contains pictures comparing the initial blast from a 0.5g Detasheet charge buried at three depths of burial. These tests were conducted at the University of Maryland Dynamic Effects Lab. The first column is a charge buried at 0.19", the middle column is a charge buried to 0.69", and in the third column the charge is buried to a depth of 1.19". Each frame is a picture taken by a high speed camera at a 40μs interval, starting with the first frame immediately after the explosion. Comparing the images between the different tests can provide insight into the effect of burial depth on the loading of a target above an exploding charge.

The most apparent difference between the tests is the difference in velocity of the ejecta and detonation products as the depth of burial changes. The ejecta from the charge buried to 0.19" travels significantly faster than the ejecta from the charges buried at deeper depths. By the last frame, the ejecta from the 0.19" charge has traveled approximately twice the distance of the 0.69" charge, and over four times the distance of the 1.19" charge. This difference in velocity may be a result of the additional mass of soil from the deeper burial depths.

The flow is also more horizontal for shallower depths of burial. At the 0.19" burial depth the plume expands upward and outward, whereas at the 0.69" and 1.19" burial depths the plume is primarily dome-shaped for the region tested. The additional soil surrounding the deeper buried charges restricts the radial flow of the detonation products. Constrained by the crater walls, the expanding gas is forced to flow upward in a more vertical direction compared to the shallower charges.

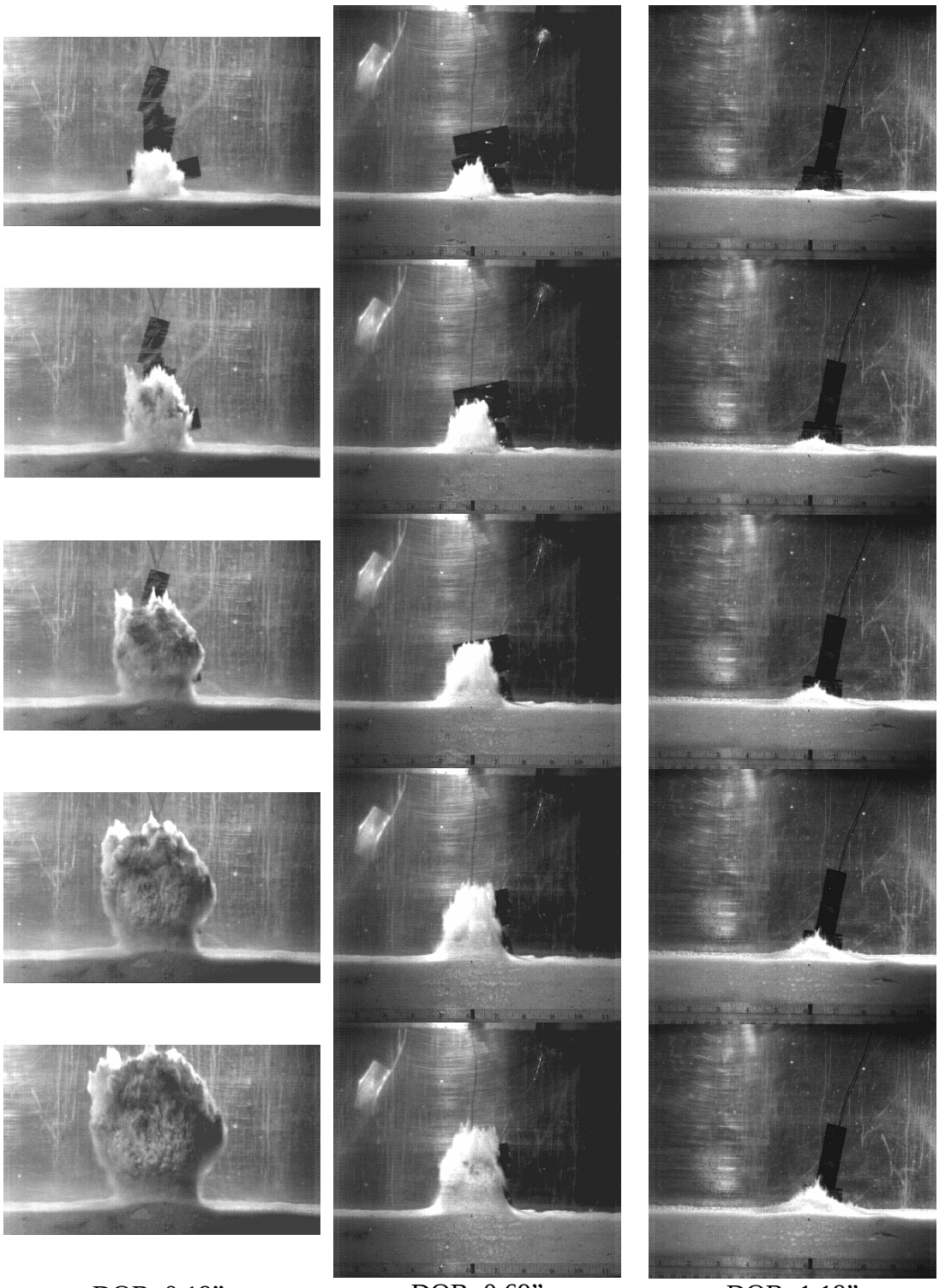

DOB: 0.19” DOB: 0.69” DOB: 1.19”

Figure 1.8: Elapsed Time (40μs/frame) of Buried Charge Explosion for 3 DOBs

1.5.3 Soil Condition

The condition of the soil, particularly the saturation level, has a significant effect on the loading mechanism. High levels of water saturation reduce the shear strength of the soil, which decreases the amount of energy required to displace it [1]. The rate of soil movement during the gas bubble phase is dependent on the porosity and bulk density of the soil, which in turn is mainly dependent on the water content. Wet or saturated soils contain pores filled with water and are more resistant to crushing [4]. This constrains the gas bubble and prevents the gas from being dispersed throughout the soil, which results in more energy directed to the target.

1.5.4 Target Shape

Vehicle geometry can have a channeling effect that either diverts the blast effects away from the target, or traps them and causes damaging overpressures. South African vehicle designers began incorporating angles into the underside of vehicles in the late 1970's [13]. The Casspir armored personnel carrier (Figure 1.9) is one such example. Testing on angled plates angled between 0° and 30° using air blasts revealed that loading decreased significantly as the plate angle increased within the range tested [4]. Similar results should be expected in soil.

Figure 1.9: Casspir APC

1.6 Blast Scaling

Scaled testing is one of the most common forms of explosive testing. A full scale test can cost many thousands of dollars, require specialized equipment and training, and take months to set up and run. Smaller scale tests on the order of a few pounds are less expensive and take far less time to set up, but still require specialized blast chambers or testing sites. Very small scale testing, on the order of a few grams or less, is far less expensive and can be conducted indoors. The University of Maryland Dynamic Effects Lab specializes in small scale testing, with charge sizes up to 8 grams. The Dynamic Effects Lab primarily uses Hopkinson-Cranz scaling to scale between small-scale and full-scale test results.

Hopkinson-Cranz scaling, or cube-root scaling, is based on the theory that similar blast waves are produced at the same scaled distance when the scaled charge geometry, explosive, and atmospheric conditions are the same [5]. For small time scales, air is assumed to be a perfect gas and gravity is assumed to have a negligible effect. Hopkinson scaling is used to scale air blast (shock) and underwater shock, and has also been used for scaling other effects from buried charges. Hopkinson scaling is so prevalent that almost all data is presented in terms of the parameters Z (reduced distance), τ (reduced time), and ζ (specific reduced impulse). R, t, i, W are the unscaled distance, time, specific impulse, and charge weight.

$$Z = \frac{R}{W^{\frac{1}{3}}} \qquad \tau = \frac{\mathrm{t}}{\mathrm{W}^{\frac{1}{3}}} \qquad \zeta = \frac{i}{W}$$

Although charge weight is the primary term used for Hopkinson scaling, total energy is an alternative scaling term. Hopkinson scaling is designed for use with ideal explosives, and fails to scale non-ideal explosive compositions. Chock [6] suggests that energy is a much more "physically realistic" parameter, and Fu [7] was able to properly scale non-ideal explosives through a correlation factor based on detonation energy. Weight is a sufficient parameter for the majority of scaling research. Scaling between full-scale and small scale tests on the order of a few pounds has been confirmed down to research scale weights below 100 grams [7]. The region between 100g and 1g (the scale used in the Dynamic Effects Lab) has also shown good behavior, but requires more study [3].

Chapter 2: Research Equipment

Overview

The specific demands of plate impulse testing required specialized pieces of equipment to be custom fabricated for the Dynamic Effects Lab. Other components had to be modified or specially protected in order to withstand the rigors of blast testing. The choice of sensor equipment and test bed allowed for repeated tests once setup was completed.

2.1 Explosive Charge

The charge (Figure 2.1) consisted of 0.9g of Detasheet (63% PETN by weight, or 567 mg PETN) detonated by an RISI RP-87 EBW (exploding bridge wire) detonator (26mg PETN initiating explosive, 43 mg RDX output explosive). PETN is Pentaerythritol Tetranitrate, a very stable explosive commonly used in commercial applications. RDX is cyclonite, a common military explosive component. The total explosive mass of this charge was 636 mg.

Figure 2.1: 636 mg Charge

2.2 Phantom Digital Camera System

The displacement of the plate was measured visually using high speed digital cameras. The original camera used was the Vision Research Phantom v4.1, a monochrome high speed digital camera which was operated at 1000 pictures per second at pixel resolutions of 512x512. A Nikon 28-80mm f/3.5-5.6D lens was mounted to the camera to focus the image. Later on in the testing, the lab obtained a new Phantom v7.1 digital camera (Figure 2.2), which was operated at 8000 pictures per second at 512x512 resolution. Focus was achieved through the use of a Tamron (IF) 28-75mm 1:2.8 MACRO Φ67 lens. The selection of frame rate and resolution was largely dependent on the memory capacity and performance capability of the cameras. The Phantom v4 contains 256 megabytes of memory and could take 1000 pictures at full resolution. The Phantom v7 contained 2 gigabytes of memory and could capture over 8000 pictures at full resolution. The sharper image and faster frame rate of the v7.1 made it a superior platform compared to the v4.1.

Figure 2.2: Phantom v7.1 High Speed Digital Camera [12]

Data was collected by the camera and then transmitted to a personal computer. The camera was either connected by a FireWire cable (Phantom v4) or CAT5 cable (Phantom v7). The FireWire cable was more susceptible to outside electrical interference and repeatedly caused signal loss. This could cause the camera to lose connection with the PC or fail to trigger the camera during a test. The connection could be restored by resetting and reconnecting the camera and PC.

The digital camera was mounted on a standard duty, fluid head tripod mount sold by Vision Research (Figure 2.3). A foam skirt protected the stand from flying soil and water. The camera itself was protected by a translucent plastic case. The front of the container was removed and replaced with a clear pane of acrylic plastic, while the rear was cut out to allow the wiring to connect to the camera.

Figure 2.3: Phantom v7, Camera Stand, Protective Skirt, and Cover

2.3 Phantom Software

Phantom cameras utilize proprietary software to analyze the recording (Figure 2.4). The control software allows the user to control resolution, frame rate, exposure time, zoom, picture quality, and other options. The control software also contains integrated filtering imagery that can sharpen a picture. The view window shows exactly what the camera sees in real time, allowing the researcher to determine precisely how the recording should look. The controller can either trigger the camera from the software, or place the camera in "Capture" mode and trigger using an external device. The Phantom software also allows the user to record movement, scale distances from a reference, and determine angular and linear acceleration and velocity.

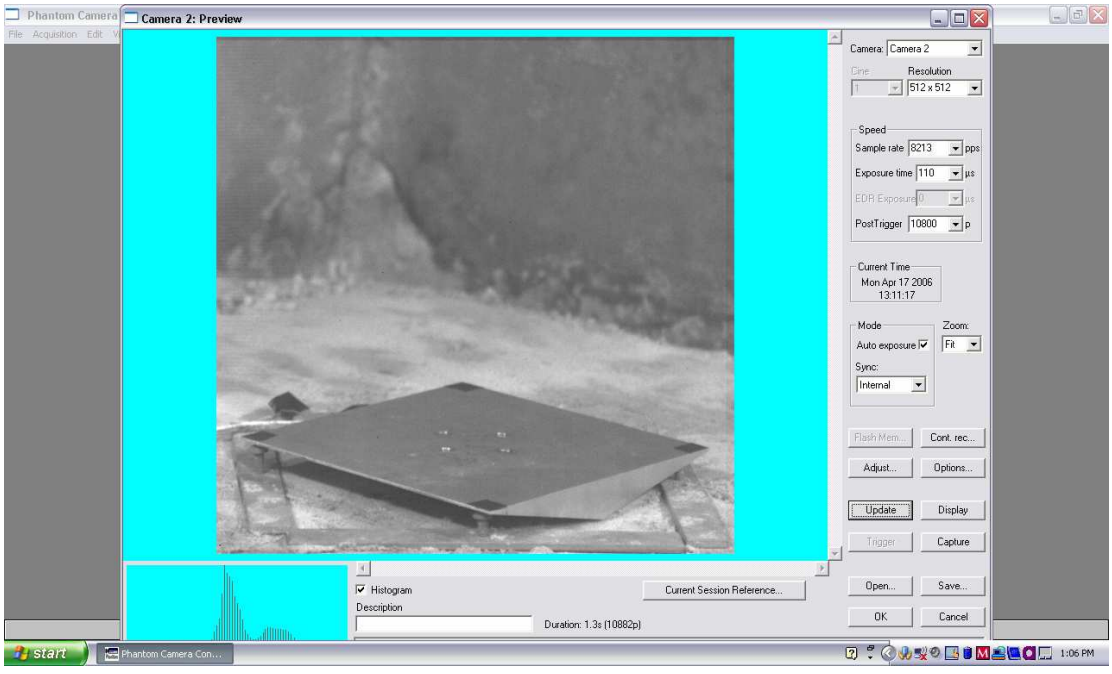

Figure 2.4: Phantom Camera Control Software

2.4 Firing System

The charge is detonated with a Reynolds Industries Inc FS-10 EBW firing system [11] (Figure 2.5). This battery-operated firing system is charged from an 110V power source, and uses coaxial cable to connect to the charge leads. A trigger system is connected from the firing module to the camera via coaxial cable. The FS-10 is designed specifically to fire exploding bridge wire detonators.

The firing system consists of a control unit and firing module; in Figure 2.5 the firing module is the metal box in the upper-right corner. The control unit provides between 32 and 40 volts to the firing module, which charges a 1μF capacitor to 3000V. When a 30V pulse is applied to the red terminal on the module, the capacitor discharges 3000V into the lead (upper right) terminals. The detonator will fire 10μs after the 30V pulse is applied to the module. A safety interlock key ensures the control unit will not fire until the key is inserted in the proper location.

Figure 2.5: FS-10 EBW Firing System

2.5 Dummy Charge

The camera is tested three times before each test to ensure the data will be collected. Testing the firing and data collection system requires the use of a bridge wire gap "dummy charge" that does not contain explosive powder (Figure 2.6). A dummy charge consisting of two leads inserted into a block of graphite inside an aluminum tube is used to ensure the firing system is functioning. The gap between the two wires is approximately 1/8". When the firing system is initiated a 3000V pulse runs across the leads. This pulse causes a visible spark that is recorded by the camera.

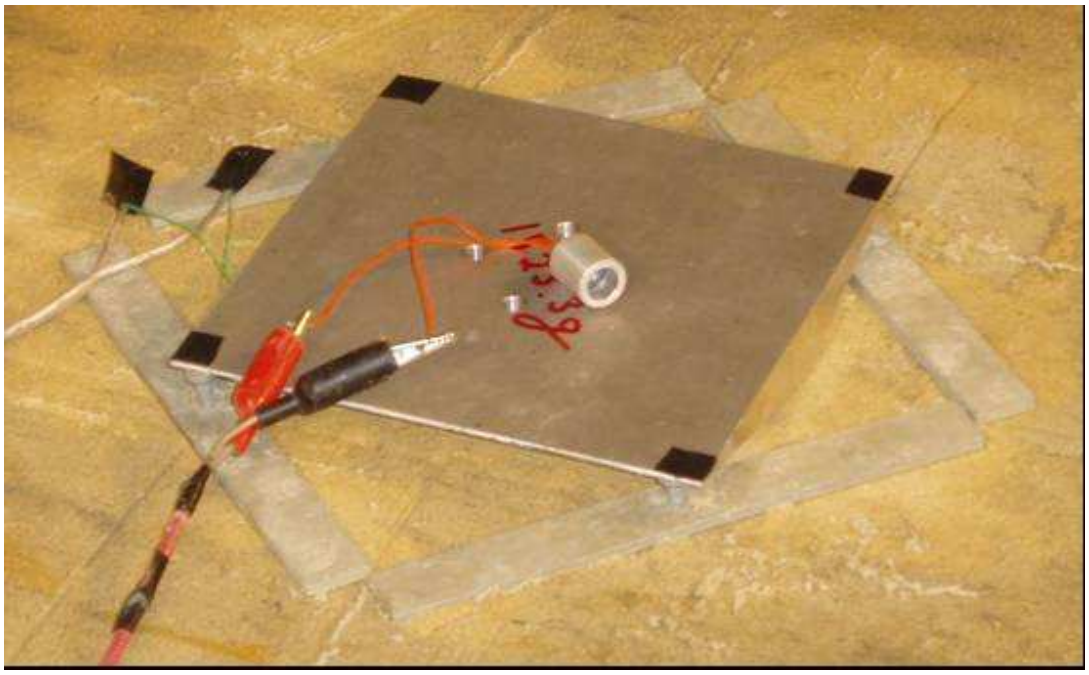

Figure 2.6: Dummy Charge

2.6 Trigger Mechanism

The camera can be remotely triggered by sending an electrical pulse to the trigger (red) coaxial lead on the camera. The trigger lead is kept at +5V when the camera is powered and running properly. If a -5V pulse is sent along the trigger lead, it causes the voltage to drop and triggers the camera. When the 30V activation pulse is transmitted, the trigger mechanism converts this into a -5V pulse that triggers the camera. Figure 2.7 shows the trigger mechanism, with the coaxial cable on the left leading to the camera and the red and white wires on the right connecting to the firing module.

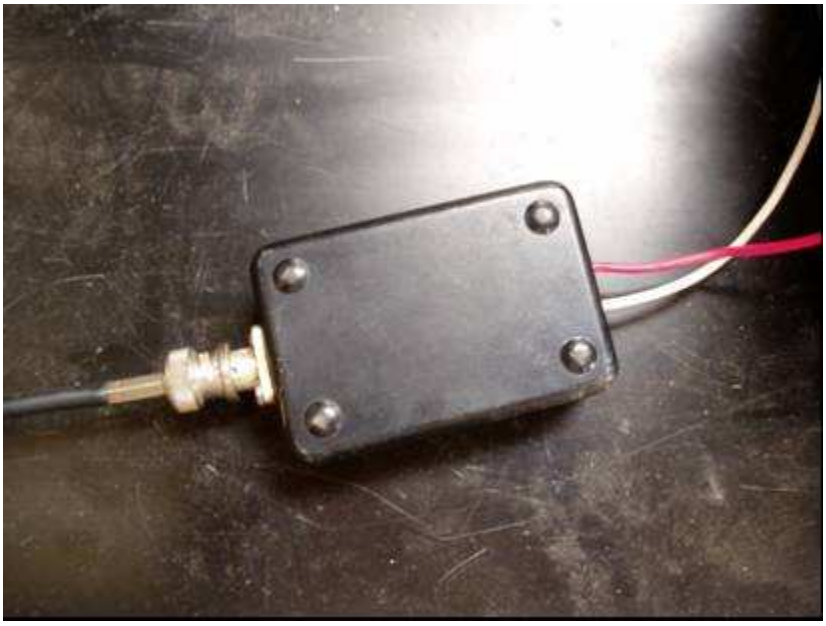

Figure 2.7: Trigger Mechanism

2.7 Test Bed Area

The test bed is a 1.5 meter by 1.5 meter steel tank measuring 0.6 meters deep (Figure 2.8, left). The bottom of the tank is filled with coarse gravel covered by a geotextile mesh blanket. A 25cm layer of HD-2 uniformly graded medium quartz sand lies on top of the mesh. Piping to the underside of the tank allows the test bed to be evenly saturated with water (Figure 2.8, right). The saturation system uses a stand column to move water into the underside of the tank and upwards into the sand bed. Equilibrium is established when the water level inside the water column equals that of the test bed. A drainage valve on the lowest part on the system allows the tank to drain completely. It takes approximately fifteen minutes to saturate the tank.

Six 500W halogen work lights on three stands provide illumination for the test setup. Lights are located in each of the three corners opposite the target plate. The work lights must be capable of withstanding repeated sprays of sand and water.

Figure 2.8: Test Bed Setup and Saturation System

2.8 Target Plates

A wide variety of shapes were tested to examine the effect of shape on total captured impulse from the detonation of a buried charge. These shapes included a grid of pyramids (similar to some forms of acoustic paneling), plates bent into dihedral shapes, and plates machined into pyramid and dihedral shapes. The plates were machined from 6061-T6 free machining aluminum to be 8" x 8" in the plane parallel to the soil, and to have a mass of approximately 1500 grams. The dimensions and mass of the plates are the standard size used at the Dynamic Effects Lab for the given charge size, and were shown to provide good results in previous tests [14]. Table 2.1 lists the various plate shapes tested and their respective masses.

Plate Shape	Mass (g)
0° Plate	1525
7° Dihedral Plate (1)	1458
7° Dihedral Plate (2)	1556
7° Pyramid Plate	1500
13° Dihedral Plate (1)	1506
13° Dihedral Plate (2)	1523
20° Dihedral Plate	1519

Table 2.1: Plate Shapes and Properties

Figure 2.9: Plate Angle

Figure 2.9 shows the angle referenced in Table 2.1; it is the angle between the front face of the plate and a line parallel to the ground. The 0° plate shape refers to a flat plate of material (Figure 2.10, Top). This geometry served as a baseline to compare the performance of other target shapes. Dihedral shapes (Figure 2.11, Bottom Left) are solid plates machined into an angled form with a triangular cross-section. The single pyramid shapes (Figure 2.10, Bottom Right) are solid plates machined into a pyramid form.

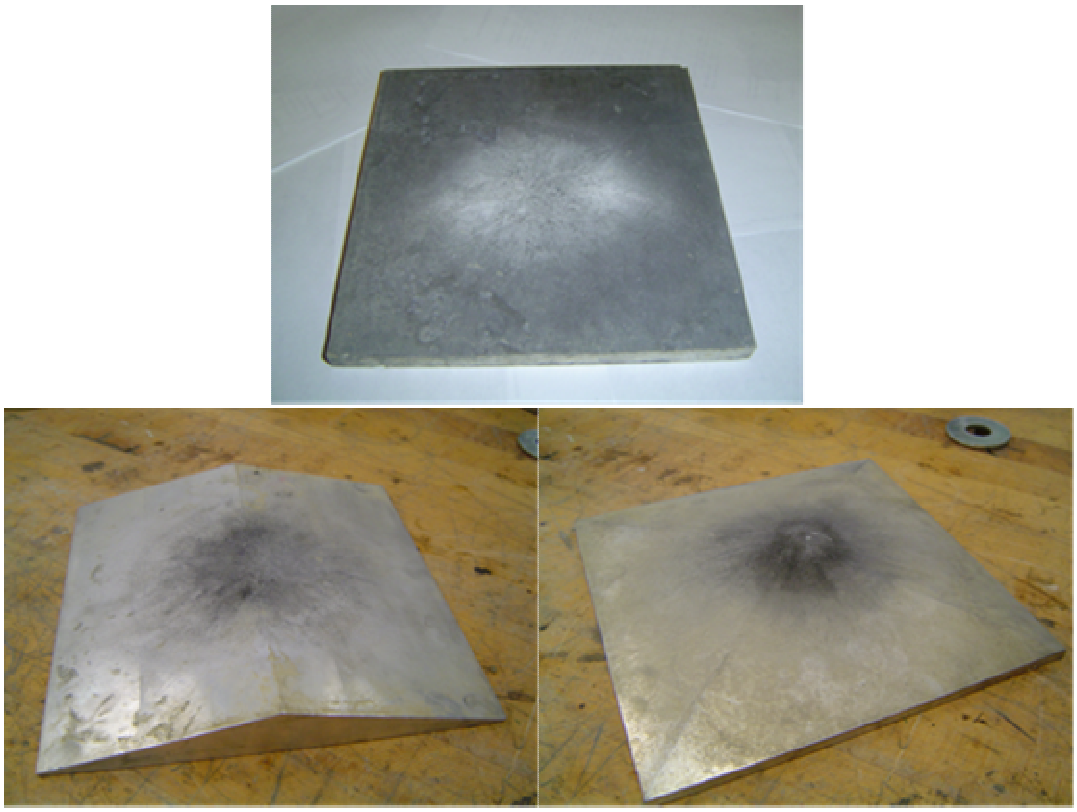

Figure 2.10: 0° plate, 13° Bent Plate, 13° Single Pyramid

The most extensive testing was done on the dihedral test plates, and in fact so much testing was conducted that two of the plates (the 7° and 13° plates) had to be replaced midway during the test. The decision to replace the plates was based on observations made over time. Although erosion was initially felt to be a significant factor, repeated tests revealed that plate wear had a minor effect on the total impulse captured by a dihedral target plate. The 7° pyramid plate was compared to the 7° dihedral plate at the 0.04" standoff distance to further examine the effects of target geometry on total impulse. Additional testing was conducted with alternate plate shapes; the results of these tests are in Appendix B.

Chapter 3: Research Methodology

Overview

In order to determine the impulse transmitted to a plate by explosive loading, the initial velocity imparted to the plate is required. High speed digital imaging captured the movement of the plate in response to the blast. Specialized software was used to analyze the video to determine displacement, and the data points were then fitted to a curve to find the initial velocity. Common problems encountered during testing included spray obscuring the video, camera failure, and dud charges.

3.1 Dihedral Plate Fabrication

The unusual geometry of the angled plates requires specialized fixturing and machining techniques to fabricate. Figure 3.1 shows the fixture and aluminum plate before machining. All parts have a nominal tolerance of 0.05”.

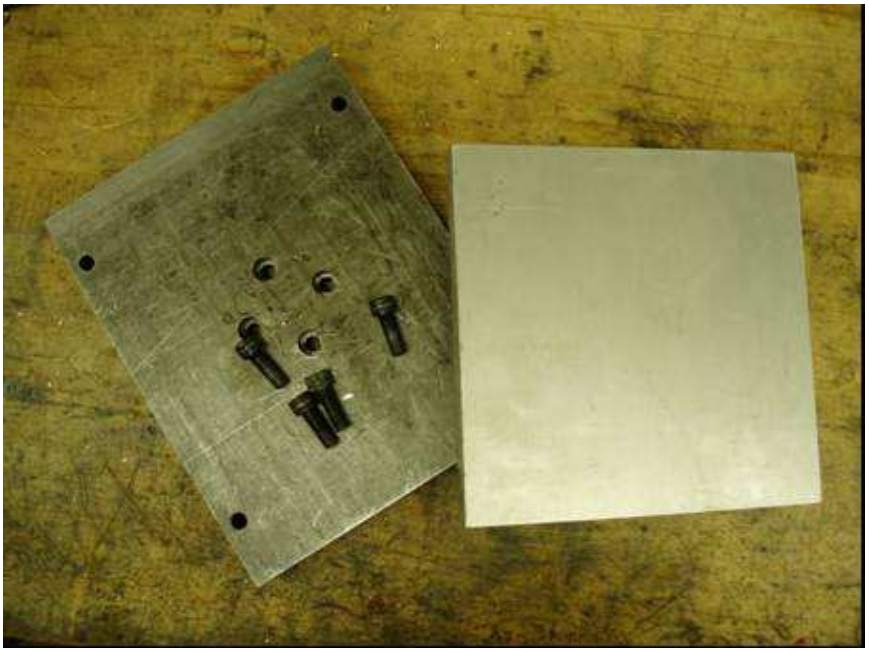

Figure 3.1: Fixture Plate, Bolts, and Aluminum Plate

The fixture plate is a 1” thick steel plate measuring 8” x 10”. Four 3/8” holes in a square pattern were drilled and countersunk into the center of the plate. The coordinates of the four holes with the center of the plate as the origin are (1”, 0”), (-1”, 0”), (0”, 1”), and (0”,-1”). 1” long 3/8”-16 socket cap bolts were used to hold the aluminum block to the fixture plate.

The initial dimensions of the aluminum plate depended on the angle of the target to be fabricated. All aluminum plates required an 8” x 8” billet. All targets were fabricated to a nominal mass of 1.5 kg (3.306 lbs), which requires a total of 33.9 in^3 (55.6 cm^3) of aluminum. Figure 3.2 and Table 3.1 show the dimensions of each target plate. The 20° target plate required the removal of 9.86 in^3 of material from the back of the plate to meet the specified mass, as can be seen in Figure 3.3.

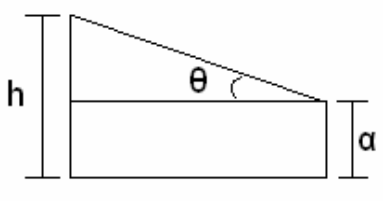

Figure 3.2: Target dimensions

θ°	h (in.)	α (in.)
0	0.500	0.500
7	0.487	0.286
13	0.900	0.080
20	1.368	0

Table 3.1: Target Dimension Values

Figure 3.3: Underside of 20° Plate (note removed material)

3.1.1 Dihedral Plate Machining Procedure

The aluminum plate was clamped to the mill bed, with a machined edge placed against the reference posts (Figure 3.4). A piece of stock between the plate and the table allowed the edges of the plate to be milled in a single pass. The corners of the plate were then indexed using an edge finder.

Figure 3.4: Clamping Aluminum Plate to Mill Table

The plate was milled until it was square and dimensioned as close to 8” x 8” as possible (Figure 3.5). Tolerances were less than 0.05”, and surface finishes were not important at this stage.

Figure 3.5: Milling the Edges of the Target Plate

Figure 3.6 shows the drilling and tapping of the machined and dimensioned stock plate. With the center of the plate as the origin, the coordinates of the hole pattern were (1”, 0”), (-1”, 0”), (0”, 1”), and (0”,-1”). The holes diameters were 5/16” and approximately 0.5” deep. The tap size was 3/8”-16.

Figure 3.6: Tapping the Drilled Hole Pattern

The plate was then removed from the table, cleaned, and then tightly bolted to the fixture plate as seen in Figure 3.7. The bolt heads needed to be flush with the surface of the fixture plate.

Figure 3.7: Mounting Aluminum Plate to Fixture Plate

Figure 3.8 shows the installed and adjusted angled mill table.

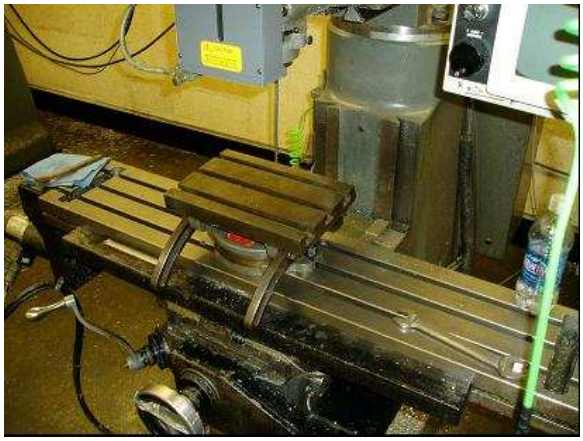

Figure 3.8: Angled Mill Table

The fixture plate was clamped to the angled mill table as shown in Figure 3.9.

Figure 3.9: Clamping Fixture Plate to Angled Mill Table

A facing cutter was run across the plate (Figure 3.10) until the reference dimensions reach the values specified in Table 3.1.

Figure 3.10: Facing the Target Plate

The fixture was then unclamped, rotated 180°, and then clamped to the milling table again. The facing operation was then repeated on the other side of the target. Figure 3.11 shows a completed target plate.

Figure 3.11: Finished 13° Target Plate

3.2 636 mg Charge Fabrication

Fabricating the 636 mg charge required 0.9g of Detasheet, an RP-87 detonator, a delrin ring, and 5-minute epoxy (Figure 3.12). The delrin ring has an inner diameter of 33/64", an outer diameter of 9/16", and a nominal height of 0.3". The inner diameter is the most critical dimension. Wax paper prevents the Detasheet from sticking to any surfaces, and a ½" brass rod is useful for tamping the explosive.

Figure 3.12: 636 mg Charge Fabrication Components

The charge is fabricated by first firmly tamping the explosive into the delrin ring. A RP-87 is then pushed into the center of the detasheet approximately 1/8"deep. The back of the charge and the detonator wire leads are then sealed with epoxy and allowed to dry (Figure 3.13).

Figure 3.13: 636 mg Charge

3.3 Initial Setup and Testing

3.3.1 Test Bed Setup

Setting up the test bed properly is crucial for consistent results. The process involves disturbing and compressing the sand, burying the charge, setting the target plate, and finally saturating the soil. The sand in the bed had to be reasonably dry before beginning; it took approximately an hour after draining the tank from saturation for the soil to be dry enough. Disturbing the soil a few minutes after all the water had drained accelerated the drying process.

First, the sand needed to be completely turned over using a scoop. Once the soil was disturbed a cinder block was used to pound the sand down into a compacted form (Figure 3.14). If the sand bed was not dry enough, compacting the sand forced water up through the sand bed. If this happened, the sand bed was given another 30 minutes to dry.

Figure 3.14: Compacted Sand Bed

The sand bed was then planed to a level shape, as seen in Figure 3.15. Once planed, a small trench was dug around the edge of the sand to help distribute the water.

Figure 3.15: Test Bed and Sand Plane

Figure 3.16 shows how the charge was wired to the firing system leads. The firing system was disconnected before the charge was wired, and the leads were sealed with electrical tape.

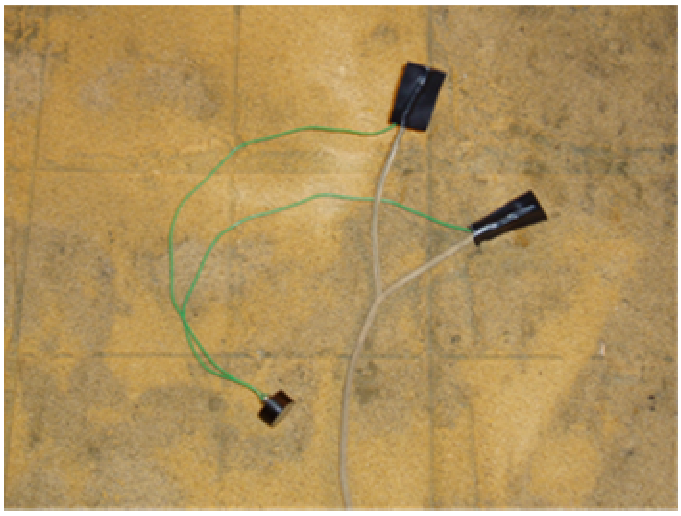

Figure 3.16: Wired 636 mg Charge

The charge was placed by first marking two very long, perpendicular lines in the soil using a ruler, and then creating a 7” x 7” square with the intersection of the two lines in the center (Figure 3.17). For tests using a 636mg charge and 8” by 8” plate the edges of the square were at least a foot from any wall of the tank.

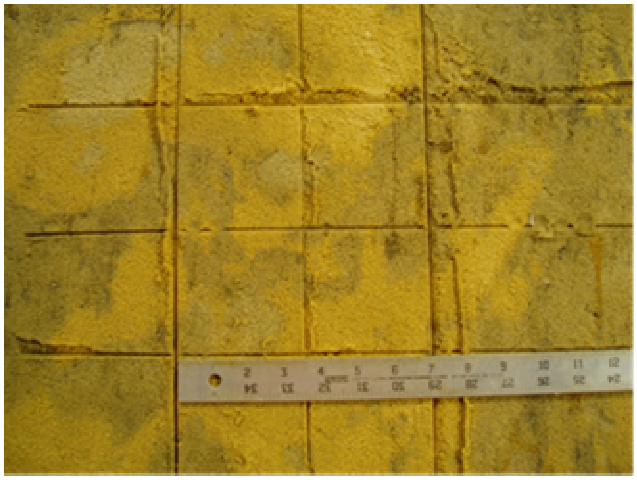

Figure 3.17: Placement Grid for Charge and Plate

The charge was then buried in the center of the square, and a caliper was used to measure the depth of burial as seen in Figure 3.18.

Figure 3.18: Confirming Depth of Burial

Once the charge was buried to the correct depth, the top was covered with sand and gently compacted with a small block of wood. A standoff post was placed at each corner of the previously marked square (Figure 3.19), and their height adjusted so that the bottom of the plate was at the required standoff distance.

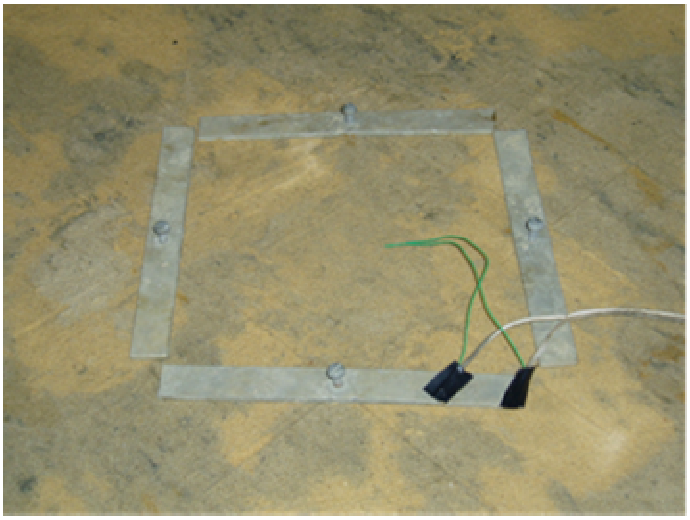

Figure 3.19: Standoff Posts and Buried Charge

The standoff distance was measured by first finding the distance from the top of the plate to the ground (Figure 3.20), and then subtracting the plate thickness.

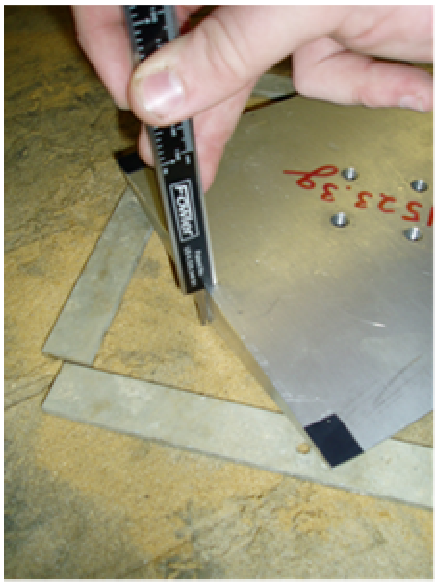

Figure 3.20: Measuring Standoff Distance

The plate was then leveled and centered over the charge using the centerlines marked in the soil (Figure 3.21). The standoff distance was then checked again.

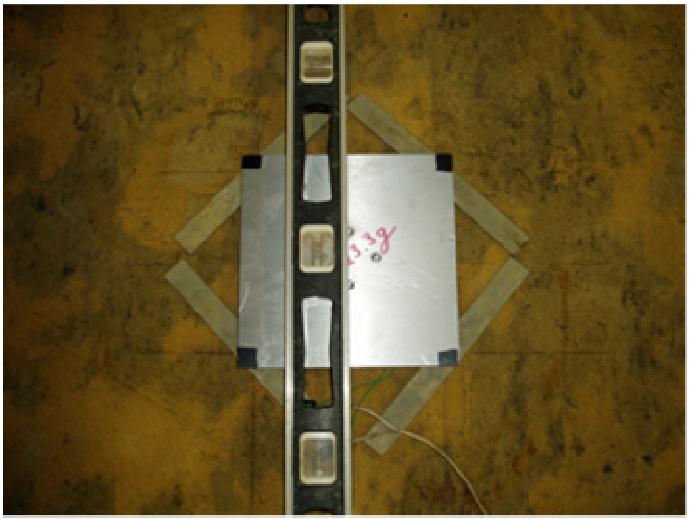

Figure 3.21: Leveled Target Plate

Once the plate was accurately positioned the tank was filled with water until the sand was saturated. When properly saturated the sand developed a light sheen (Figure 3.22, Right). If the sand was oversaturated (Figure 3.22, Left) then the tank was drained until the water level reached an acceptable height. Figure 3.23 shows a completed test bed setup with properly saturated sand around the target plate.

Figure 3.22: Oversaturated Sand (Left) and Properly Saturated Sand (Right)

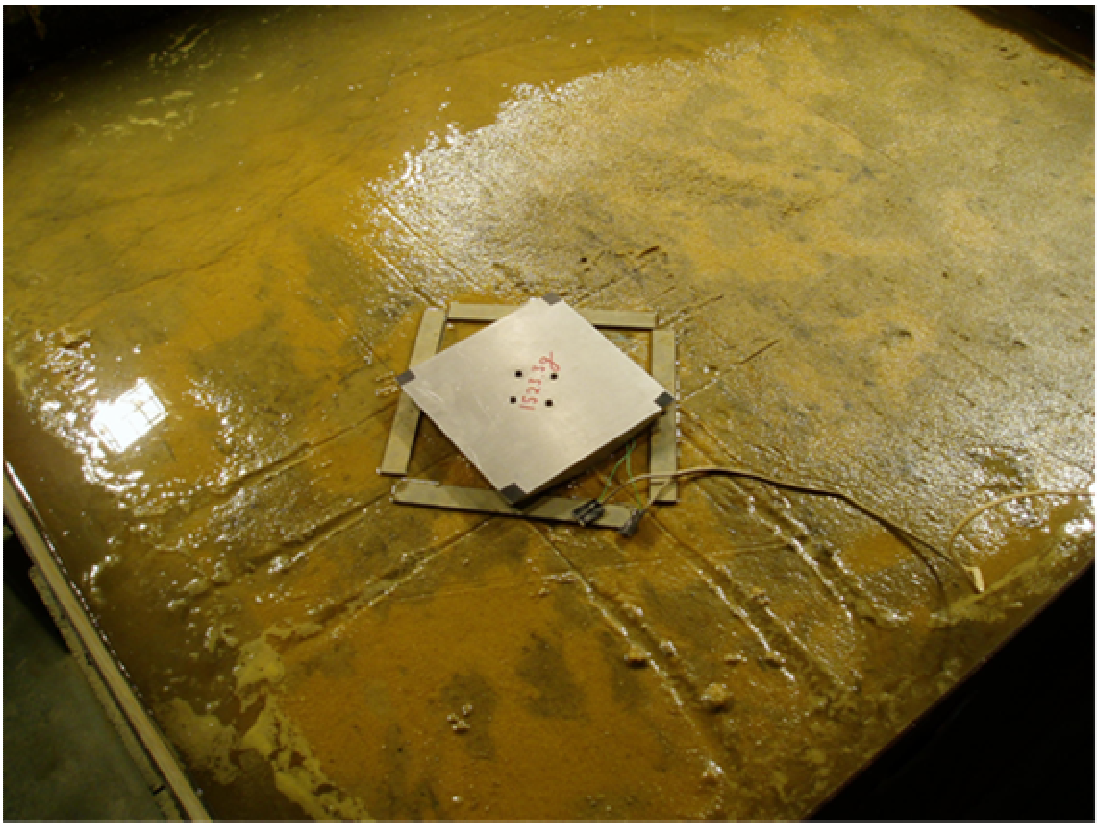

Figure 3.23: Completed Test Setup

3.2.2 Camera Setup

The camera was set up facing one of the corners of the plate, raised high enough that all four plate corners can be seen. The precise height was not important because the variation caused from the change in perspective is insignificant. The camera was zoomed and tilted so that the plate filled the view window horizontally (Figure 3.24). The software settings depended on the camera model, as seen in Table 3.2. The image quality settings (brightness and contrast) were adjusted during each test depending on the light conditions.

	Phantom v4	Phantom v7
Frame rate:	1000 pps	8213 pps
Exposure Time:	594 µs	120 µs
Post Trigger:	1000 p	10802 p
Resolution:	512x512	512x512
Zoom:	Fit	Fit
Exposure:	Auto	Auto

Table 3.2: Camera Settings

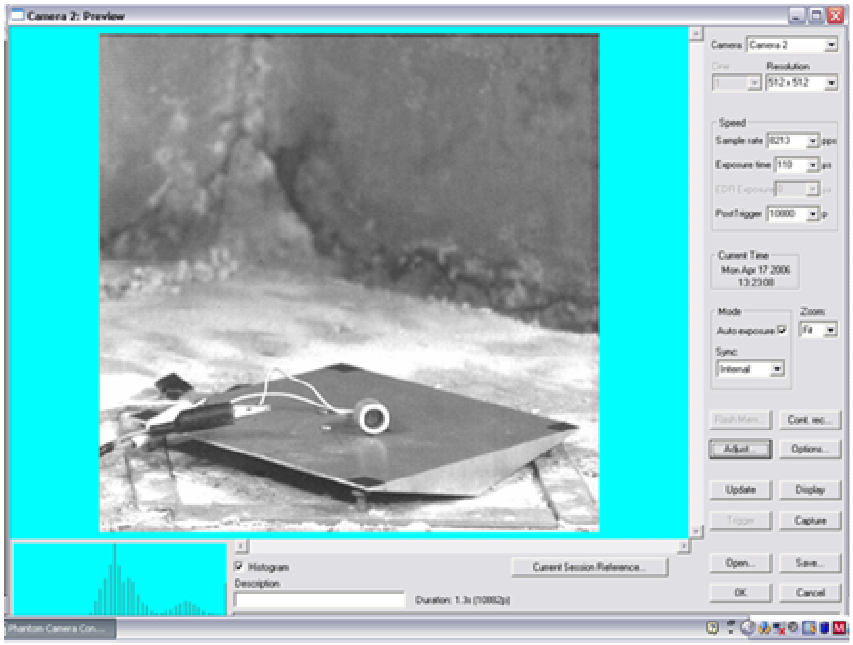

Figure 3.24: Camera Configuration and Plate Display

3.2.3 Testing

The next step was to ensure the camera and trigger system were functioning properly. The dummy charge was connected to the detonator leads and placed on top of the plate. The camera was set to receive the trigger signal, and the dummy charge was detonated. If the system was working properly, the video showed the dummy charge flashing at the same time the timer indicated the charge had detonated. The test was repeated twice for a total of three successful trial runs. The dummy charge was then removed, the leads were connected to the live charge, the camera was reset, and then the live test was conducted (Figure 3.25).

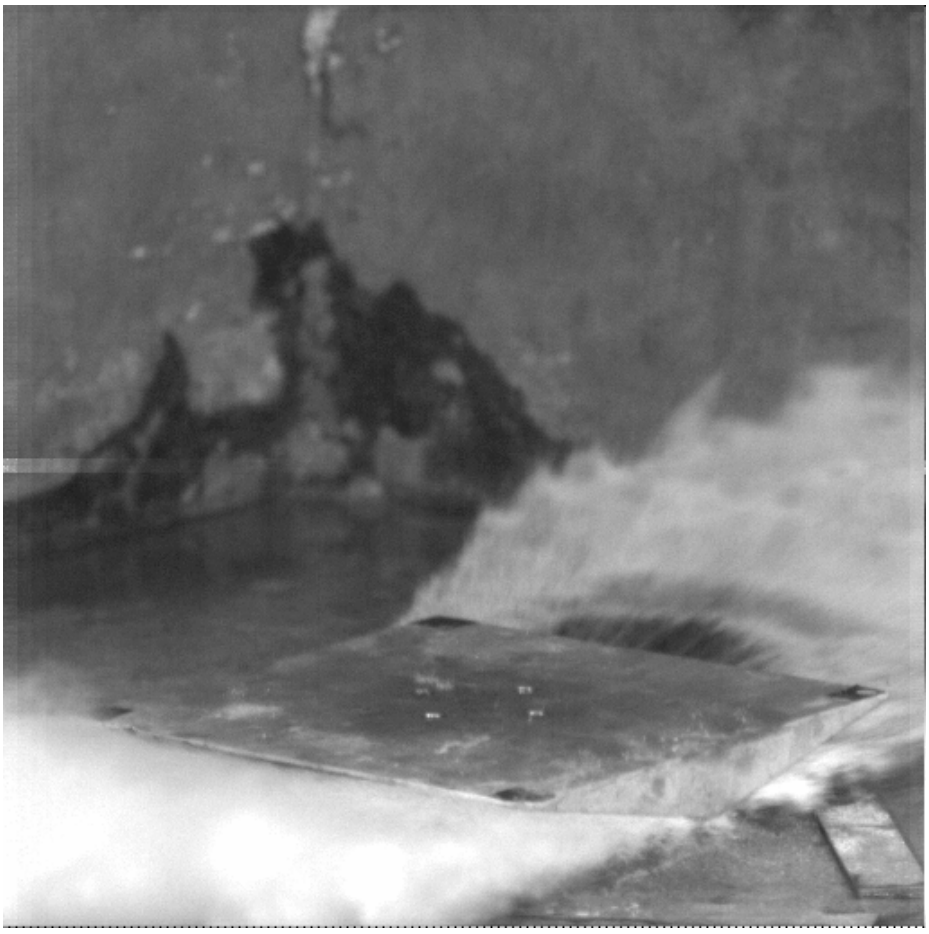

Figure 3.25: Typical Buried Charge Test

3.4 Data Collection and Analysis

3.4.1 Collection of Data

The Phantom camera recorded the movement of the plate in .cin files which can only be read by the Phantom camera software. The movies were truncated to reduce their size; a full size movie using the Phantom 7 takes up two gigabytes of hard drive space. The movie was cut to only show a few frames before the trigger event, and then every frame until the target plate was no longer on screen. Any video of the descent of the plate was considered unusable because the target plates typically hit the ceiling.

The four corners of every target plate were marked with black electrical tape in order to make recording plate displacement easier. Each corner was designated by its position relative to the camera. The left and right corners were located to the camera's left and right respectively, the front corner was closest to the camera, and the back corner was furthest.

The displacement of selected points on the plate was manually measured using tools contained within the software suite. The software was set to read inches, and the distance between the left and right corners of the plate was used to calibrate the scale. The position of the four corners in each frame were captured and measured independently. Data points were gathered from the first 50 to 100 frames, and then every 10^{th} frame afterwards until the plate was out of view. The first 50 to 100 points were needed to fully characterize the initial displacement. Once the data was collected, Microsoft Excel was used to translate the raw text files produced by the

Phantom software into readable spreadsheets. The Y position and time after trigger were the only columns needed.

The most common hindrance to recording the displacement of the target plates was spray obscuring one or more corners. This was partially overcome by zooming in to observe the movement of a specific point, or by using the image processing filters to sharpen the image. The location of a corner could also be extrapolated by intersecting the lines of each edge. If the data point was too obscured, then it was not recorded.

If the sand was found to be oversaturated, then the test was thrown out and repeated. Over saturation was detected by observing the condition of the sand during a test. If the sand was oversaturated it appeared "soupy" in consistency, similar to the sand in Figure 3.26 (Left). Properly saturated sand flew in chunks as seen in Figure 3.26 (Right).

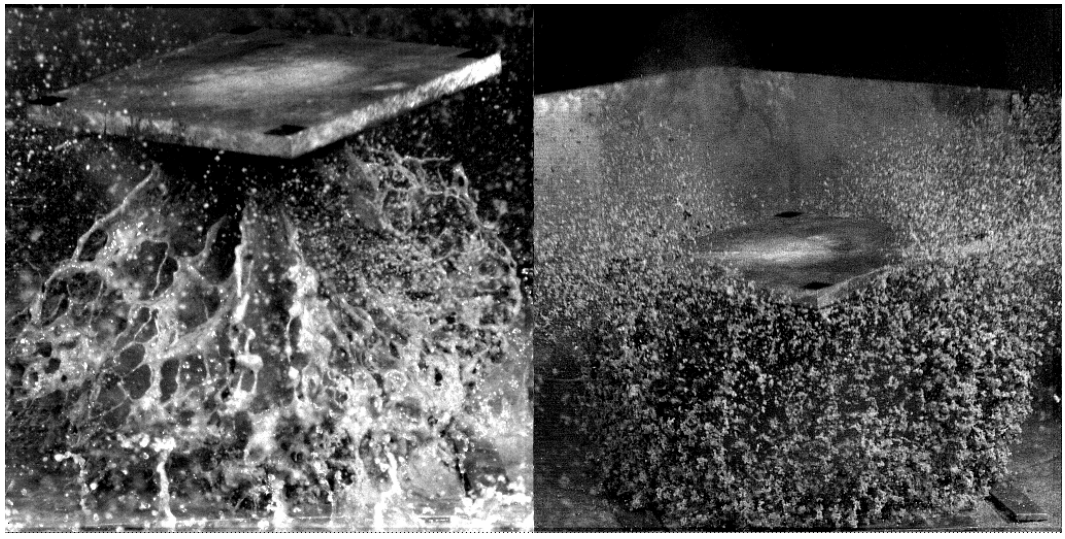

Figure 3.26: Oversaturated Sand (Left) and Properly Saturated Sand (Right)

3.4.2 Analysis of Data

The data was analyzed using curve fitting through Microsoft Excel. The vertical displacement was graphed with respect to time, and a curve was fit to determine the initial velocity. Different curve fit methods were used to determine the initial velocity from the displacement data. The effectiveness of each method depended on the number of the points captured and the time interval between them.

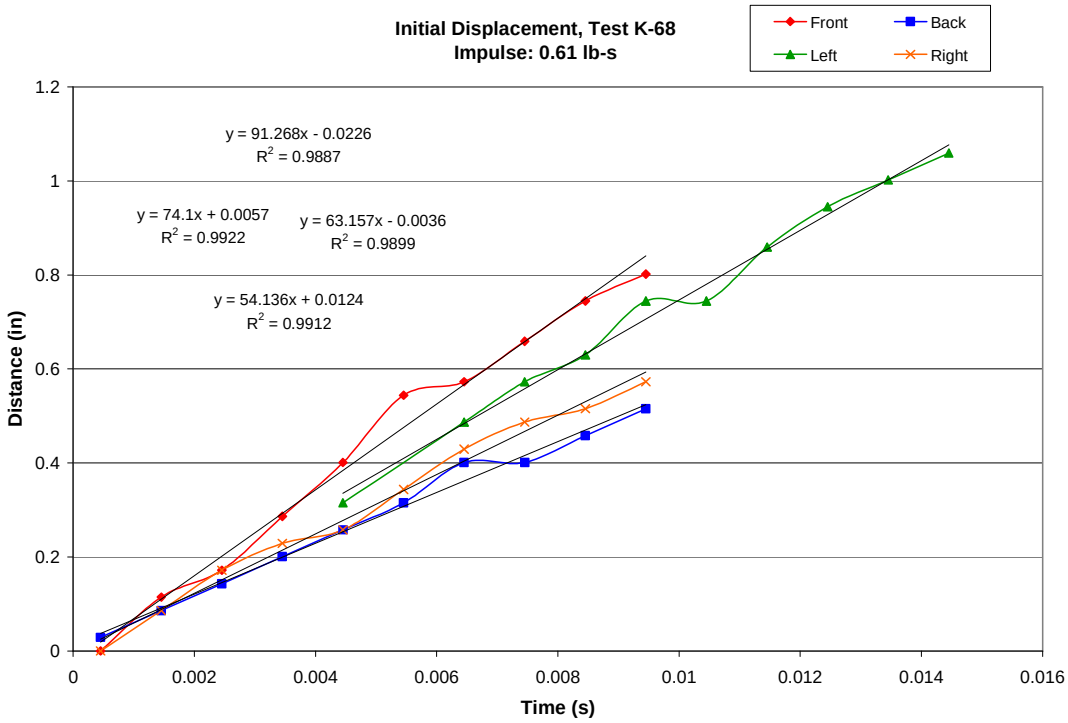

Figure 3.27: Initial Displacement Curve Graph

The first method fit the first ten frames to a linear fit (Figure 3.27). The slope of the fit line was taken as the initial velocity. This method was mostly used with the Phantom v4 camera with its relatively low frame rate. The higher frame rate of the Phantom v7 had too much scatter within the first ten frames to produce viable results with this method. This method was also ineffective if the initial data points were

obscured by water spray or flying soil. Another method involved fitting a linear curve to the data points within the first two inches of travel. This method was more effective with the Phantom v7 camera and was less affected by flying debris and soil.

The entire recorded displacement was also fit to a parabolic curve to obtain another equation of motion. This method had the advantage of not being significantly affected by obscuring spray and ejecta, but was less useful if the plate rotated or flipped. The parabolic curve fit produced a quadratic equation ($Ax^2 + Bx + C$) that could be compared to the displacement equation

$$x(t) = (\frac{1}{2})gt^2 + V_O t + X_O$$

where t is time, g is acceleration due to gravity, V_o is the initial velocity, and X_o is the initial position. If the A term (acceleration term) of the fitted curve equation was close to -198 (half the acceleration due to gravity in in/s^2) then the B term was considered a good value for the initial velocity. Deceleration due to air drag was considered negligible for this analysis, but deceleration of the plate from the collapse of the bubble was considered a potential factor if the parabola was imperfect. Figure 3.28 shows a typical displacement plot, in this case for a 20° dihedral plate with a 0.04" DOB and 0.5" SOD.

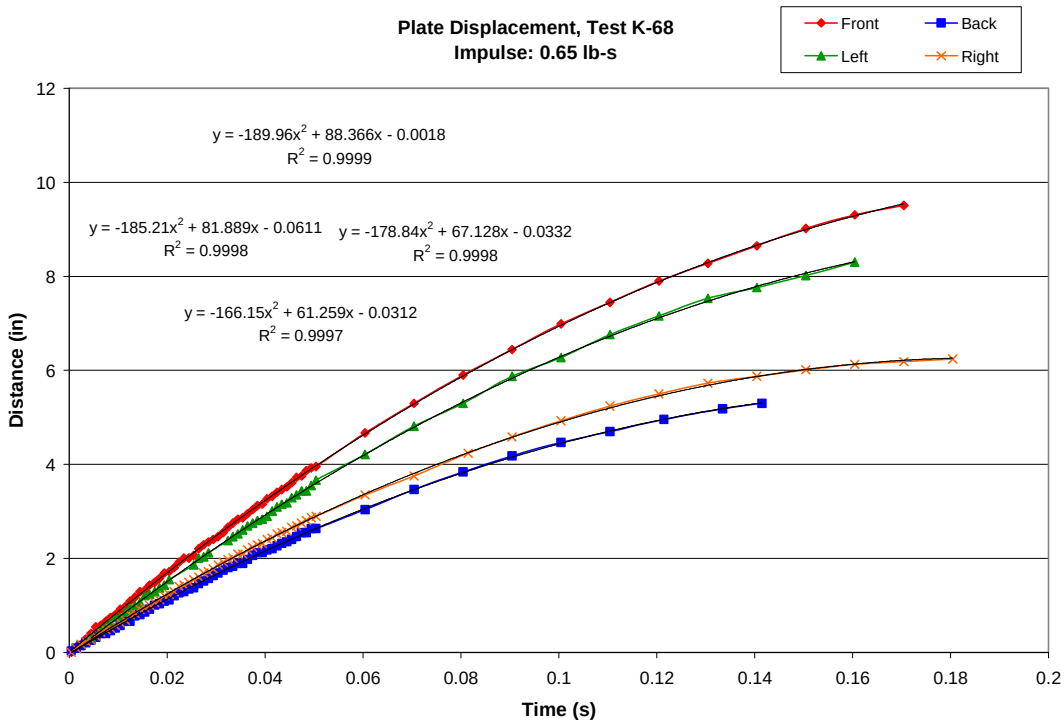

Figure 3.28: Total Displacement Curve Graph

For each method, the velocities for each corner were averaged and the result was multiplied by the plate mass to obtain the impulse. The impulse reading and R^2 value for each method was compared and each curve was examined visually for anomalies and degree of scatter. The linear fit to the initial displacement was generally used as the impulse result for the test. The parabolic fit to the total displacement was used when the initial displacement was obscured by flying sand or water. The difference between impulse values was typically 10%.

Chapter 4: Results

Overview

This chapter presents the findings on testing of the effect of variations in plate angle, standoff distance, and depth of burial on the impulse transmitted by a buried charge to a suspended target plate.

Section 4.1 presents the primary results from the impulse testing in the form of eleven surface graphs. In each graph one of the four standoff distances, the three depths of burials, or the four plate angles is held constant. Any specific trends within the graph are examined and discussed.

Section 4.2 discusses these findings and analyzes the effect of variations in target shape, standoff distance, and depth of burial on impulse. Trends between the individual graphs are linked to establish conclusions regarding the interaction of the variables. This section will also present potential explanations for the trends found in the data.

Section 4.3 discusses inconsistencies found between the results of 0° plate testing and expected values derived from previous experiments. It also explains how the small size Detasheet charge may be responsible for these inconsistencies.

Section 4.4 discusses the effects of repeated tests on the target plates, and how the wear pattern supports the presence of the impact load and a dispersed load components.

4.1 Presentation of Target Shape Findings

Sections 4.1.1 through 4.1.3 contain surface graphs depicting impulse as a function of depth of burial, standoff distance, and dihedral plate angle. For each graph one of the variables is held constant, and the other two are plotted in the X and Y directions. The Z direction is always impulse in lb-s. The color of the surface graph corresponds to the height. Each of the blue dots represents a single data point; multiple points at the same location indicate repeated tests.

Section 4.1.4 contains a line graph comparing impulse as a function of standoff distance for two different plate shapes (pyramid and dihedral) at a constant depth of burial. The X axis is standoff distance, while the Y axis is total impulse. The different color lines represent different target shapes (either the pyramid or dihedral shape).

4.1.1 Results at Constant Depth of Burial

Figure 4.1 and Table 4.1 show total impulse as a function of standoff distance and plate angle for a constant depth of burial of 0.04". At this shallow depth of burial there is little soil to impact against the target, which means most of the load comes from the expanding gas. The impulse falls quickly as the standoff distance increases to 0.5" and then levels off as the standoff distance increases further. The decrease in impulse with standoff distance becomes less pronounced as the plate angle increases. The difference in total impulse with constant 0.0" standoff distance is peculiar; there is a large change in impulse between the 7° and 13° angles, but at smaller and larger angles the effect of plate angle is negligible . A similar phenomena occurs at the 0.5" standoff distance.

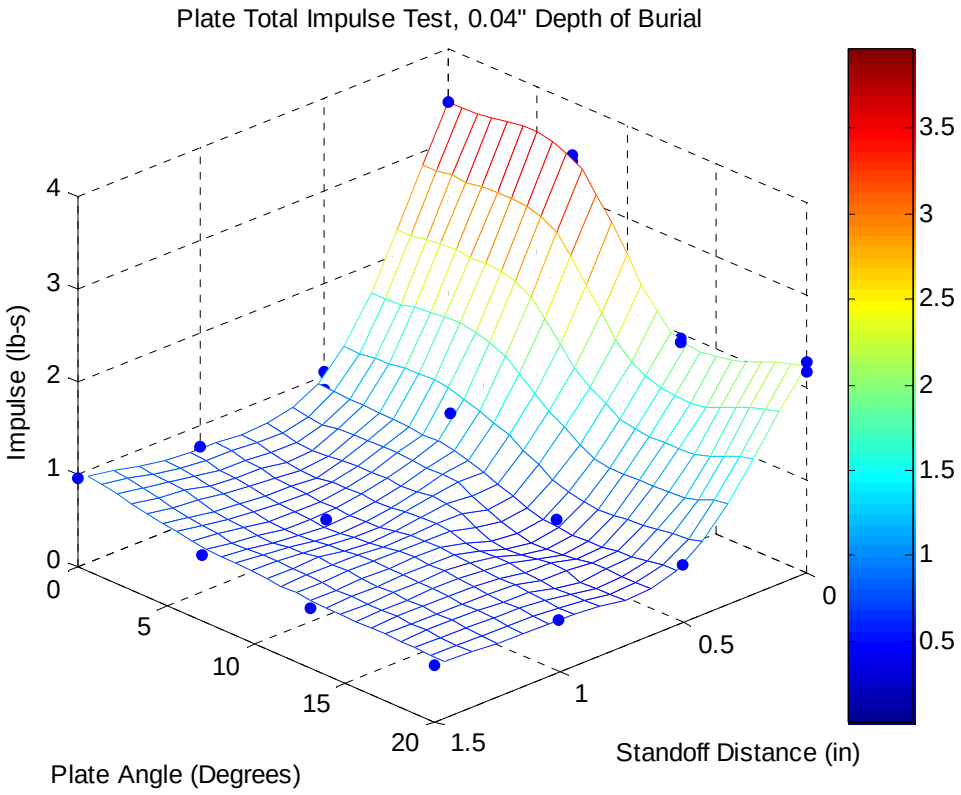

Figure 4.1: Total Impulse Tests at Constant 0.04" Depth of Burial

Angle \ Standoff Distance	0"	0.5"	1"	1.5"
0°	3.42	0.98	0.75	0.96
7°	3.39	0.88	0.57	0.71
13°	1.93	0.52	0.65	0.63
20°	2.23	0.61	0.56	0.60

Table 4.1: Average Total Impulse Values (lb-s) at 0.04" Depth of Burial

Figure 4.2 and Table 4.2 show the total impulse as function of standoff and plate angle when the depth of burial is 0.25". This deeper depth of burial means there is more soil above the charge. This added soil may change the loading mechanism by dispersing the gas bubble and increasing the amount of momentum transfer through soil impact. At the smaller standoff distances the impulse captured by the plate is roughly inversely proportional to the angle of the plate. More refined testing with additional standoff distances and plate angles is needed to better understand the relationship. The addition of more ejecta due to the deeper depth of burial may have increased the effect target geometry has on total impulse at smaller standoffs. At the 1.0" and 1.5" standoffs, the loading is roughly constant regardless of target angle. This suggests the presence of a loading component unaffected by target shape or standoff distance (within the range tested), perhaps the soil cap impacting against the underside of the plate.

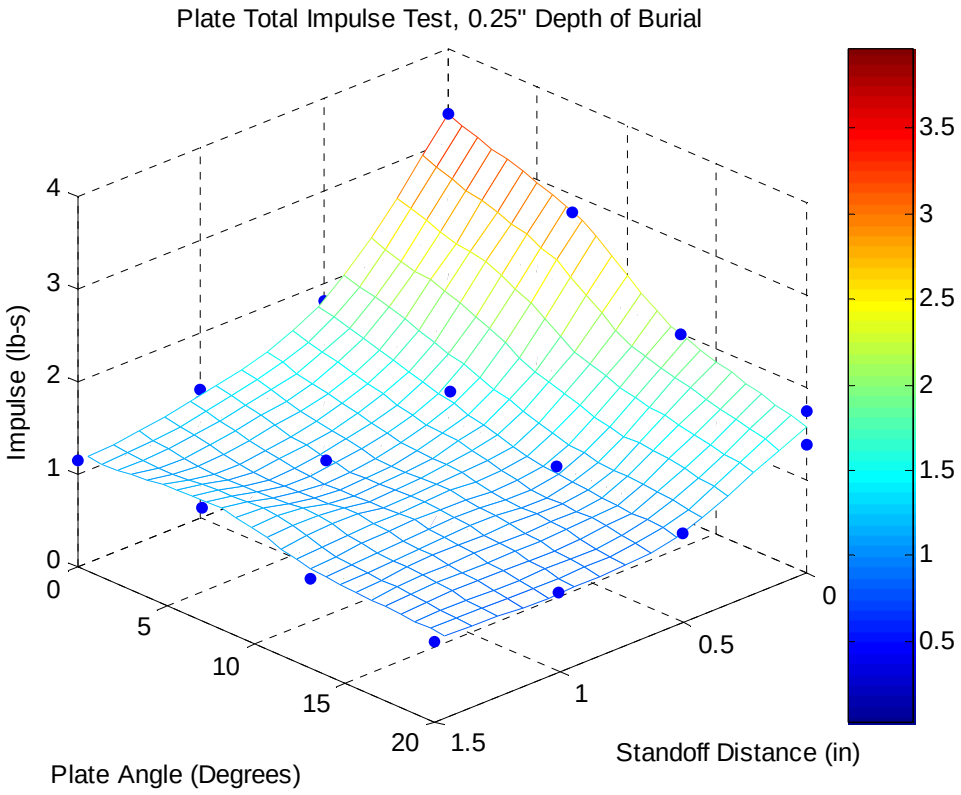

Figure 4.2: Total Impulse Tests at 0.25” Depth of Burial

Angle \ Standoff Distance	0"	0.5"	1"	1.5"
0°	3.28	1.80	1.33	1.16
7°	2.81	1.40	1.05	1.23
13°	1.99	1.09	1.05	0.96
20°	1.57	0.96	0.85	0.87

Table 4.2: Average Total Impulse Values (lb-s) at 0.25” Depth of Burial

Figure 4.3 and Table 4.3 show total impulse as a function of standoff distance and plate angle at a 0.5” depth of burial. At the 0” standoff distance the impulse values are unusual; the impulse drops between the 0° and 7° plates, remains constant between the 7° and 13° plates, and then drops again as the dihedral angle increases to 20°. One possible explanation for this phenomenon is the direction of the blast. Deeply buried charges are believed to have more vertical soil movement than shallow charges, and the target may need to have a greater angle to deflect that blast. At the 0.5” standoff distance there is little difference between the 13° and 20° plates. At greater standoff distances there is a negligible difference among all of the angles tested.

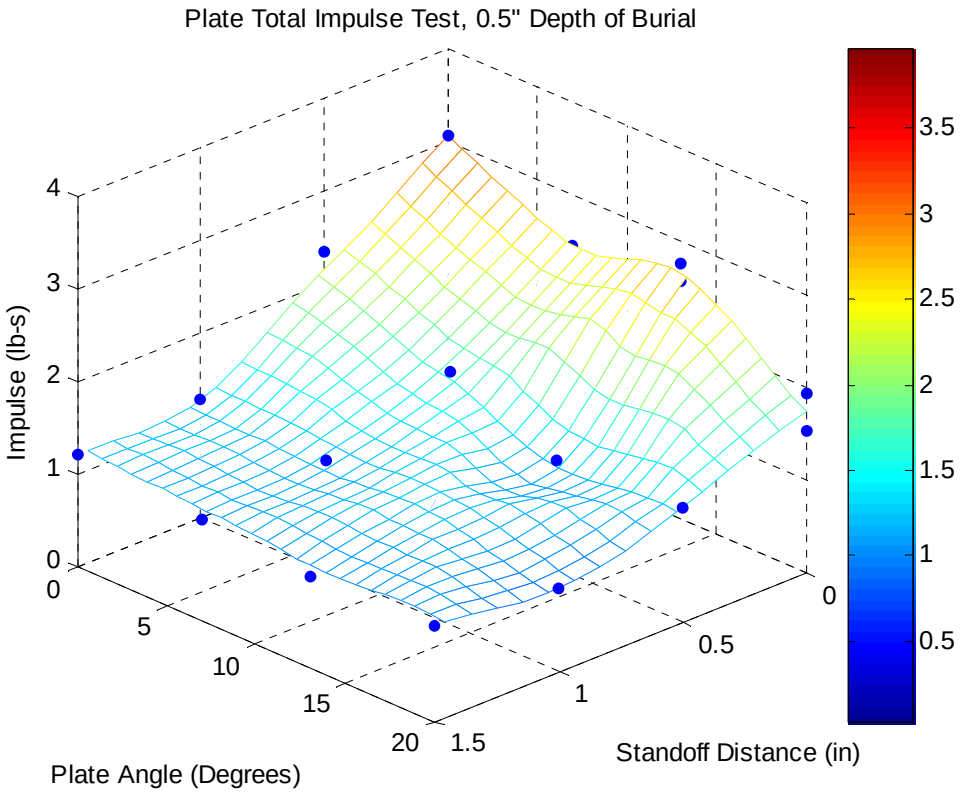

Figure 4.3: Total Impulse Tests at 0.5" Depth of Burial

Angle \ Standoff Distance	0"	0.5"	1"	1.5"
0°	3.06	2.14	1.27	1.21
7°	2.45	1.62	1.20	1.10
13°	2.66	1.17	1.23	0.99
20°	1.74	1.23	0.90	1.03

Table 4.3: Average Total Impulse Values (lb-s) at 0.5" Depth of Burial

4.1.2 Results at Constant Plate Angle

Figure 4.4 and Table 4.4 present captured impulse as a function of standoff distance and depth of burial for a 0° dihedral target plate. The total impulse is greatest at the 0" standoff distance, and decreases steadily as the standoff distances increases up to the 0.5" standoff distance. The total impulse then levels out between the 0.5" and 1.5" distances. The performance of the 0° plate with respect to depth of burial is dependent on the standoff distance. At 0" standoff distance, the total impulse decreases slightly as the depth of burial increases. At 0.5" standoff, the impulse increases with depth of burial, while at 1.0" and 1.5" the impulse increases slightly between 0.04" and 0.25" depth of burial, and then levels off as the depth reaches 0.5". The performance of the 0° plate is used as a baseline against which the other angle plates are compared.

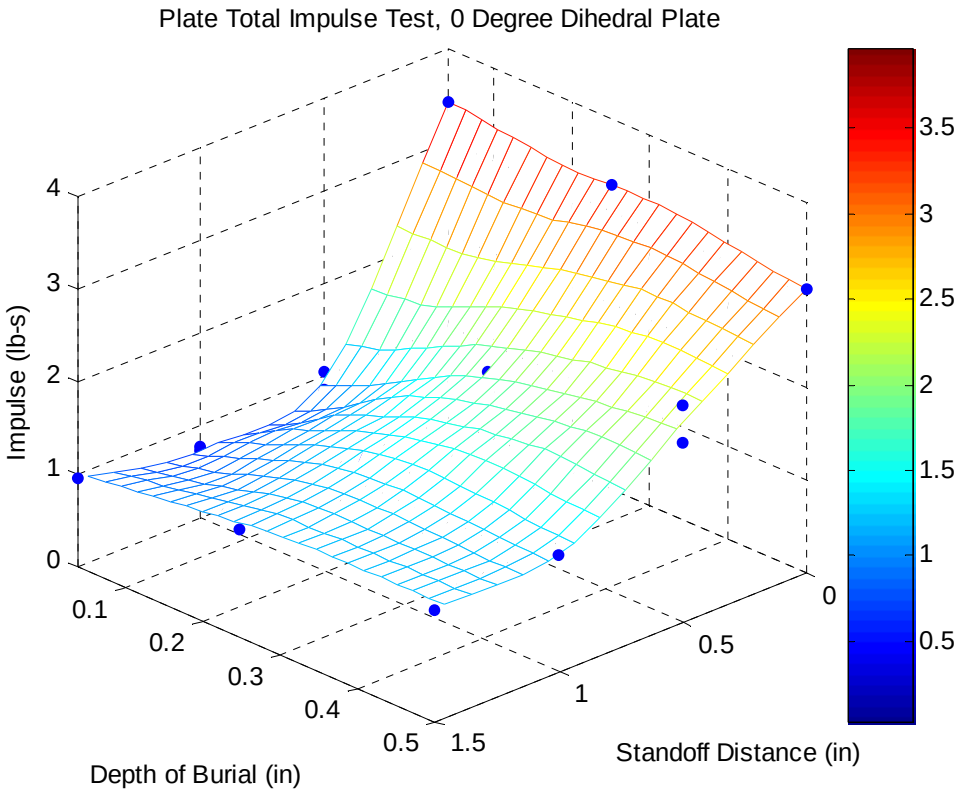

Figure 4.4: Total Impulse Tests with 0 Degree Angled Plate

Burial Depth \ Standoff Distance	0"	0.5"	1"	1.5"
0.04"'	3.42	0.98	0.75	0.96
0.25"	3.28	1.80	1.33	1.16
0.5"	3.06	2.14	1.27	1.21

Table 4.4: Average Total Impulse Values (lb-s) with 0 Degree Angled Plate

Figure 4.5 and Table 4.5 show captured impulse as a function of standoff distance and depth of burial for a 7° dihedral target plate. Seven degrees is the shallowest nonzero plate angle tested, and overall this provided trends similar to those of the 0° plate. The highest impulse is located at 0.0" standoff and 0.04" depth of burial. For all depths of burial the impulse decreases gradually as standoff distance is increased. As with the 0° plate, the change in impulse with respect to depth of burial depends on the standoff distance. At 0.0" standoff the impulse steadily decreases with increasing depth. At the other standoff distances the impulse increases slightly between the 0.04" and 0.25" depths and the levels off between the 0.25" and 0.5" depths. Overall the impulse is lower than that of the 0° plate. This implies that the plate angle, when loaded in the center, deflects some of the ejecta to the sides. This reduces the total vertical impulse.

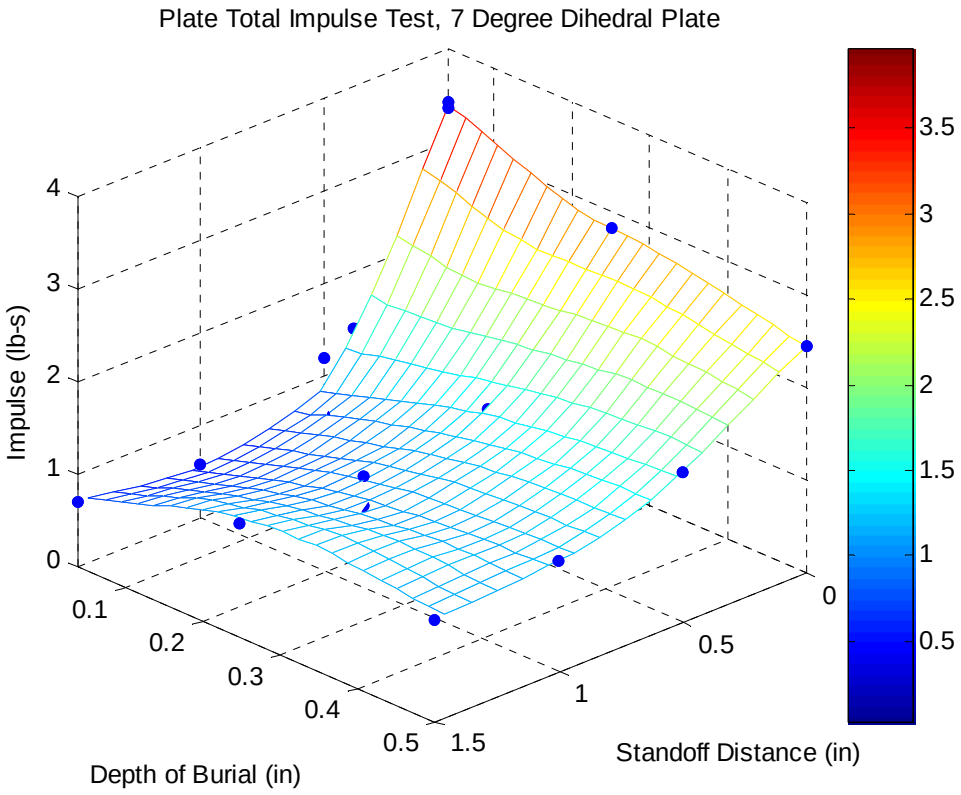

Figure 4.5: Total Impulse Tests with 7 Degree Angled Plate

Burial Depth	Standoff Distance 0"	0.5"	1"	1.5"
0.04"'	3.39	1.37	0.88	0.57
0.25"	2.81	1.40	1.05	1.23
0.5"	2.45	1.62	1.20	1.10

Table 4.5: Average Total Impulse Values (lb-s) with 7 Degree Angled Plate

Figure 4.6 and Table 4.6 display captured impulse as a function of standoff distance and depth of burial for a 13° dihedral target plate. As with the 0° and 7° plates, the impulse decreases as the standoff distance goes from 0" to 1.0", and then levels off between the 1.0" and 1.5". For the 0.5", 1.0", and 1.5" standoff distances, the impulse trends are similar to the other dihedral plates; the impulse increases slightly between the 0.04" and 0.25" depths of burial, and then levels off between the 0.25" and 0.5" depths. At the 0.0" standoff distance, the impulse captured by the 13° plate remains level between the 0.04" and 0.25" depth of burials, and then increases as the depth of burial goes to 0.5". This behavior at the 0.0" standoff is different from the other target shapes used in this test series. This behavior can be explained by the presence of increasingly vertical flow of the ejecta as charge depth increases, as seen in Section 1.5.2. As more of the ejecta flows at an angle close to perpendicular with respect to the surface, a steeper dihedral angle is required in order to better deflect the blast effects.

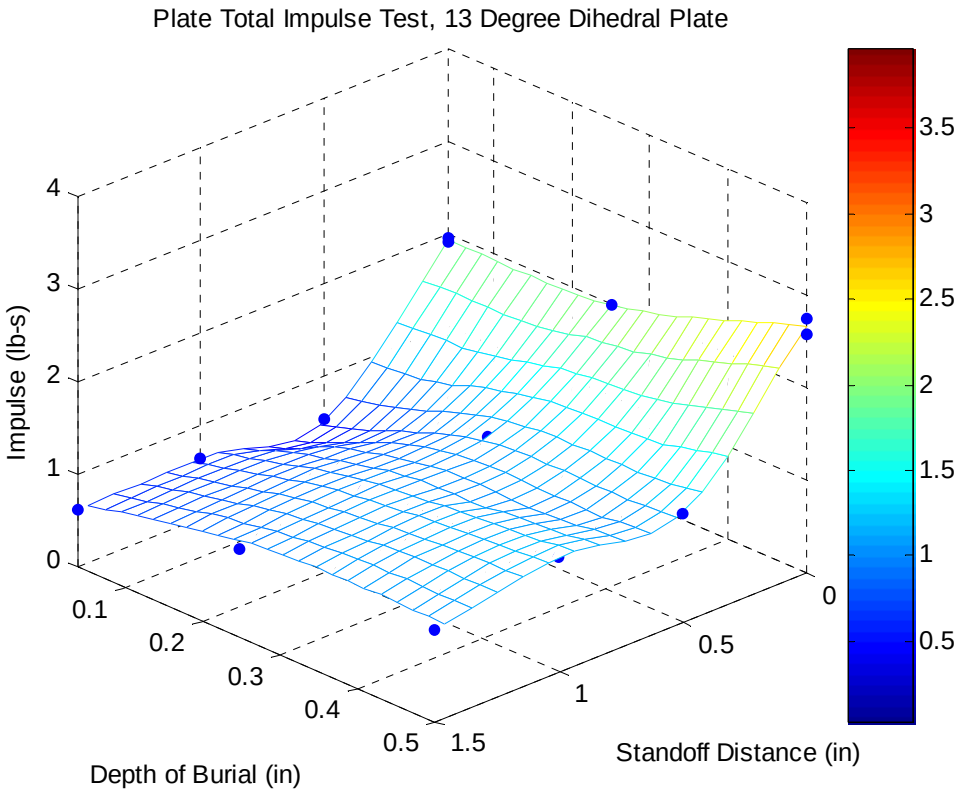

Figure 4.6: Total Impulse Tests with 13 Degree Angled Plate

Burial Depth \ Standoff Distance	0"	0.5"	1"	1.5"
0.04"'	1.93	0.52	0.65	0.63
0.25"	1.99	1.09	1.05	0.96
0.5"	2.66	1.17	1.23	0.99

Table 4.6: Average Total Impulse Values (lb-s) with 13 Degree Angled Plate

Figure 4.7 and Table 4.7 show total impulse as a function of standoff distance and depth of burial for a 20° plate. At the 0.0" standoff distance, the 20° plate demonstrates a decrease in total impulse between the 0.04" and 0.25" depth of burial, and then levels off as the depth increases to 0.5". The plate performs differently at the other standoff distances. At standoff distances greater than 0", the impulse increases slightly between the 0.04" and 0.25" depths of burial, and then the impulse levels off between the 0.25" and 0.5" burial depths. The significant reduction in total impulse (relative to the 0° plate) implies that much of the blast effects are being deflected away by the 20° plate. The similarity in performance between the 0.25" and 0.5" depths of burial at 0.0" standoff is in contrast to the 13° plate. This may mean that when facing charges buried at deeper depths, the more vertical flow of the ejecta and detonation products requires larger plate angles to maximize the deflection when compared to shallow buried charges.

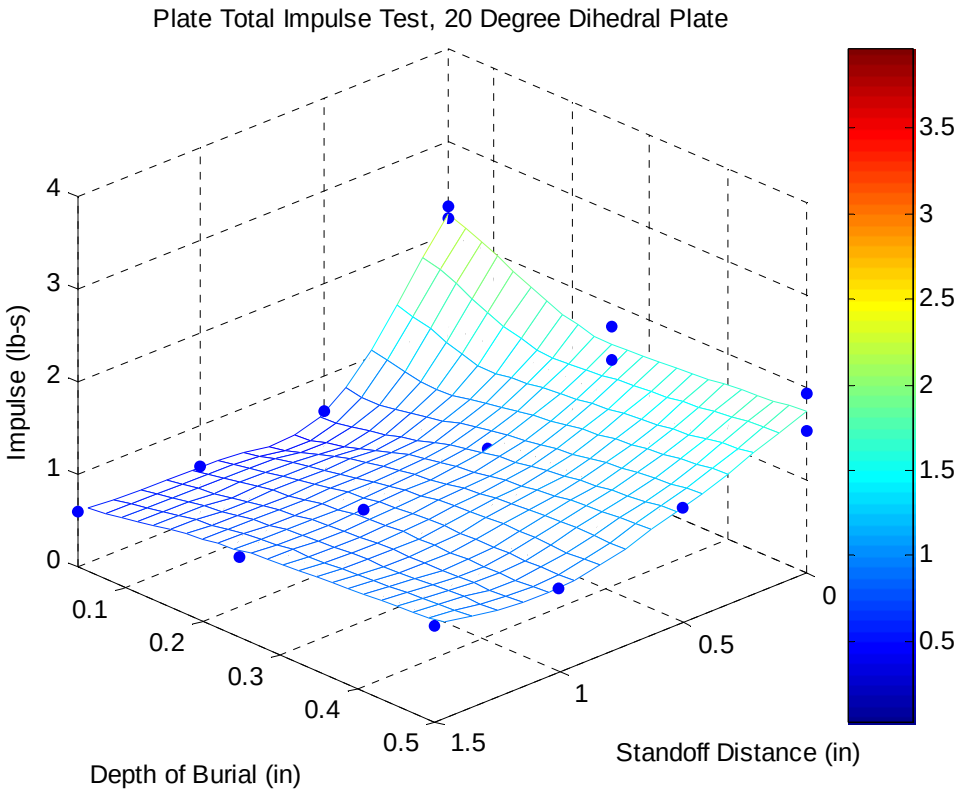

Figure 4.7: Total Impulse Tests with 20 Degree Angled Plate

Burial Depth \ Standoff Distance	0"	0.5"	1"	1.5"
0.04"'	2.23	0.61	0.56	0.60
0.25"	1.57	0.96	0.85	0.87
0.5"	1.74	1.23	0.90	1.03

Table 4.7: Average Total Impulse Values (lb-s) with 20 Degree Angled Plate

Figure 4.8 and Table 4.8 show total impulse as a function of plate angle and depth of burial at a 0.0” standoff distance. Since the target is touching the ground the shock wave is able to load the target. The close target placement also means the soil will have more time to act on the target and will be less dispersed than at greater standoff distances. This standoff distance shows the highest impulses for all depths of burial and plate shapes. The relationship between impulse and plate shape changes with the depth of burial. This may be a result of increased vertical flow of the soil and detonation products as a result of the deeper depth of burial. At the 0.0” standoff distance the ejecta would not be able to change direction significantly before it hit the target. Higher plate angles may be less susceptible to shock effects due to the greater spacing between the target surface and the ground as compared to the shallow plate angles. Since the shock wave is mitigated in the presence of an air gap, the higher plate angles provide less area for the shock wave to act on as less of the target is close to the ground.

4.1.3 Results at Constant Standoff Distance

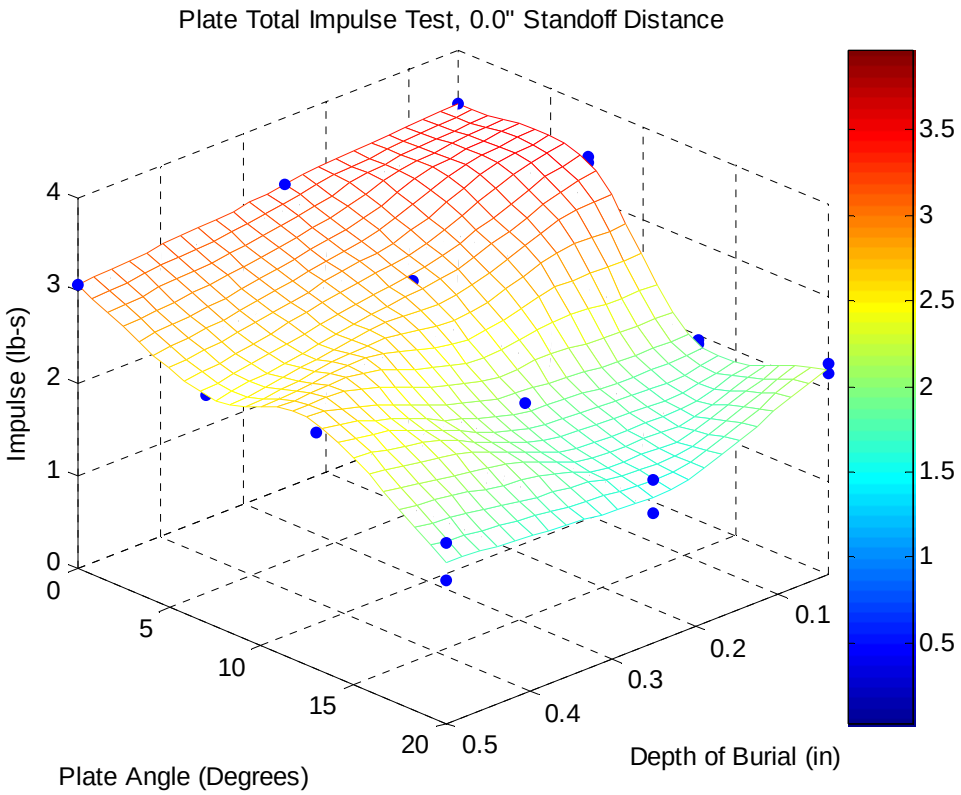

Figure 4.8: Total Impulse Tests at 0.0" Standoff Distance

Angle	Depth of Burial 0.04"	0.25"	0.5"
0°	3.42	3.28	3.06
7°	3.39	2.81	2.45
13°	1.93	1.99	2.66
20°	2.23	1.57	1.74

Table 4.8: Average Total Impulse Values (lb-s) at 0.0" Standoff Distance

Figure 4.9 and Table 4.9 display impulse as a function of plate angle and depth of burial at a 0.5” standoff distance. The presence of an air gap between the surface and the target suggests the shock wave no longer provides a significant amount of loading. Instead the target is loaded entirely by the impact and distributed load components. The 0° plate shows the greatest impulse for all depths of burial because none of the material is deflected to the side. The highest impulse is captured by the 0° plate at the 0.5” depth of burial, which suggests that the addition of soil over the charge produces an increased load on the plate. As the target angle increases, less impulse is captured for all depths of burial. There appears to be little difference in total impulse between the 13° and 20° target shapes for all depths of burial at the 0.5” standoff distance.

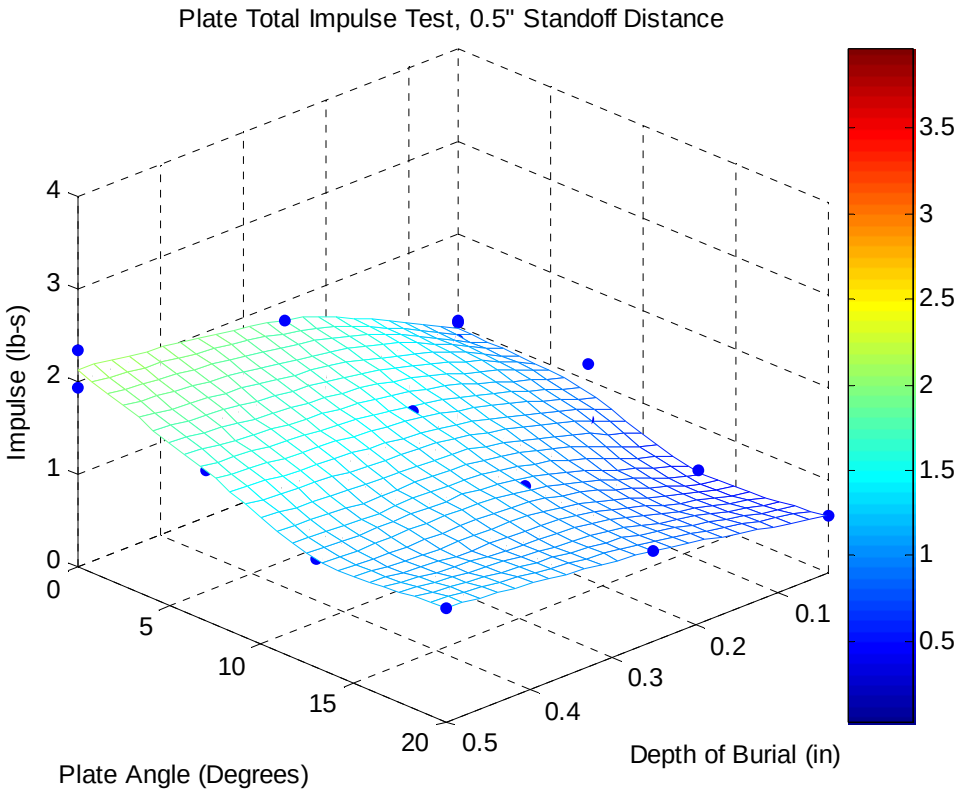

Figure 4.9: Total Impulse Tests at 0.5" Standoff Distance

Angle \ Depth of Burial	0.04"	0.25"	0.5"
0°	0.98	1.80	2.14
7°	0.88	1.40	1.62
13°	0.52	1.09	1.17
20°	0.61	0.96	1.23

Table 4.9: Average Total Impulse Values (lb-s) at 0.5" Standoff Distance

Figure 4.10 and Table 4.10 plot total impulse as a function of plate angle and depth of burial at a 1.0” standoff distance. The increased air gap between the charge and target underside allows the soil annulus and gas bubble to be more dispersed, which in turn reduces the total impulse captured by the target plate. The 0° plate captures the most impulse, but the difference in impulse between various depths of burial and plate angles is significantly less than differences seen at closer standoff distances. Total impulse increases for all angles between the 0.04” and 0.25” depth of burial. There is little change in impulse between the 0.25” and 0.5” depths of burial for all plate angles. The high standoff distance significantly reduces momentum transfer from the soil. It is the author’s opinion that the majority of the loading at the higher standoff distances seems to come from the initial impact of the soil plug, which appears to be largely unaffected by standoff distance within the range tested. If the soil plug were affected by standoff distance, the change in impulse between the 1.0” and 1.5” would be greater.

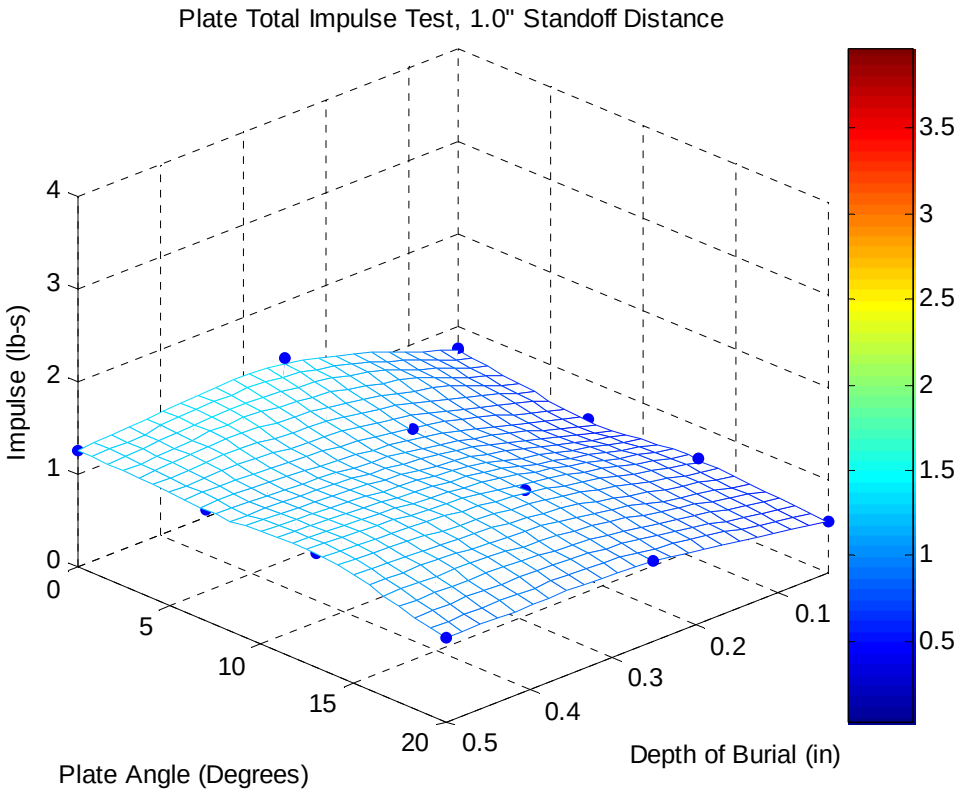

Figure 4.10: Total Impulse Tests at 1.0" Standoff Distance

Angle	Depth of Burial 0.04"	0.25"	0.5"
0°	0.75	1.33	1.27
7°	0.57	1.05	1.20
13°	0.65	1.05	1.23
20°	0.56	0.85	0.90

Table 4.10: Average Total Impulse Values (lb-s) at 1.0" Standoff Distance

Figure 4.11 and Table 4.11 show impulse as a function of plate angle and depth of burial at a 1.5” standoff distance. The 0° plate captures the most impulse, but the difference in total impulse between the 0° plate and the other shapes for a given depth of burial is minimal. As with the 1.0” standoff distance the impulse increases slightly between the 0.04” and 0.25” depths of burial, and then remains constant to the 0.5” depth for all target shapes. At lower standoff distances, where the distributed load appears to be most significant, variations in the dihedral angle of the target change the total impulse captured by the plate. At the higher standoff distances changes in geometry have a minimal effect on total captured impulse. The change in behavior of total impulse with respect to target geometry suggests that a different load mechanism is prevalent at the higher standoff distances, such as the impact load from the soil plug. This component appears to be largely unaffected by target geometry or standoff distance (within the range tested), and increases slightly as more soil is added above the charge.

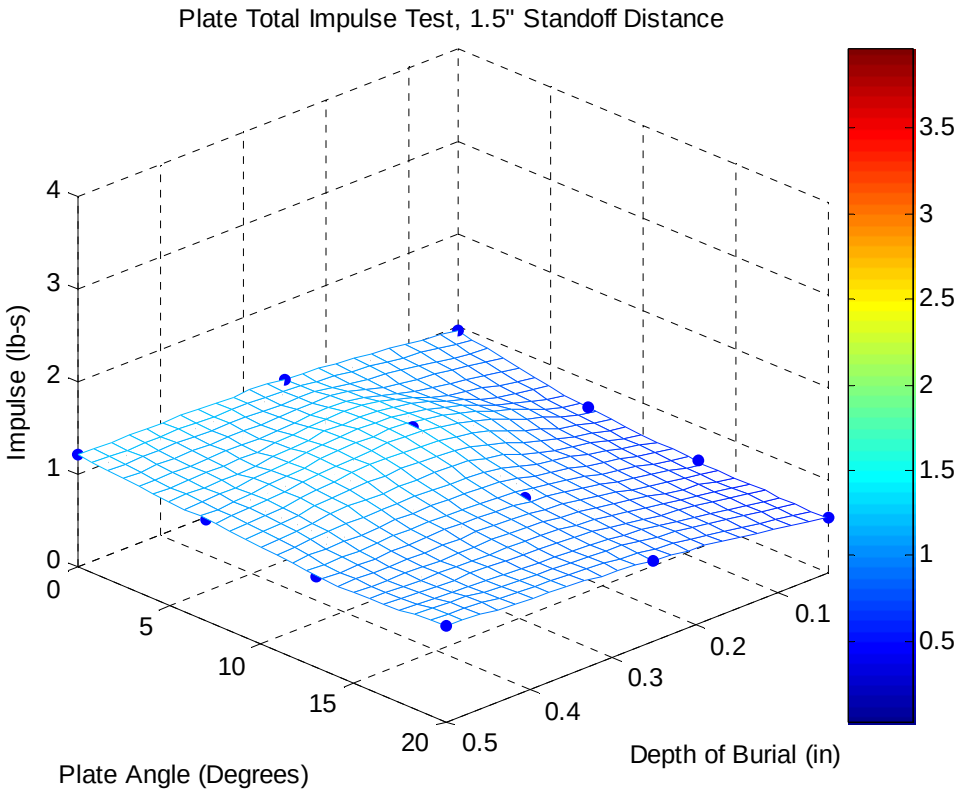

Figure 4.11: Total Impulse Tests at 1.5” Standoff Distance

Angle	Depth of Burial 0.04"	0.25"	0.5"
0°	0.96	1.16	1.21
7°	0.71	1.23	1.10
13°	0.63	0.96	0.99
20°	0.60	0.87	1.03

Table 4.11: Average Total Impulse Values (lb-s) at 1.5” Standoff Distance

4.1.4 Pyramid v. Dihedral Shaped Plates

Figure 4.12 and Table 4.12 show total impulse as a function of standoff distance for a 7° dihedral and pyramid shape at a constant 0.04" depth of burial. The X-axis is standoff distance, the Y-axis is total captured impulse, and each colored line gives the values for the two target geometries. The 7° dihedral plate (red line) captures more impulse than the 7° pyramid plate (blue line) at the 0.0" and 0.5" standoff distances, but at further standoff distances the total impulse is the same between the two. The 7° pyramid plate shows no difference between the 0.5" and 1.0" standoff distances. This suggests that at 0.5" standoff distance the 7° pyramid shape has deflected the maximum amount of impulse possible and the only component of the load remaining is one unaffected by geometry or standoff distance.

Appendix B contains additional information comparing dihedral and pyramid shapes to one another. In addition to the 7° dihedral and pyramid tests, 13° dihedral and pyramid plates are compared. The results indicate that there is no difference in total captured impulse between a 13° pyramid and dihedral plate, and furthermore that both plates captured the same total impulse as the 7° pyramid plate. The results reinforce the concept that target geometry can only deflect a portion of the total impulse, and once that portion is fully deflected further changes in geometry have no effect.

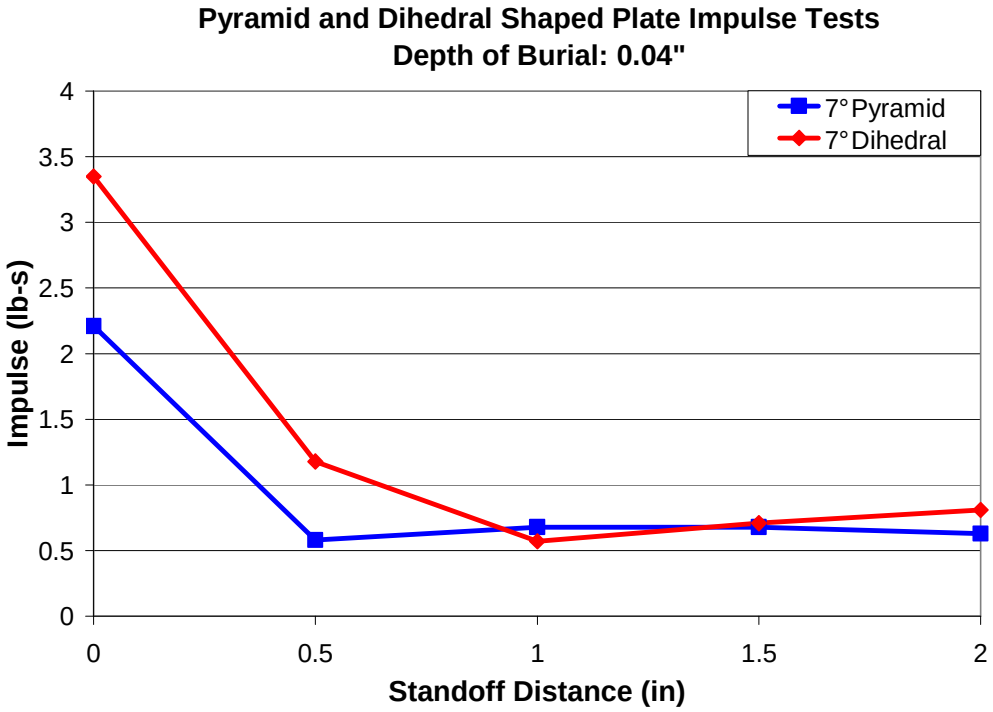

Figure 4.12: Pyramid and Dihedral Shaped Plate Impulse Tests

	Standoff Distance			
	0"	**0.5"**	**1"**	**1.5"**
7°Dihedral	3.39	0.88	0.57	0.71
7°Pyramid	2.21	0.58	0.68	0.68

Table 4.12: Pyramid and Dihedral Shaped Plate Impulse Values (lb-s)

4.2 Discussion of Target Shape Findings

4.2.1 Standoff Distance

Testing confirmed what previous studies have found regarding standoff distance. The standoff distance between the surface of the soil and the underside of the target plate has an inverse effect on the impulse captured by the target from an exploding charge. At the 0" standoff distance, when the target is physically touching the soil, energy from the explosion can be directly channeled into the plate in the form of a shock wave. In addition the close proximity of the plate to the charge maximizes the exposure of the target to soil and expanding gas. Loading from the shock wave may be mitigated in targets with a steeper dihedral angle; these shapes have less material touching or near the surface when compared to the shallow dihedral angles and flat plates. As a result the shock wave will come into contact with less material compared to a flat plate.

Figure 4.13 through 4.15 are surface graphs showing the percentage change in total impulse as the standoff distance increases. Tables 4.13 through 4.15 contain the values used to create the surface graphs. The percentage is relative to the lower value. For example, for a given combination of angle and burial depth in Figure 4.13, the percentage is the total change between 0.0" and 0.5" standoff distance, divided by the magnitude of impulse at the 0.0" standoff distance. The largest change in total impulse is seen as the target moves away from the surface to the 0.5" standoff distance. The presence of an air gap allows the soil annulus and detonation gases to expand before impacting on the target. This dispersion causes some of the ejecta to

escape without hitting the target, and as a result the impulse captured by the target plate is decreased.

The impulse was nearly constant between the 1.0” and 1.5” standoff distances. Beyond 1.0” standoff distance, the air gap disperses the soil annulus and provides room for the gas bubble to expand. It is this author’s opinion that this would minimize impulse transmitted from the soil, and as a result the impact of the soil plug (the impact load) would be the mechanism responsible for the majority of the load. The minimal change in total impulse between the 1.0” and 1.5” standoff distances for all angles suggests the soil plug is largely unaffected by standoff distance within the range tested.

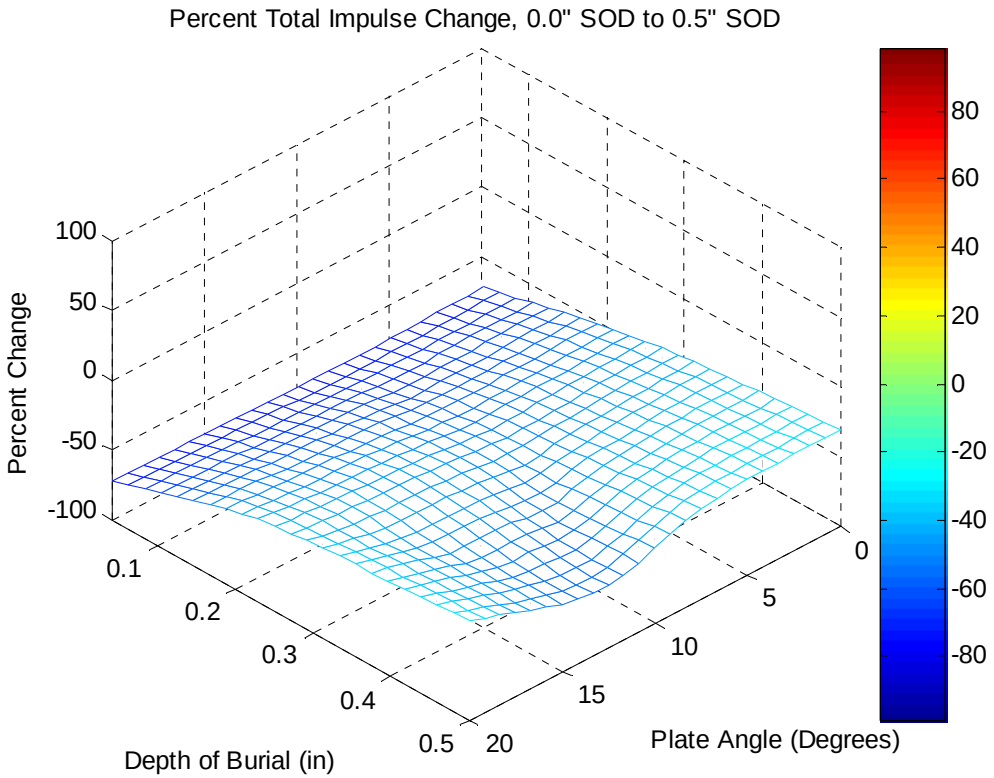

Figure 4.13: Percent Total Impulse Change from 0" to 0.5" Standoff Distance

		Depth of Burial		
		0.04	**0.25**	**0.5**
Angle	**0°**	-71.64	-45.12	-30.07
	7°	-74.04	-50.18	-33.88
	13°	-73.06	-45.23	-56.02
	20°	-72.65	-38.85	-29.31

Table 4.13: Percent Total Impulse Change Values, 0" to 0.5" SOD

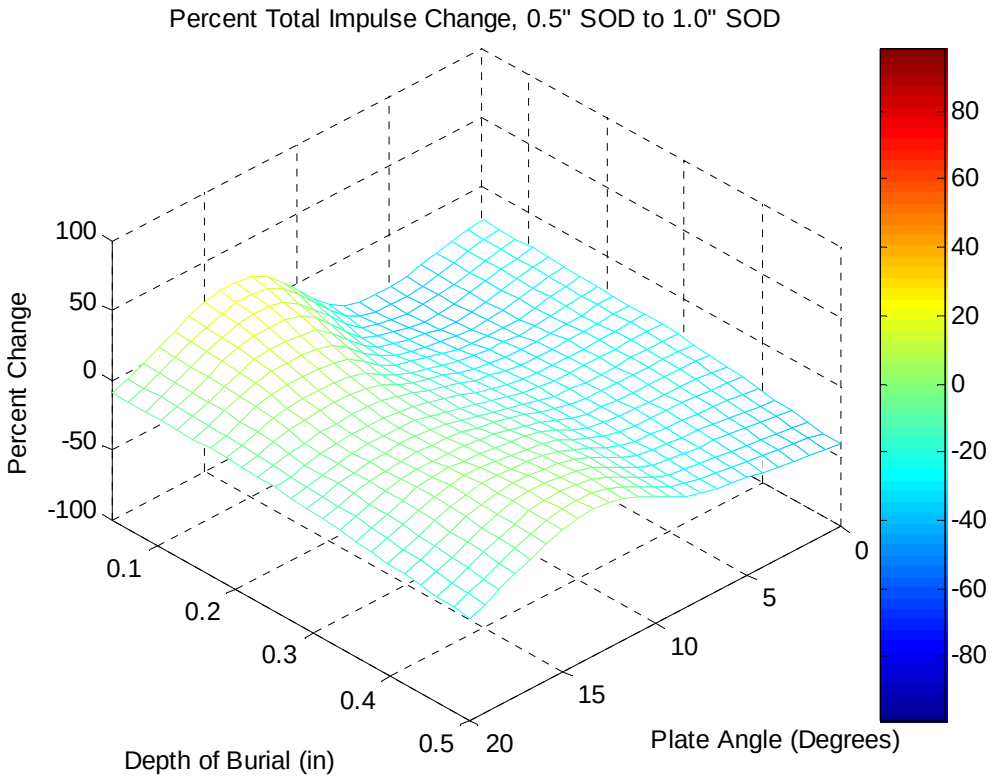

Figure 4.14: Percent Total Impulse Change from 0.5” to 1.0” Standoff Distance

Angle	Depth of Burial		
	0.04	**0.25**	**0.5**
0°	-22.68	-26.11	-40.65
7°	-35.23	-25.00	-25.93
13°	25.00	-3.67	5.13
20°	-8.20	-11.46	-26.83

Table 4.14: Percent Total Impulse Change Values, 0.5” to 1.0” SOD

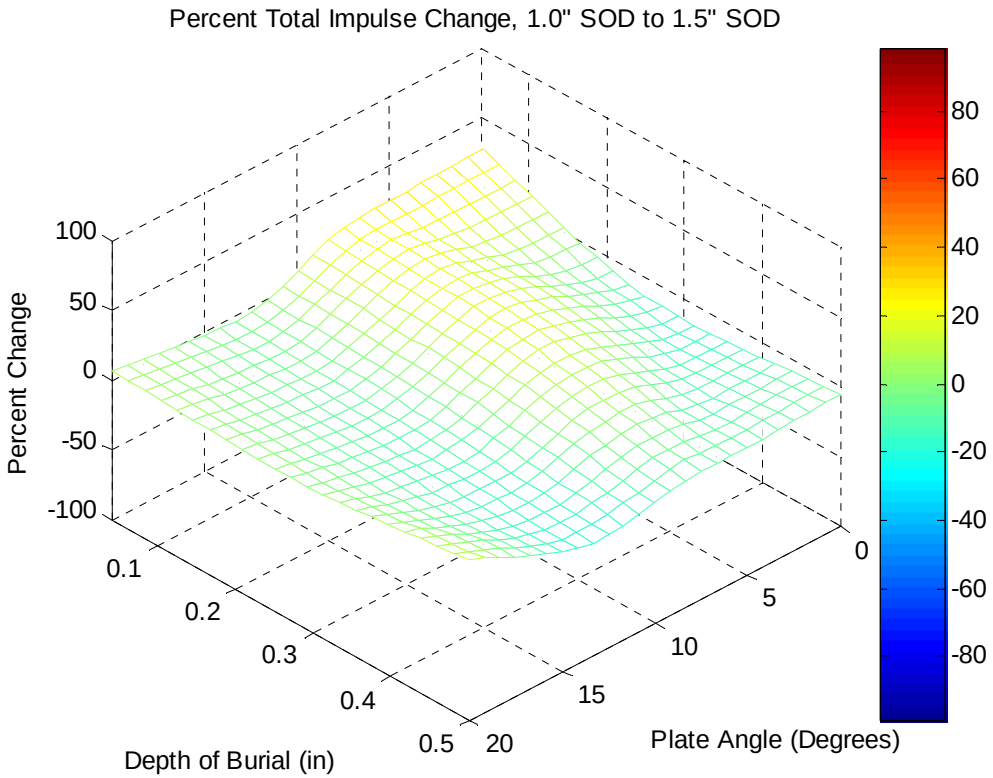

Figure 4.15: Percent Total Impulse Change from 1.0” to 1.5” Standoff Distance

Angle	Depth of Burial		
	0.04	**0.25**	**0.5**
0°	28.00	-12.78	-4.72
7°	24.56	17.14	-8.33
13°	-3.08	-8.57	-19.51
20°	7.14	2.35	14.44

Table 4.15: Percent Total Impulse Change Values, 1.0” to 1.5” SOD

4.2.2 Depth of Burial

The effect of burial depth on the impulse applied to a target by an exploding charge varies with the magnitude of that depth. Deeper burial depths provide more soil over and around the charge. At very shallow depths of burial there is little or no soil plug, and most of the impulse is transmitted through an expanding gas bubble and the impact of soil from the crater. This results in a significant decrease in impulse if the target is not very close to the charge.

Figures 4.16 and 4.18 show the percentage change in total impulse as the depth of burial increases. Tables 4.16 and 4.17 contain the values used to create the respective surface graphs. The percentages are with respect to the smaller depth of burial. The additional soil reduces the shock wave (decreasing the total impulse at the 0.0" standoff distance), but provides more mass to impact against the target. Beyond the 0.25" depth the additional soil provides a negligible increase in impulse. As a result we see the impulse increase between the 0.04" and 0.25" depths of burial for all standoff distances in which there is an air gap. This change can be seen most clearly in Figure 4.17, which is a 180° rotation of Figure 4.16. There is little change between the 0.25" and 0.5" depths as seen in Figure 4.18. The additional soil also increases the impulse at the 1.0" and 1.5" standoff distances, where the dispersed load is no longer a major loading mechanism and it is believed that most of the loading comes from the impact of the soil plug.

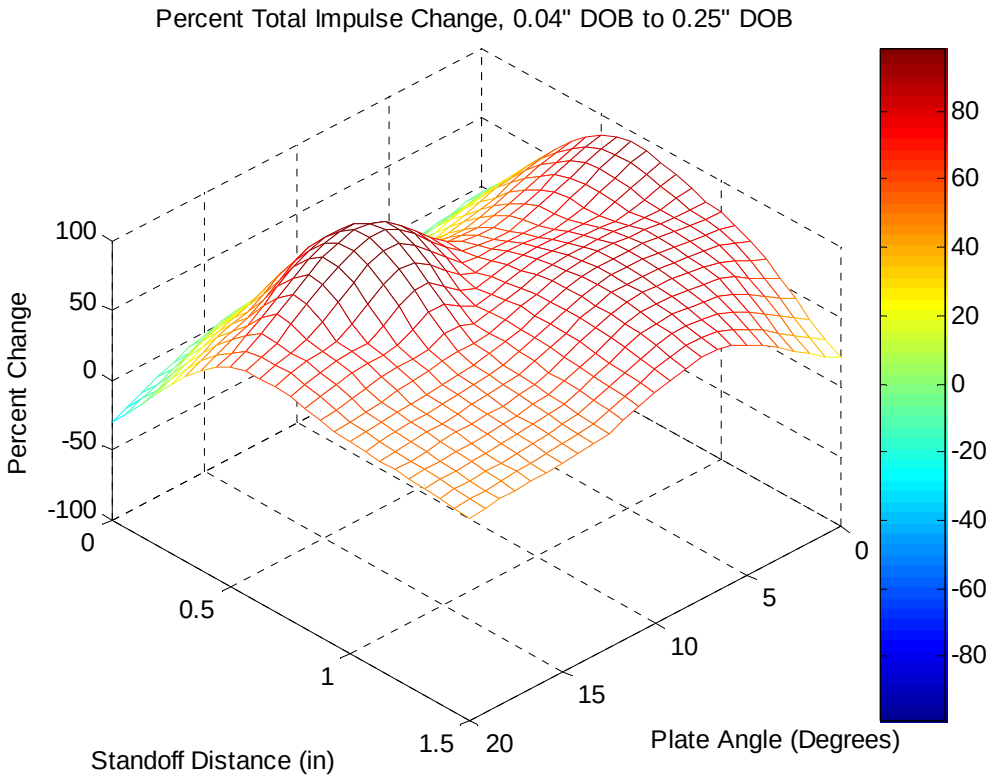

Figure 4.16: Percent Total Impulse Change from 0.04" to 0.25" Burial Depth

Angle \ Standoff Distance	0"	0.5"	1"	1.5"
0°	-4.09	85.57	77.33	20.83
7°	-17.11	59.09	84.21	73.24
13°	3.11	109.62	61.54	52.38
20°	-29.60	57.38	51.79	45.00

Table 4.16: Percent Total Impulse Change Values, 0.04" to 0.25" DOB

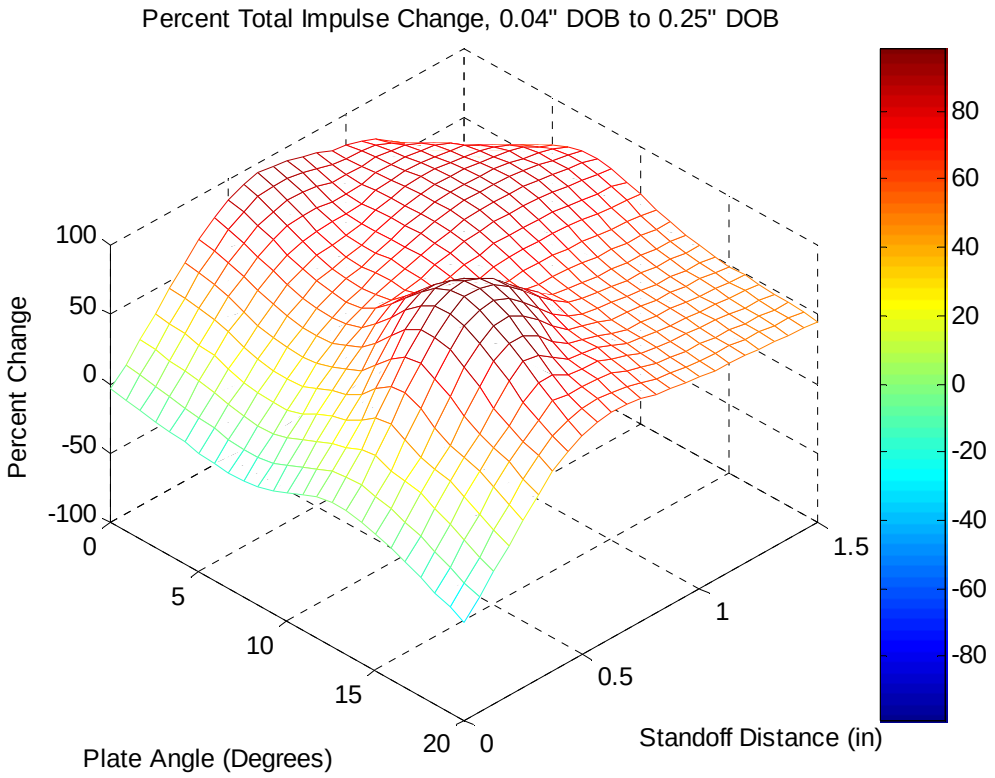

Figure 4.17: 180° Rotation of Figure 4.16

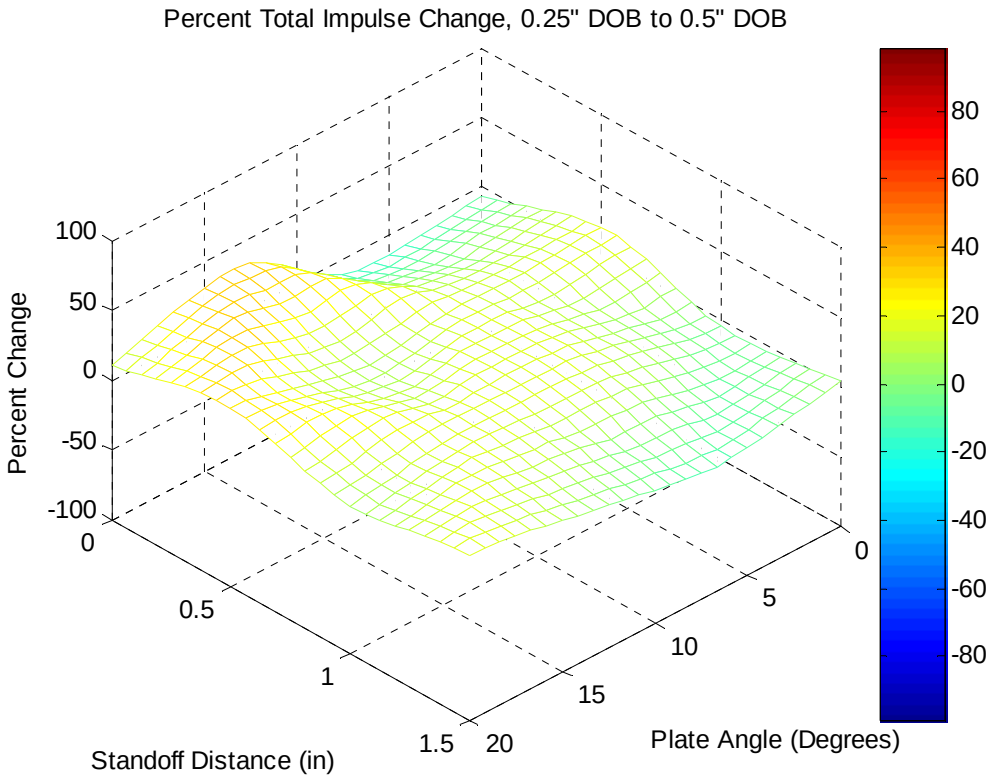

Figure 4.18: Percent Total Impulse Change from 0.25” to 0.5” Burial Depth

	Standoff Distance			
Angle	**0"**	**0.5"**	**1"**	**1.5"**
0°	-6.71	-18.89	-4.51	4.31
7°	-12.81	-15.71	14.29	-10.57
13°	33.67	-7.34	17.14	3.13
20°	10.83	-28.13	5.88	18.39

Table 4.17: Percent Total Impulse Change Values, 0.25” to 0.5” DOB

4.2.3 Dihedral Plate Angle

The shape of the target plays a significant role in determining the amount of impulse captured from an exploding buried charge, but the extent of the effect is dependent on the standoff distance and charge depth of burial. Overall, the effect plate angle has on total impulse is roughly inversely proportional to standoff distance, and approximately proportional to depth of burial. That is, as the standoff distance increases, the effect of a dihedral angle in reducing impulse compared to a flat plate at the same height goes down. In all cases the steepest plate angles captured less impulse than the shallow plate angles.

Figures 4.19 through 4.21 show the percentage change in impulse as the dihedral plate angle increases with respect to a flat plate. Tables 4.18 through 4.20 contain the values used to create the respective surface graphs. Depending on the standoff distance and depth of burial, some increases in plate angle produced significant decreases in impulse while others produced little or none. For all standoff distances in which an air gap existed, there was little difference between the 13° and 20° plate angles. At 0.0" standoff distances, the change in impulse with respect to target shape varied greatly depending on the depth of burial. At the shallow depth of burial, there was little change between the 0° and 7° targets, a large change between the 0° and 13° targets, and a similar change between the 0° and 20°. At the 0.25" depth of burial, the change was nearly linear with respect to target shape. Finally at 0.5" depth, there was a change between the 0° and 7°, a similar magnitude of change between 0° and 13°, and a larger decrease between the 0° and 20° targets.

As depth of burial increases, more soil is thrown into the air and against the target, but at a slower speed. The additional mass increases the effect of target shape on total impulse, particularly at closer standoff distances. Deeply buried charges also produce a more vertical flow of ejecta. Vertical flows require steeper angles to deflect the components away from the target, and shallow angled plates seem to act similarly to a 0° plate as the gas and soil annulus stagnate against the underside. The result is that, as the depth of burial increases, a steeper plate angle is required to deflect the ejecta and reduce the total vertical impulse applied to the plate.

Changes in target shape have little effect when the standoff distance is large. The presence of an air gap disperses the soil annulus; as the air gap increases, the soil annulus will impact over a larger area on the target. The increased dispersion allows some of the ejecta to escape from the target without impacting against it. The greatest change in impulse with respect to dihedral angle is around standoff distances close to the surface. When the target is close to the ground, changes in target shape can have a dramatic effect on impulse (on the order of a 45% reduction).

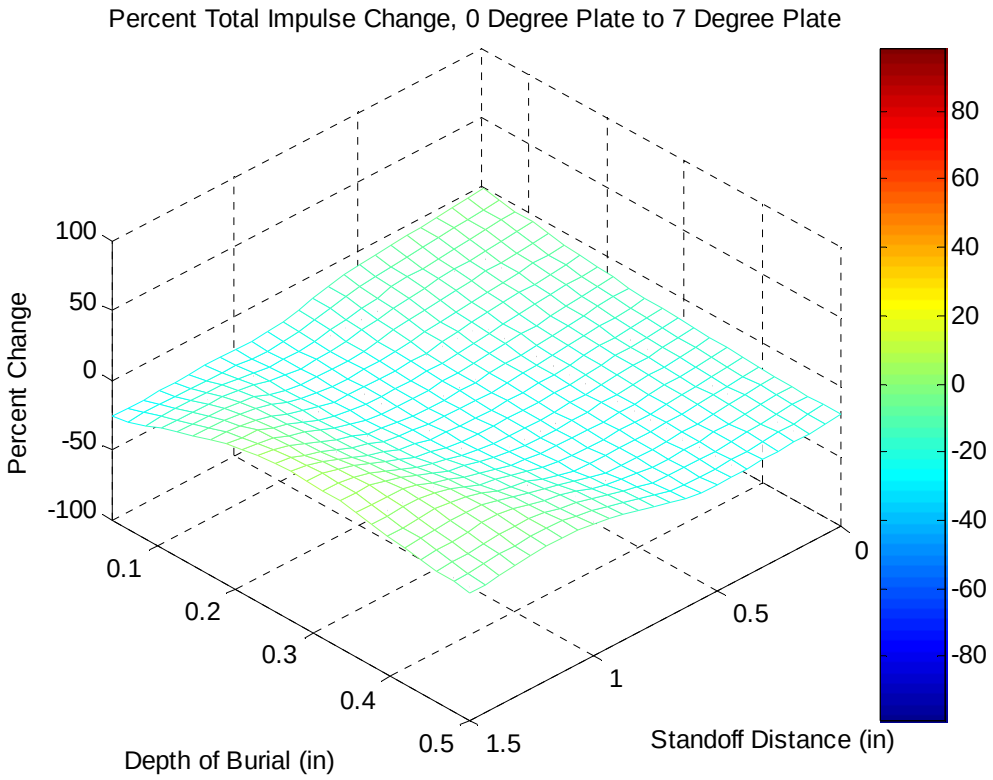

Figure 4.19: Percent Total Impulse Change from 0° to 7° Dihedral Plate

Standoff Distance \ Depth of Burial	0.04"	0.25"	0.5"
0"	-0.88	-14.33	-19.93
0.5"	-9.28	-22.22	-24.30
1"	-24.00	-21.05	-5.51
1.5"	-26.04	6.03	-9.09

Table 4.18: Percent Total Impulse Change Values, 0° to 7° Dihedral Plate

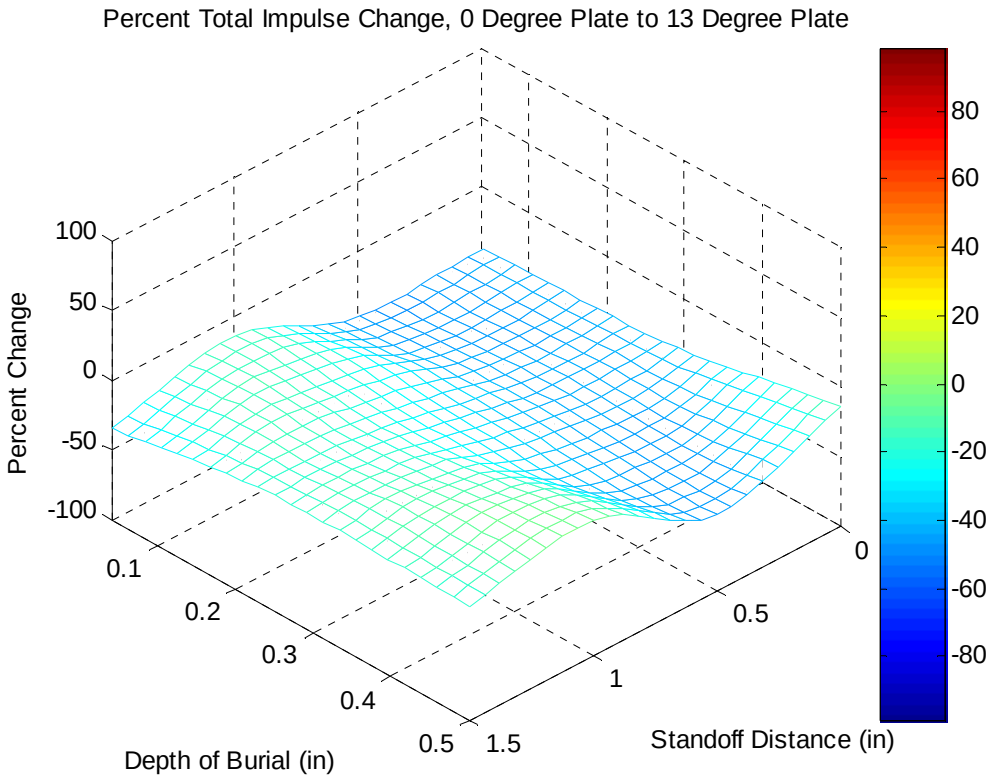

Figure 4.20: Percent Total Impulse Change from 0° to 13° Dihedral Plate

Standoff Distance \ Depth of Burial	0.04"	0.25"	0.5"
0"	-43.57	-39.33	-13.07
0.5"	-46.39	-39.44	-45.33
1"	-13.33	-21.05	-3.15
1.5"	-34.38	-17.24	-18.18

Table 4.19: Percent Total Impulse Change Values, 0° to 13° Dihedral Plate

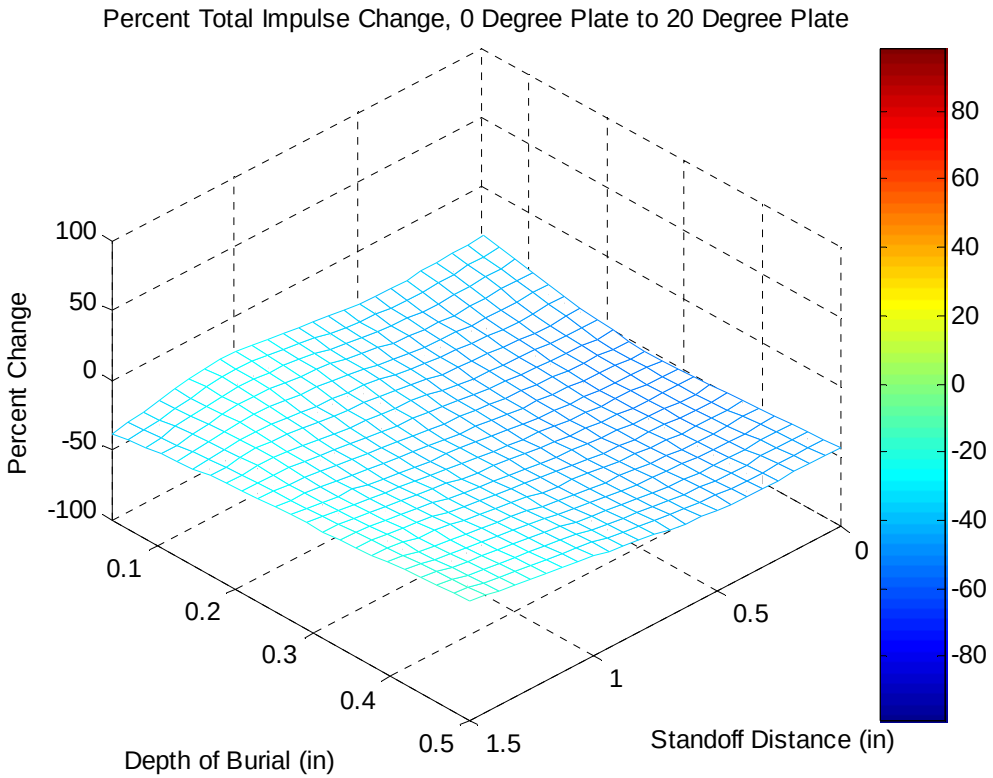

Figure 4.21: Percent Total Impulse Change from 0° to 20° Dihedral Plate

Standoff Distance \ Depth of Burial	0.04"	0.25"	0.5"
0"	-34.80	-52.13	-43.14
0.5"	-37.11	-46.67	-42.52
1"	-25.33	-36.09	-29.13
1.5"	-37.50	-25.00	-14.88

Table 4.20: Percent Total Impulse Change Values, 0° to 20° Dihedral Plate

4.3 Scaling and Expected Values

During the course of the research an attempt was made to correlate the 0° plate tests with an equation developed from small-scale tests previously conducted at the University of Maryland Dynamic Effects Lab and full scale tests conducted at the US Army Aberdeen Proving Grounds. These results were plotted to a surface graph by Mr. W. McDonald [15], and an equation was derived from the result. The equation is presented below, and Figure 4.22 shows the data points and the resulting surface graph from the equation. Red dots represent the 24 small scale tests (.609 g charges using Reynolds detonators), and blue dots are the seven full scale (Table 4.21) tests. In order to compare the values across difference scales, the values were reduced to units that are independent of scale. Standoff distance (called HOT, or height of target in the figure) and depth of burial are in units of $in/\sqrt[3]{lb}$, and impulse is in units of $lb-s/lb$.

$$I(d,h)/W = 3077 + 128\left(\frac{d}{W^{1/3}}\right) - 9.37\left(\frac{d}{W^{1/3}}\right)^2 - 624\left(\frac{h}{W^{1/3}}\right) + 65.1\left(\frac{h}{W^{1/3}}\right)^2 - 2.22\left(\frac{h}{W^{1/3}}\right)^3$$

The derived equation was then used by LC Taylor at the Dynamic Effects Lab to determine expected reduced total impulse with respect to reduced depth of burial when the reduced standoff distance was held constant [15]. The equation is limited by the data it was derived from, and as a result may not be accurate for combinations of variables that are outside the range tested. The depth of burial tested ranged from a reduced value of 1.86 to about 14 $in/\sqrt[3]{lb}$. Reduced target height ranged from 0 to 14 $in/\sqrt[3]{lb}$, however most of the tests were conducted at a reduced height of target of 3.7 to 6.89 $in/\sqrt[3]{lb}$.

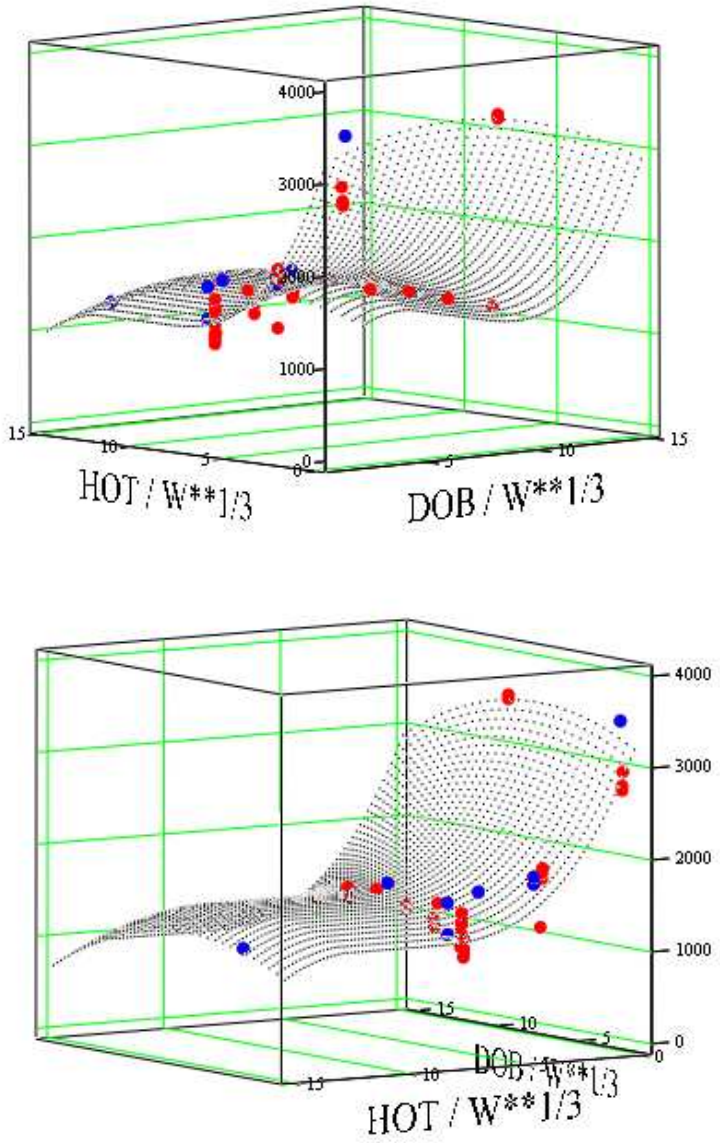

Figure 4.22: Surface Graph of Reduced Small and Full Scale Tests Values [15]

The equation was used to examine how well the results of the flat plate testing in this research compared to results from previous impulse testing. External correlation is important in order to validate the results and ensure that the data are useful for directly predicting full scale results. The data developed in this research are internally consistent, meaning repeated tests show little variation and valid conclusions can be drawn by comparing one data point to another within these test

results. External consistency would mean that data coincides with results from other tests, and that valid expectations can be drawn directly regarding full scale values.

Figures 4.23 through 4.25 compare the expected impulse values from the model equation (dashed line) with the actual results found during shaped target testing (solid line) for three constant reduced heights of target. Table 4.22 displays the small scale test values.

Charge lb	DoB in	Reduced DoB in/(lb^[1/3])	HoT in	Reduced HoT in/(lb^[1/3])	Reduced Impulse (lb-s)/lb	Expected Impulse (lb-s)/lb
0.001402	0.04	0.36	0.50	4.47	691	1435
0.001402	0.25	2.23	0.50	4.47	1283	1630
0.001402	0.5	4.47	0.50	4.47	1384	1775
0.001402	0.04	0.36	1.00	8.93	528	1160
0.001402	0.25	2.23	1.00	8.93	991	1354
0.001402	0.5	4.47	1.00	8.93	906	1500
0.001402	0.04	0.36	1.50	13.40	685	1108
0.001402	0.25	2.23	1.50	13.40	827	1302
0.001402	0.5	4.47	1.50	13.40	863	1448

Table 4.21: 0° Plate Small Scale Test Results

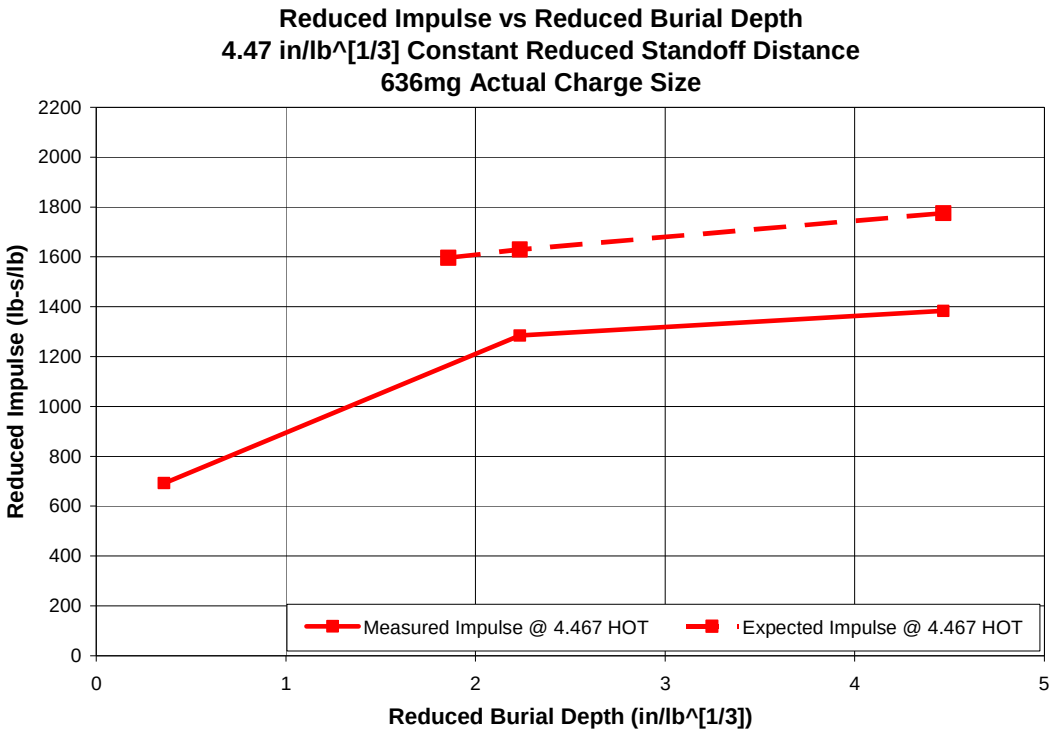

Figure 4.23: 4.467 $in/\sqrt[3]{lb}$ Reduced Impulse: Expected vs. Actual Values [15]

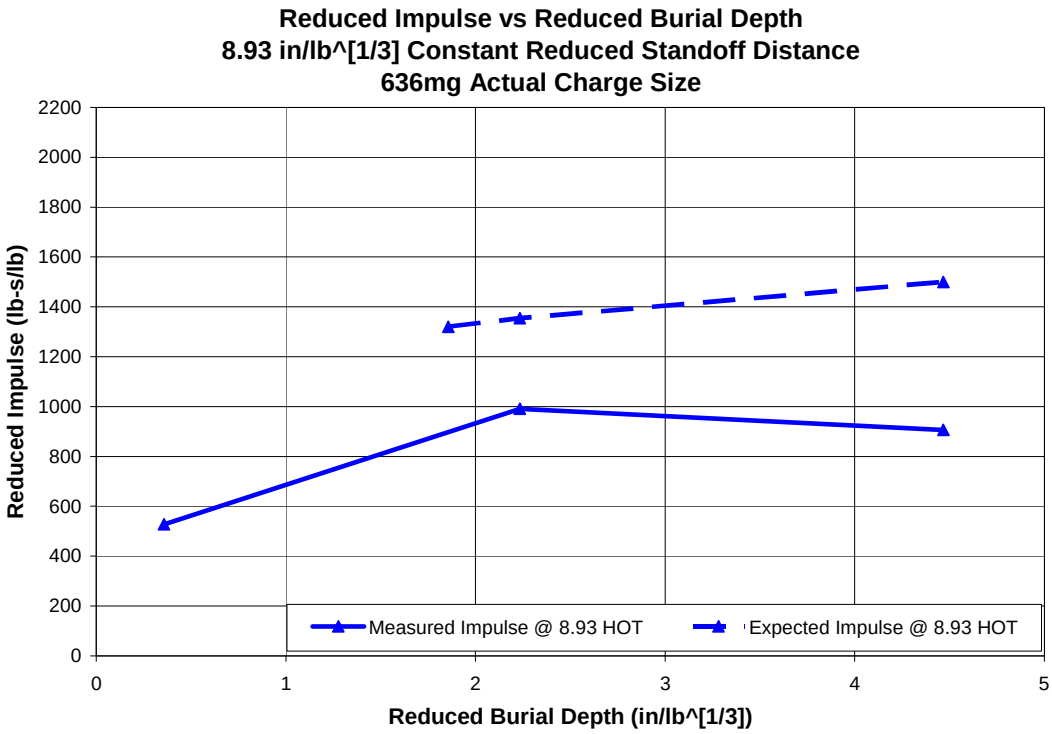

Figure 4.24: 8.93 SOD Reduced Impulse: Expected vs. Actual Values [15]

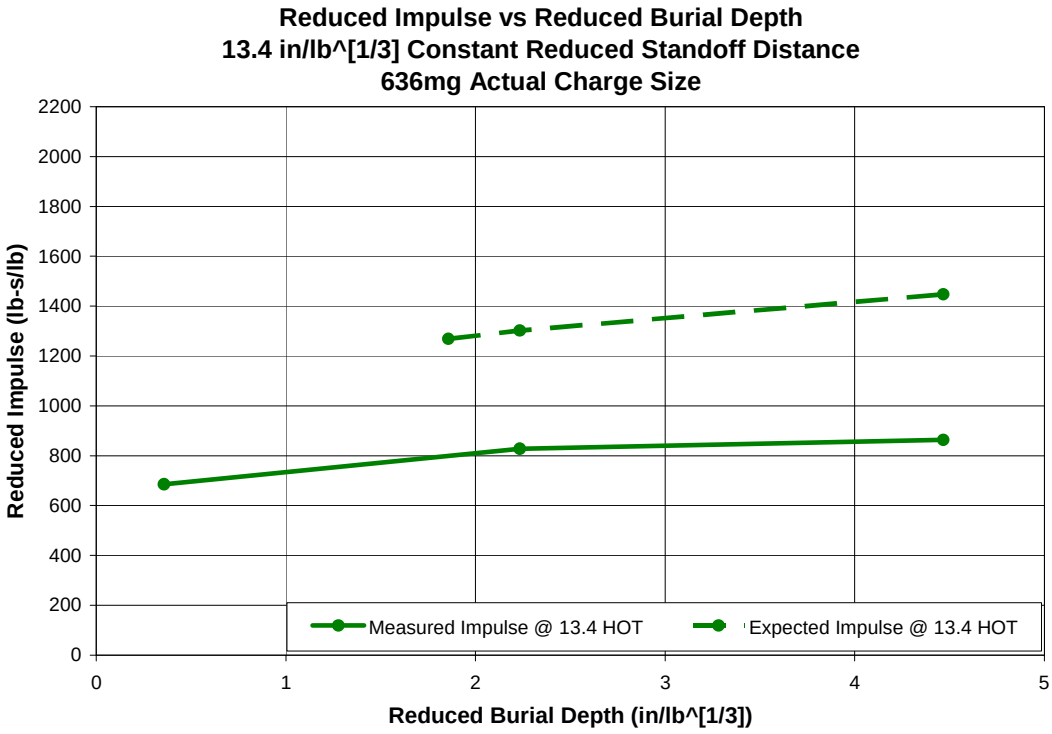

Figure 4.25: 13.4 SOD Reduced Impulse: Expected vs. Actual Values [15]

The reduced values of the flat plate tests reported in this thesis are consistently lower than the expected values calculated by the McDonald equation. Because the data used to create the McDonald equation did not contain any tests at a depth of burial less than 1.86 $in/\sqrt[3]{lb}$, the expected values at the shallower depths of burial are not predicted. The differences at the 2.23 and 4.47 $in/\sqrt[3]{lb}$ reduced depths of burial are within a region that was extensively tested and incorporated into the model, and are therefore more believable. Ignoring the values for the 0.36 $in/\sqrt[3]{lb}$ reduced depth of burial, on average the measured impulse values in this study are 31% lower than the expected values.

An inconsistency between the expected values derived from previous testing and the results obtained from the shaped target testing would indicate the presence of a problem with testing that needs to be resolved. Assuming the equation is correct, the most likely source of error is miscalculation of charge size. Hopkinson scaling only applies to ideal explosives, so a correlation factor may be required if the charge output is not what is expected.

The equation and test data have similar trends with regards to impulse as a function of height of target, as seen in Figure 4.26.

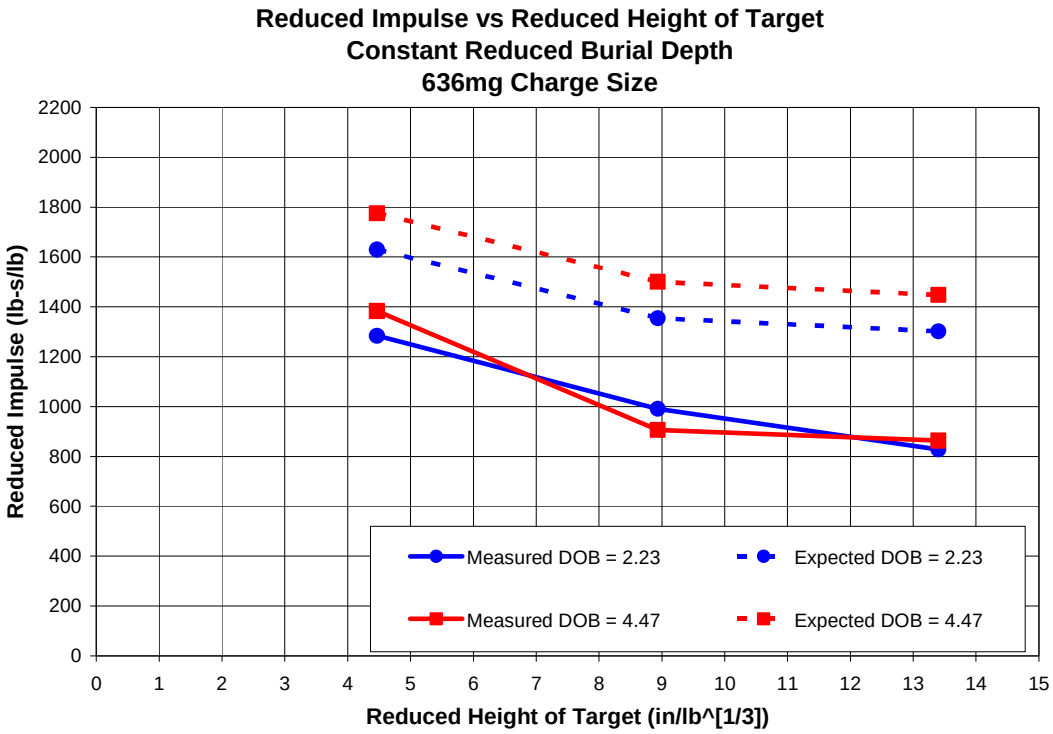

Figure 4.26: Measured vs Expected Total Impulse for Constant Reduced DoB

For the reduced depths of burial within the range of the model, the expected and measured values show similar trends with respect to the different heights of target.

Comparisons show that the total impulse measured using the flat plate for the given height of target and depths of burial are consistently lower than what the McDonald equation predicts for a 636mg size charge. Although the output of the charge is less than expected, it is consistent among repeated tests. This suggests that the results from this research using the 636mg charge may be compared to external data if a correlation (or "correction") factor is used for the charge size. Since the charge output is consistent but lower than expected, we can correlate the results by using an effective charge size that is smaller than the 636mg of output explosive used.

This is similar to the use of a correlation factor suggested by Fu [7] when scaling nonidealized explosives.

The expected values from the McDonald equation coincide more closely with the reduced values from the 0° plate tests if a charge size of 460mg is used instead of 636mg, as seen in Figures 4.27 through 4.29 and Table 4.22.

Charge lb	DoB in	Reduced DoB in/(lb^[1/3])	HoT in	Reduced HoT in/(lb^[1/3])	Reduced Impulse (lb-s)/lb	Expected Impulse (lb-s)/lb
0.001014	0.04	0.40	0.50	4.98	956	1360
0.001014	0.25	2.49	0.50	4.98	1775	1571
0.001014	0.5	4.98	0.50	4.98	1913	1715
0.001014	0.04	0.40	1.00	9.95	730	1176
0.001014	0.25	2.49	1.00	9.95	1371	1387
0.001014	0.5	4.98	1.00	9.95	1252	1531
0.001014	0.04	0.40	1.50	14.93	947	933
0.001014	0.25	2.49	1.50	14.93	1144	1144
0.001014	0.5	4.98	1.50	14.93	1193	1289

Table 4.22: 0° Plate Small Scale Test Results for 460mg Effective Charge Size

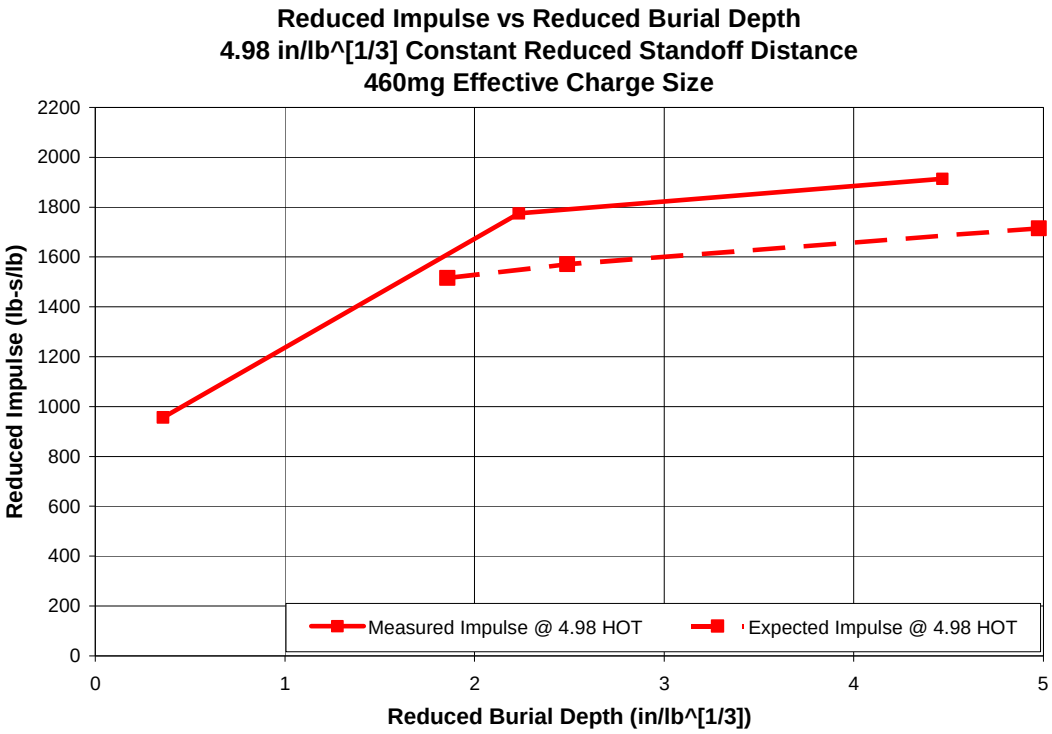

Figure 4.27: 4.98 $in/\sqrt[3]{lb}$ Reduced Impulse Values for 460mg Charge Size

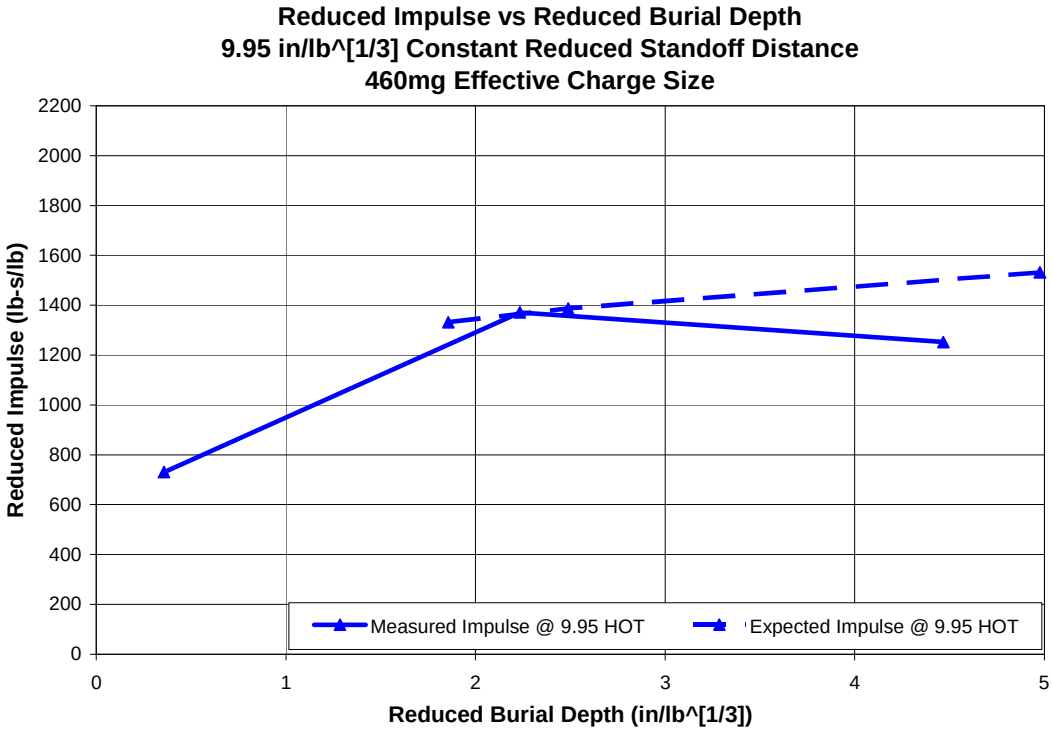

Figure 4.28: 9.95 SOD Reduced Impulse Values for 460mg Charge Size

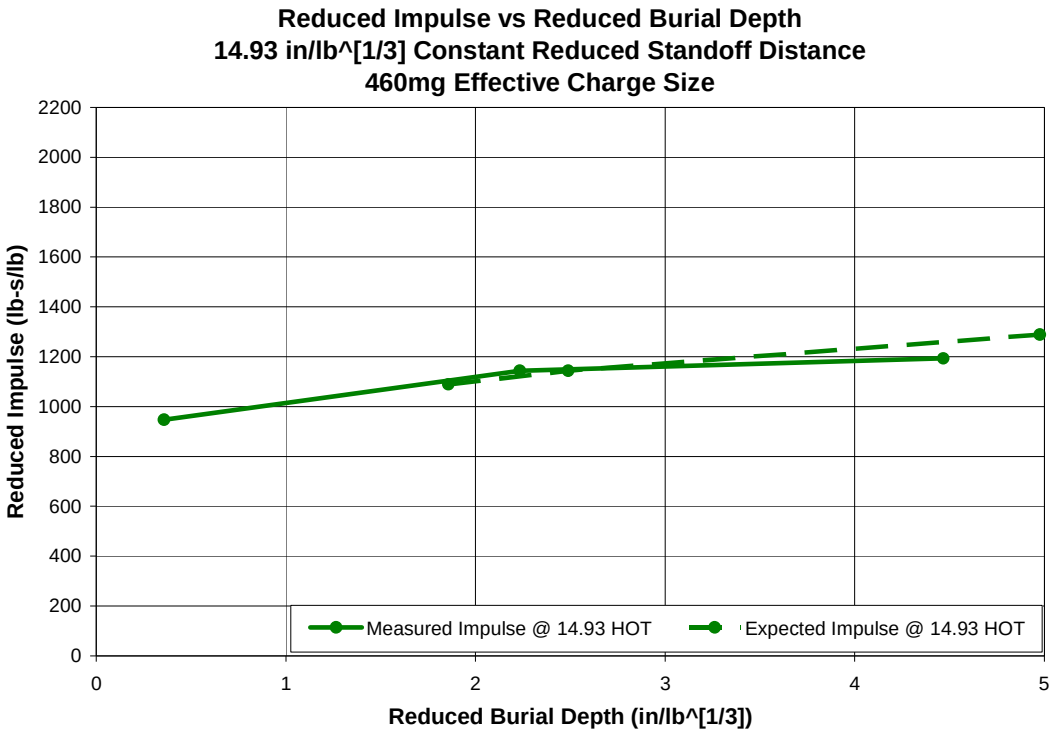

Figure 4.29: 14.93 SOD Reduced Impulse Values for 460mg Charge Size

Scaling the results with a 460mg effective charge size places the expected and actual reduced impulse values much closer than if they were scaled with the actual charge size of 636mg. Ignoring the values at the 0.36 $in/\sqrt[3]{lb}$ reduced depth of burial (since this value is outside the range of validity for the McDonald equation), the average difference between the measured and expected values is 9%, with the greatest difference at 18%. In particular, the measured 14.93 $in/\sqrt[3]{lb}$ height of target values (green lines in Figure 4.29) are right on top of their expected values. Using the 460mg effective charge size as a correlation factor allows the results of the small scale shape tests to be reduced and compared to tests conducted at other scales. In order to determine if the difference between measured and expected values was due to charge size, a series of tests involving three separate charge sizes was conducted.

0° plate impulse tests were conducted with 0.636g, 1.0g, and 2.5g charges. There was no agreement between expected and measured values until the charge size was 2.5g. Values at the 2.5g charge size were within 10% of those predicted by the McDonald equation. In order to validate this correlation, larger scale testing should be conducted and the results compared to both the small scale tests and the McDonald equation.

4.4 Blast Damage Effects: Erosion and Impact

Testing of the flat and dihedral plates produced wear on the target faces from repeated detonations. Analysis of the worn target plates provided additional information about the loading mechanisms experienced by the plate from the detonation of a buried charge. Repeating tests with a new and worn plate indicated that change in total captured impulse due to wear on the plate was within 10% scatter. Figure 4.30 compares a new 13° dihedral plate to one damaged after multiple tests.

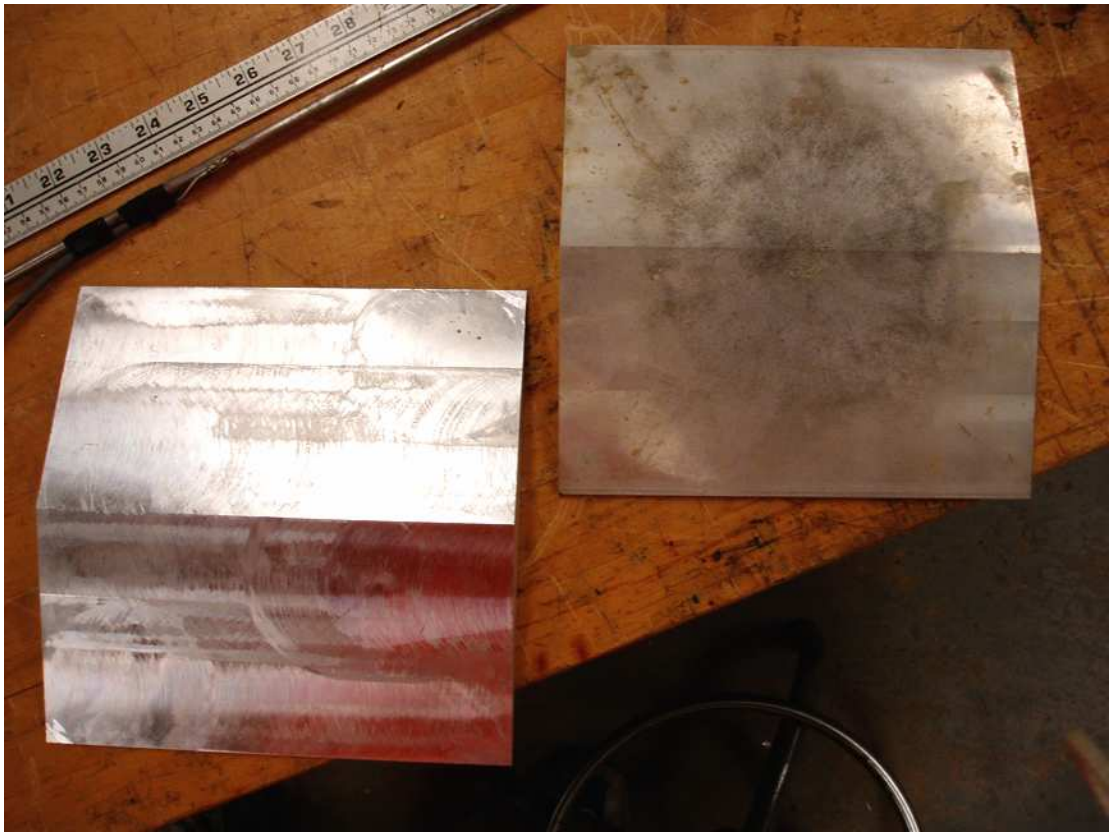

Figure 4.30: New and Worn 13° Dihedral Target Plates

Close examination of the damage to the worn plate shows two regions. The target face is radially eroded and pitted in a large circle, a result of sand tangentially striking the plate during the course of repeated blasts. This area of effect will be referred to as the erosion region. In the center of the plate is a distinct crater with a wear pattern different from that of the erosion region. This area will be called the impact region. Figures 4.31 and 4.32 show the target plate and the approximate distribution of the impact and erosion damage regions.

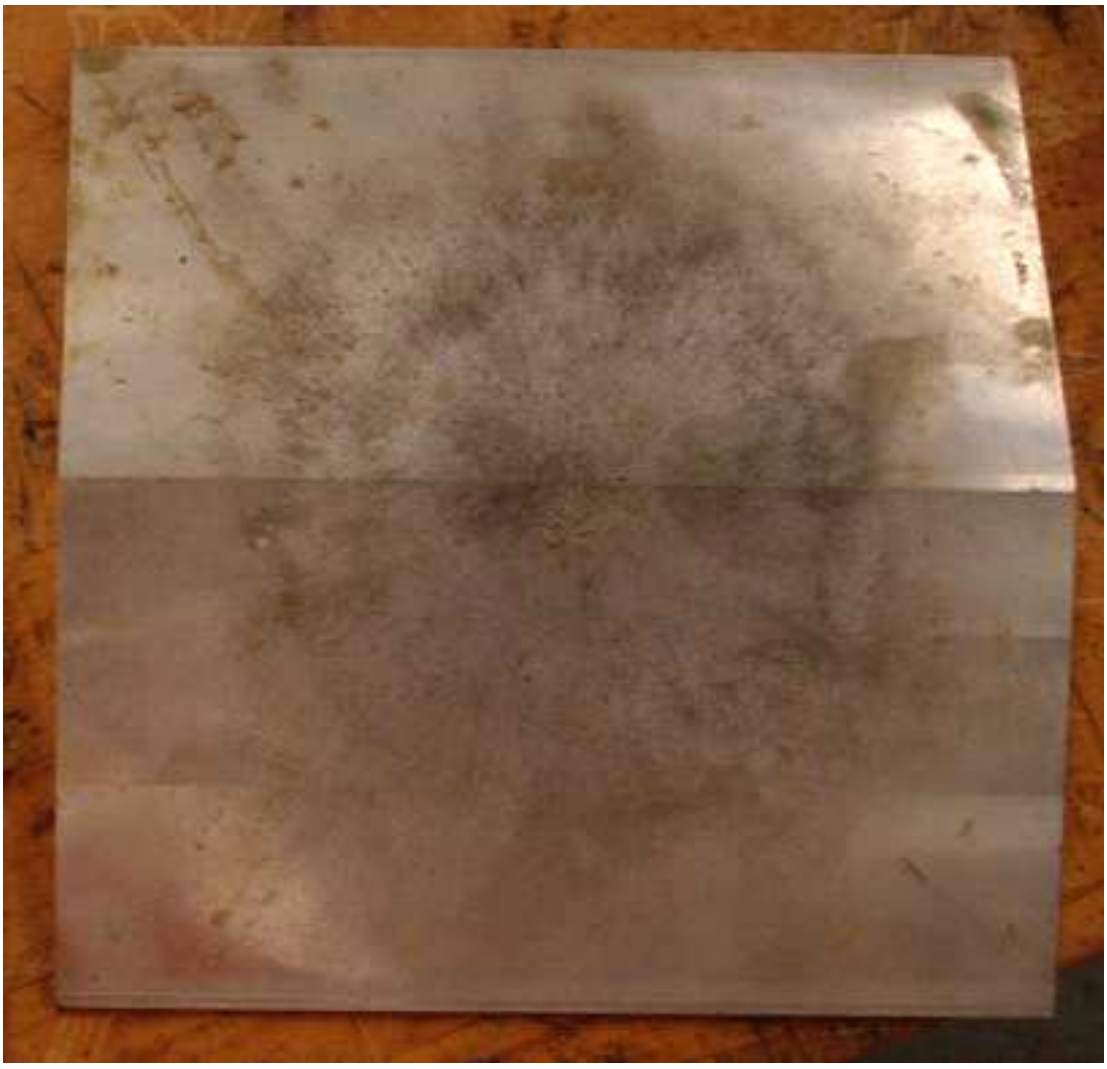

Figure 4.31: Worn 13° Plate

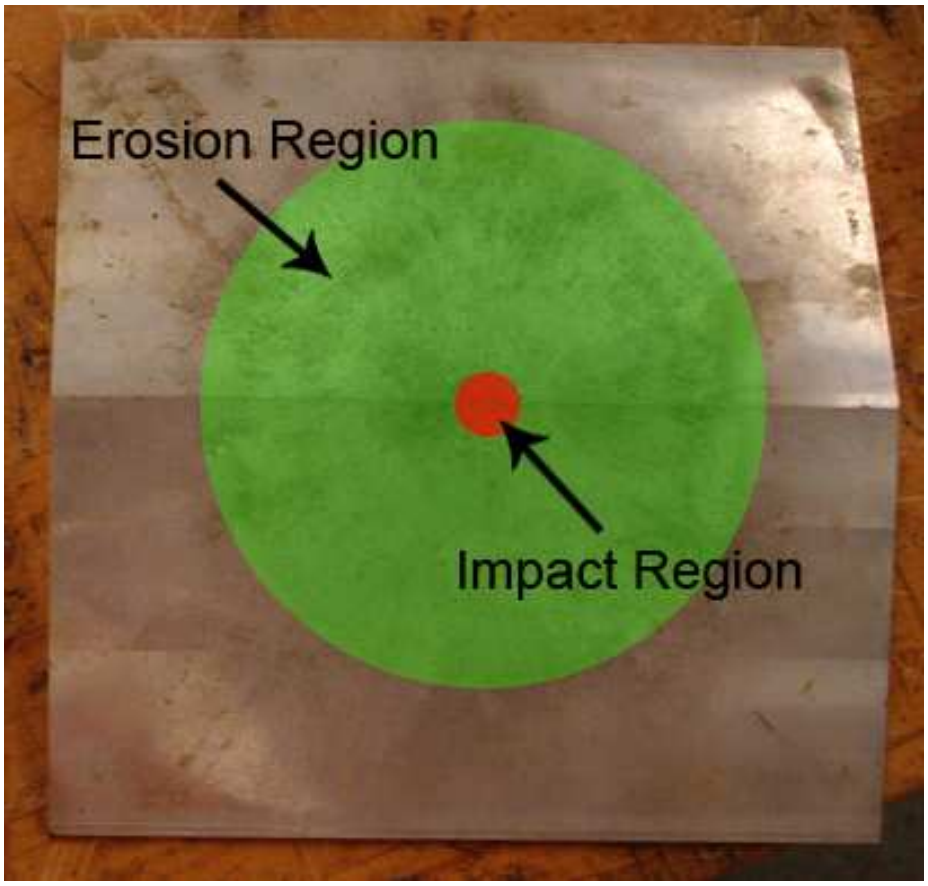

Figure 4.32: Erosion and Impact Damage Regions

Figure 4.33 is a picture of the underside of the 13° plate after a test. The plate flipped over after being loaded by the charge detonation, which preserved the sand pattern. The center of the target plate features a glob of sand over the impact region. A radial pattern of scorch marks and sand spray splays out from the center, and is surrounded on the outside by arcs of sand. Because only one pattern was recorded, further research is required before any assertions can be made regarding this phenomena.

Figure 4.33: Spray Pattern on the Underside of the 13° Plate

4.4.1 Impact Region

The impact of ejecta against the center of the target left it deeply pitted (Figure 4.34). The walls of the impact region are concave, and there is a distinct lip at the edge of the crater. The appearance of the center of the plate suggests that the sand that hit the center traveled perpendicular to the surface of the ground. Using the circles pictured in Figure 4.32 as a reference, the impact region was struck by sand traveling perpendicular to the surface. This is in contrast to the surrounding region, where the pitting travels outward in a radial direction. The sand seen in the center of the plate in Figure 4.33 completely covers the impact region.

Figure 4.34: Impact Crater Close-Up

The cratered shape of the impact region supports the presence of an intense, concentrated loading acting against the center of the plate. The most likely candidate for this load comes from the impact of the soil plug as it is propelled by the rapidly expanding detonation gases beneath it. The collision of the soil plug against the target plate deformed the center, and eventually a crater was formed after repeated strikes from testing. The size of the crater is slightly larger than the diameter of the 636 mg charge used in the impulse testing (Figure 4.35). The similarity in size between the charge and the impact region supports the idea that the cratering is from the impact of the soil plug against the target.

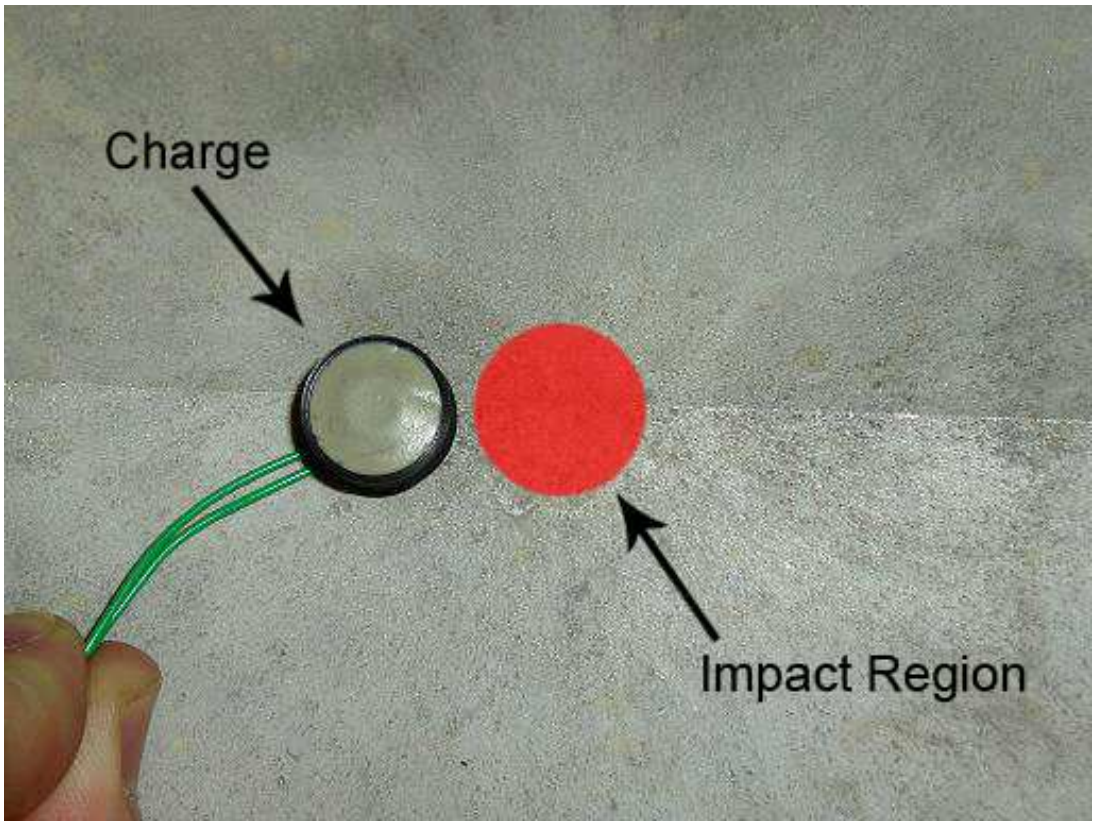

Figure 4.35: Impact Region as Compared to 636 mg Charge

4.4.2 Erosion Region

Surrounding the crater is an area pitted and worn in a radial pattern emanating outward from the center. This damage region is evenly distributed over a wide area on the plate, and hints at the presence of sand tangentially impacting against the surface of the target. The sand is most concentrated in two perpendicular lines, forming an "X" across the center of the target. The "X" pattern of soil and scorch marks in Figure 4.33 is spread out radially from the center of the target, and partial arcs of sand surround the outside.

The sand pattern in Figure 4.33, as well as the wear pattern in Figure 4.32, supports the presence of a distributed load mechanism acting over a wide area of the plate. The spray of ejecta from the charge located underneath the center of the target impacted over the surface the target in an outward direction, which caused the radial pitting seen in Figure 4.33. Portions of the spray struck and then stuck to the target, and formed the arcs seen in Figure 4.33. The "X" shape of the spray pattern suggests that the distributed load is influenced by the target shape. The regions of the dihedral shape closest to the surface are clean of spray, as are the center of the dihedral faces.

Chapter 5: Summary & Conclusions

5.1 Summary

Research was conducted to examine the effect of changes in target geometry on loading applied by a blast from a buried charge centered under the target plate. The testing involved very small scale charges (636mg of explosive) and utilized high speed digital imagery to capture the motion of specially fabricated target plates. The primary test set involved charges buried in saturated sand at three depths (0.04", 0.25", and 0.5" to the top of the charge). The targets were aluminum billets machined into non-deforming shapes with 0°, 7°, 13°, and 20° dihedral angles. The plane area parallel to the soil surface and target mass were held constant. The target plates were suspended at four different heights from the surface: 0", 0.5", 1", and 1.5". The height (called the standoff distance) was measured from the surface to the lowest point on the target. Analysis of high speed video was used to determine the total impulse transmitted from the detonated charge to the target plate.

The blast from a buried charge can act on the target plate with three distinct mechanisms. The first is a shock wave transmitted from the explosive directly into the target. This loading mechanism only affects the target when it is touching the surface, or at extremely low standoff distances. The other two loading mechanisms are caused by the expanding detonation gases in the form of a gas bubble. The second loading mechanism is the perpendicular impact of the soil above the charge (the soil plug) against the target. The expanding gas acts on the soil directly over the charge to propel the soil plug upward like a piston. The third loading mechanism is a

distributed load from an annulus of soil and ejecta thrown from the charge area by the expanding gas bubble. The distributed load is responsible for most of the total impulse, and in most cases is also the most affected by target geometry and standoff distance. Analysis of the damage caused to the plate by repeated tests supports the division of the load into an impact and distributed mechanism.

5.2 Conclusions

The dihedral angle of the target plays a significant role in reducing the total impulse applied to a target by the explosion of a buried charge. For a given standoff distance and depth of burial, there is a cutoff angle beyond which there is no reduction in total impulse over the range of variables investigated. This cutoff angle increases with depth of burial, and decreases with standoff distance. Comparisons between dihedral and pyramid target shapes confirmed the idea that only a portion of the total impulse (the distributed load mechanism) is affected by target geometry. Once the distributed load has been mitigated (and only the impact load remains), further changes in target geometry will not affect total impulse.

Changes in the depth of burial affect the amount of ejecta that was flung towards the plate and the size of the soil plug. Increases in depth of burial increase total impulse up to a point, beyond which changes had a negligible effect within the range of depths tested. The addition of more ejecta from increasing the depth of burial increases the influence of plate shape on total impulse.

Standoff distance has a roughly inverse relationship with total impulse; at higher standoff distances, the impulse is lower. For a given plate shape and depth of burial, there appears to be a cutoff height at which increases in standoff distance caused negligible changes in total impulse (within the range tested). Standoff distance determined the proportion of loading mechanisms. At extremely close distances, the shock wave imparts significant impulse to the target. Increasing standoff creates an air gap that mitigates the effect of the shock wave. At large

distances the distributed load mechanism is significantly reduced. The speculated impact load is largely unaffected by standoff distance within the range tested.

Comparisons between the test data and a model derived from previous experiments revealed a disparity. The measured total impulse per gram of explosive in this research seems to be lower than the expected values. The model itself has provided predicted results that are consistent with previous small-scale testing, and as a result the problem appears to be with the charge size. The lower values (relative to the expected values) suggest the possibility that the charge output may not be as much as the total explosive mass suggests it should be. Correlations between this data and the model were more successful when an effective charge weight approximately 70% that of the actual charge weight was used.

5.3 Future Work

There are several areas that need additional research. Additional standoff distances, plate angles, and depths of burial should be tested in order to refine the matrix and obtain a better understanding of the transition regions and cutoff angles. Particular attention should be paid to standoff distances and depths of burial near to the surface, since these areas show the greatest sensitivity to changes in the parameters. New plate shapes incorporating additional dihedral angles, as well as other geometries such as rounded shapes, should be tested. A new testing regimen involving charges placed in areas other than directly underneath the plate is needed to replicate the fact that most explosions do not occur directly underneath the center of the vehicle. Additional focus should be placed on the spray pattern on the underside of the plates after a test, as they provide insight into the distribution of load mechanisms on the target. Finally, larger scale tests should be conducted to ensure proper consistency between very small and full scale events. The research discussed in this thesis only scratches the surface of the dynamic effects surrounding a buried charge explosion. Further experiments based on results found here and elsewhere will eventually provide insight, but there remains an extensive amount of work to be done

Appendix A: Deformable Plate Shapes

In the earliest stages of this research, an attempt was made to fabricate a target plate by bending a flat plate of aluminum into a dihedral shape. A 0.125” wide by 0.375” deep channel was milled out of the center of an 8” x 8” x 0.5” aluminum plate to provide a bending axis (Figure A.1). When bent, the plate formed a dihedral angle of approximately 13 degrees. Testing used a charge consisting of 3 RP-80 detonators laid side-by-side; the total charge size was 609mg (Figure A.2). A total of three tests were conducted before the plate was too damaged by erosion to use. By the third test a crack had formed in the center of the plate into the milled channel.

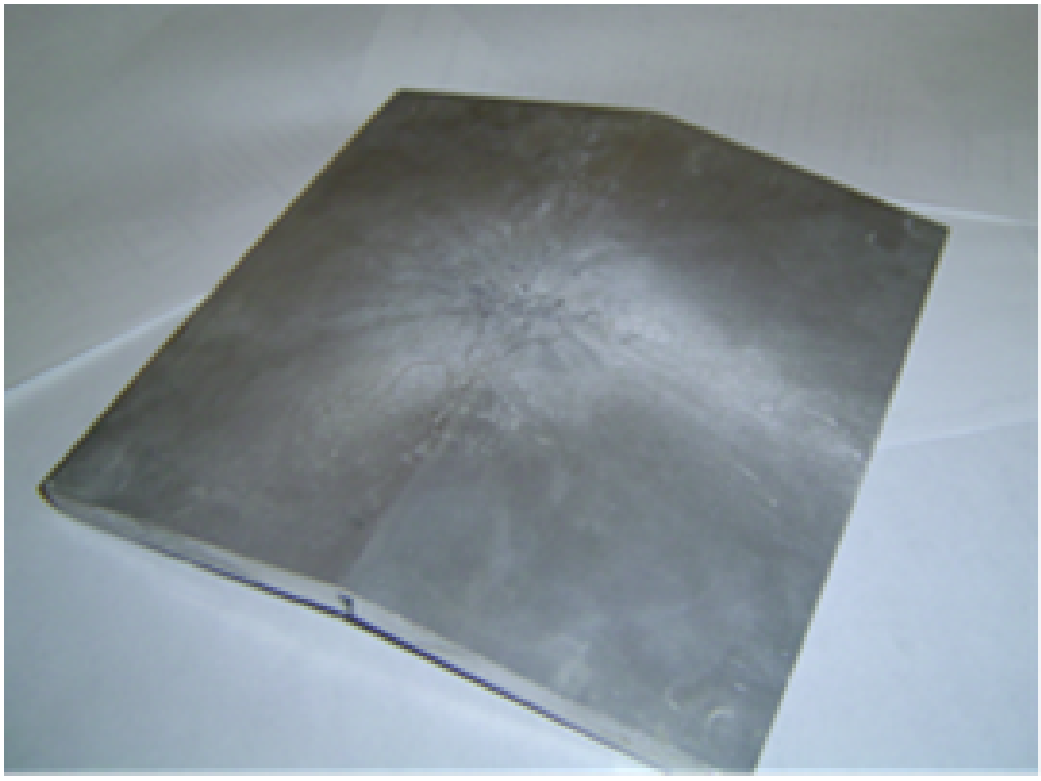

Figure A.1: 13° Deformable “Bent” Plate

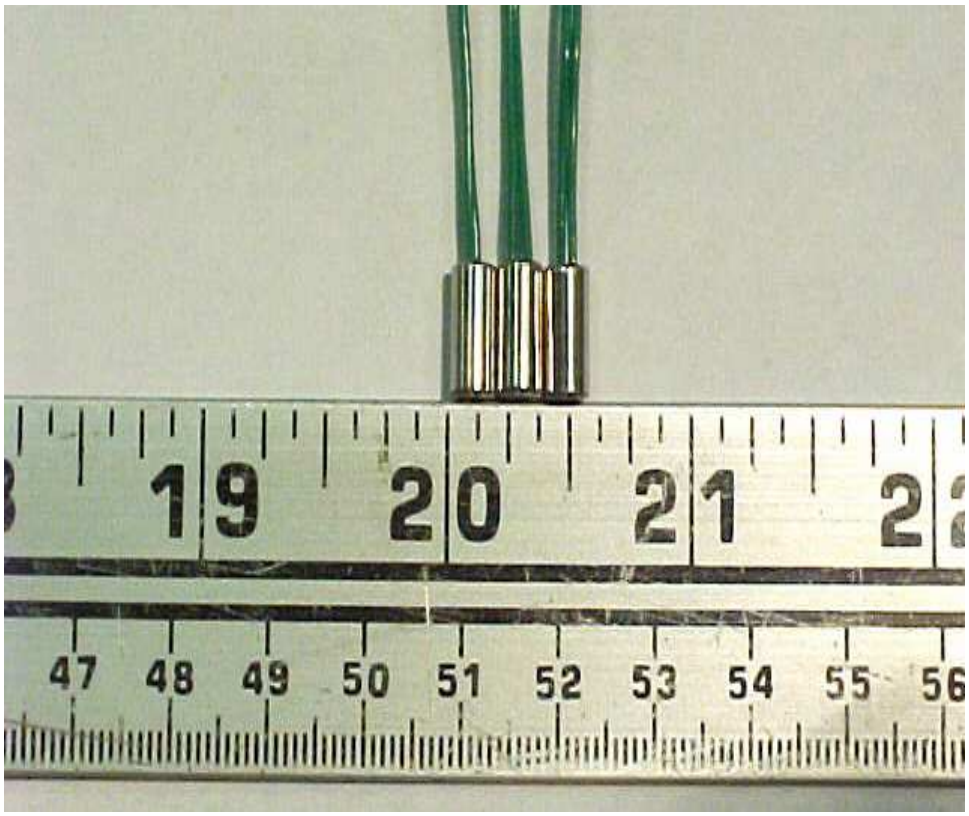

Figure A.2: 609mg Charge Consisting of 3 RP-80 Detonators

Testing of the bent plate revealed that during the initial stages of loading the plate would deform before it displaced. Figure A.3 is a series of images showing the first 5ms of the bent plate being loaded by a buried charge in saturated soil. The test was conducted at a 0.04" depth of burial and a standoff distance of 0.11". In the first frame we see the target resting before the charge is detonated. 1ms later we see the charge detonate and an initial spray of ejecta. 1 ms later the center locally deforms and flattens out to an angle of 4°. The plate does not experience any global movement. 3 ms after the explosion, in the third frame, the plate begins to move with rigid body motion. The plate regains a portion of its original shape between the third and fourth frame. After the test the plate was found to have a dihedral angle of 10°, indicating that a portion of the deformation was plastic.

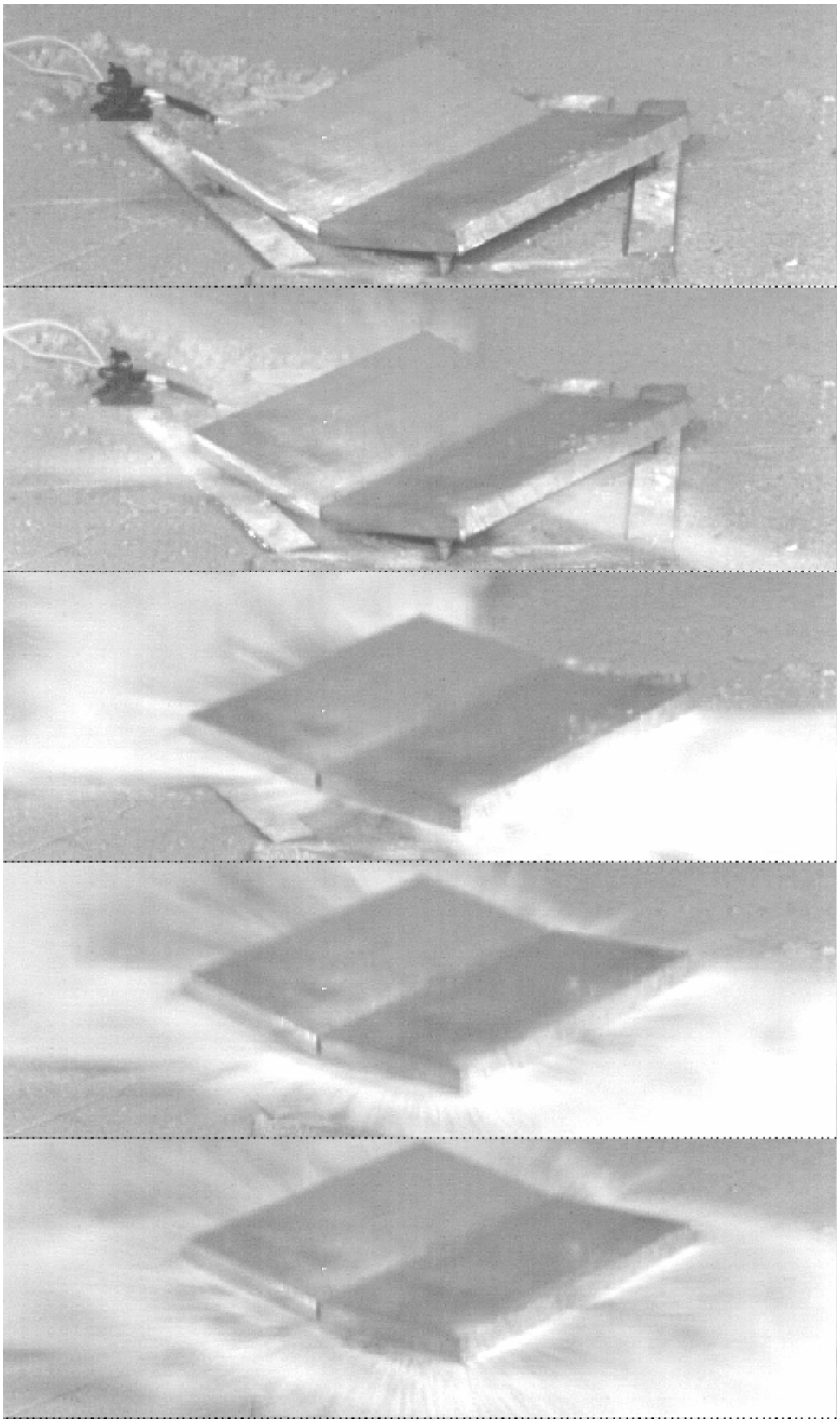

Figure A.3: Time Elapse (1 ms/frame) of Bent Plate Starting at 0ms

Since the bent plate deforms during loading, it was less useful for examining the role shape plays in reducing total impulse from a buried charge. Testing was instead conducted with solid plates machined out of solid aluminum billets, which maintained their shape during loading. While they did not solve the problem they were designed for, the bent plate tests provided an opportunity to examine how deformation affects the total impulse captured by a shaped plate.

Figure A.4 compares the reduced impulse values of the bent plate tests to the 13° dihedral tests for the same 0.04" depth of burial. The X-axis is reduced standoff distance, the Y-axis is reduced total captured impulse, and the three colored lines are three different targets. The black line is the 0° plate, the red line the deformable 13° plate, and the blue line the rigid 13° plate. The circles, triangles, and squares represent the data points rigid 13°, and deformable 13°, and 0° plates respectively. The reduced values are used because of the different charge sizes; 609mg is used to scale the bent plate values, and the effective value of 460mg from Section 4.3 is used to scale the 0° and rigid 13° plate values. Table A.1 contains the impulse values for Figure A.4.

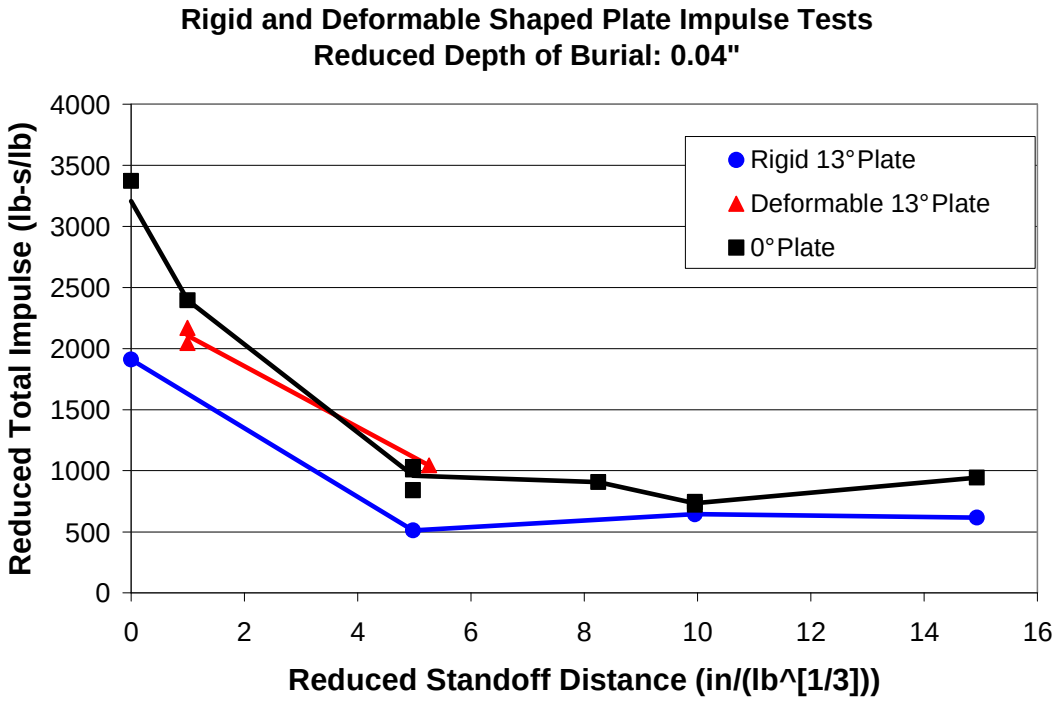

Figure A.4: Rigid and Deformable 13 Degree Plates at 0.04" Burial Depth

Plate	Charge g	Reduced SD in/(in^[1/3])	Reduced Imp lb-s / lb
Deformable 13° Plate	0.609	1.00	2044.56
	0.609	1.00	2170.14
	0.609	5.26	1044.88
Flat Plate	0.460	0.00	3371.88
	0.460	4.98	840.20
	0.460	4.98	1010.90
	0.460	4.98	1030.85
	0.460	9.95	722.70
	0.460	9.95	744.87
	0.460	14.93	944.39
	0.460	19.91	625.16
	0.609	1.00	2394.53
	0.609	8.25	907.58
Rigid 13° Plate	0.460	0.00	1910.95
	0.460	4.98	512.10
	0.460	9.95	645.11
	0.460	14.93	616.29
	0.460	19.91	563.09

Table A.1: Rigid and Deformable Plate Impulse Test Values

In Figure A.4 we see the bent plate consistently shows higher levels of total impulse within the range of standoff distances tested compared to the rigid shape. The values of the bent plate coincide very closely with those of the 0° plate, even though the bent plate still had a 10° dihedral angle after being loaded by the buried charge. Although more tests are required to confirm these results, the initial data suggests that the deformation of the bent plate can have a significant effect on total captured impulse. The impulse captured by the bent plate is the same as a flat plate. The deformable target is formed by the blast into a flatter shape that captures more impulse than a rigid target.

Appendix B: Additional Target Shapes

A small series of tests was conducted in order to compare the total impulse captured by a dihedral shape to a single pyramid shape of the same angle (Figure B.1, Top). Two angles were tested: 7° and 13°. A second series of tests were conducted comparing shapes with a grid of 45° pyramids (Figure B.1, Bottom). Two pyramid heights were tested: 0.5" and 0.25". Pyramid grid height refers to the distance from the base of the pyramid to the top point. Two different charges were used dependeing on the test. The first was the 609mg RP-80 charge described in Appendix A, and the second was the 636mg charge described in Section 2.1. In order to compare the results the standoff and impulse values were reduced to a scale-independent form. The effective charge size of 460mg from Section 4.3 was used for the 636mg charges.

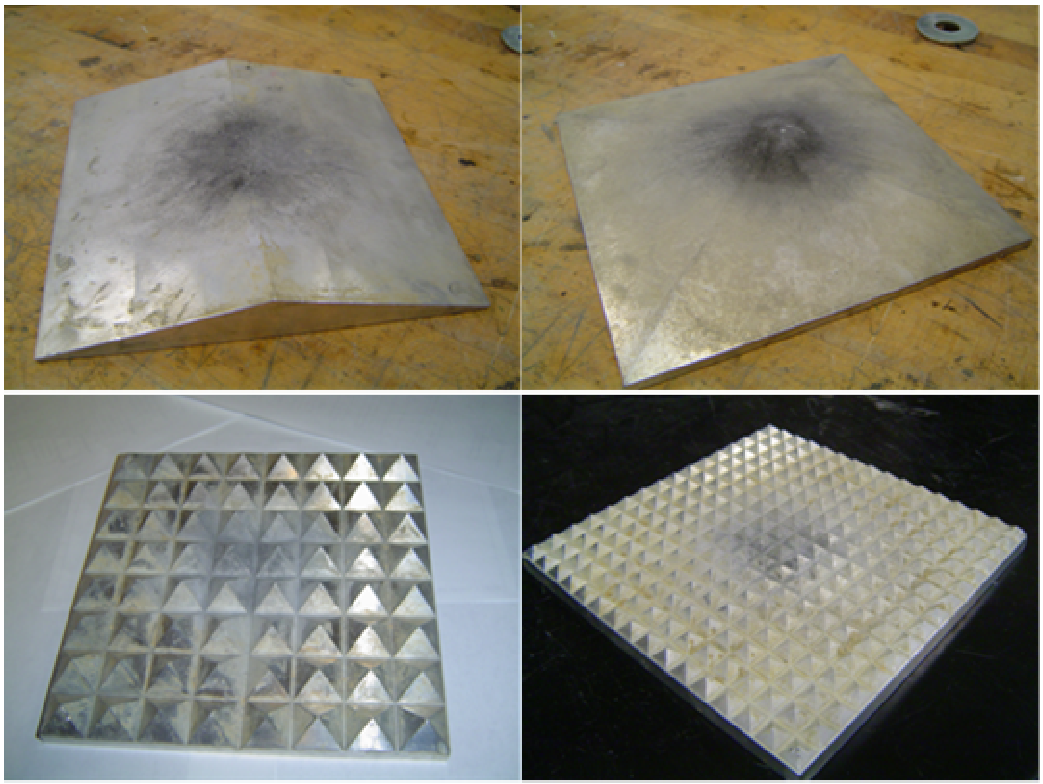

Figure B.1: 13° Dihedral & Pyramid (Top) and Pyramid Grids (Bottom)

B.1 Pyramid and Dihedral Shapes

Table B.1 and Figures B.2 and B.3 present the scale-independent values recorded from a series of tests comparing 7° and 13° dihedral and pyramid shapes. All values are presented in a scale-independent reduced format.

Plate	Charge g	Reduced SOD in / (in^[1/3])	Reduced Impulse lb-s / lb
0° Flat Plate	0.460	0.00	3371.88
	0.460	4.98	840.20
	0.460	4.98	1010.90
	0.460	4.98	1030.85
	0.460	9.95	722.70
	0.460	9.95	744.87
	0.460	14.93	944.39
	0.460	19.91	625.16
	0.609	1.00	2394.53
	0.609	8.25	907.58
7° Dihedral	0.460	0.00	3300.94
	0.460	3.78	1352.30
	0.460	4.98	558.65
	0.609	0.00	1850.32
	0.609	0.00	2550.25
	0.609	3.44	941.07
	0.609	7.25	654.73
	0.609	18.13	606.17
7° Pyramid	0.460	0.00	2176.98
	0.460	4.98	576.39
	0.460	9.95	671.72
	0.460	14.93	669.50
	0.460	19.91	620.73
13° Dihedral	0.460	0.00	1910.95
	0.460	4.98	512.10
	0.460	9.95	645.11
	0.460	14.93	616.29
	0.460	19.91	563.09
13° Pyramid	0.460	0.00	1857.75
	0.460	19.91	538.70
	0.609	0.00	1585.75
	0.609	4.53	532.49
	0.609	4.53	582.72
	0.609	7.25	577.70
	0.609	7.25	601.14
	0.609	9.97	592.77

Table B.1: Dihedral and Pyramid Plate Test Values

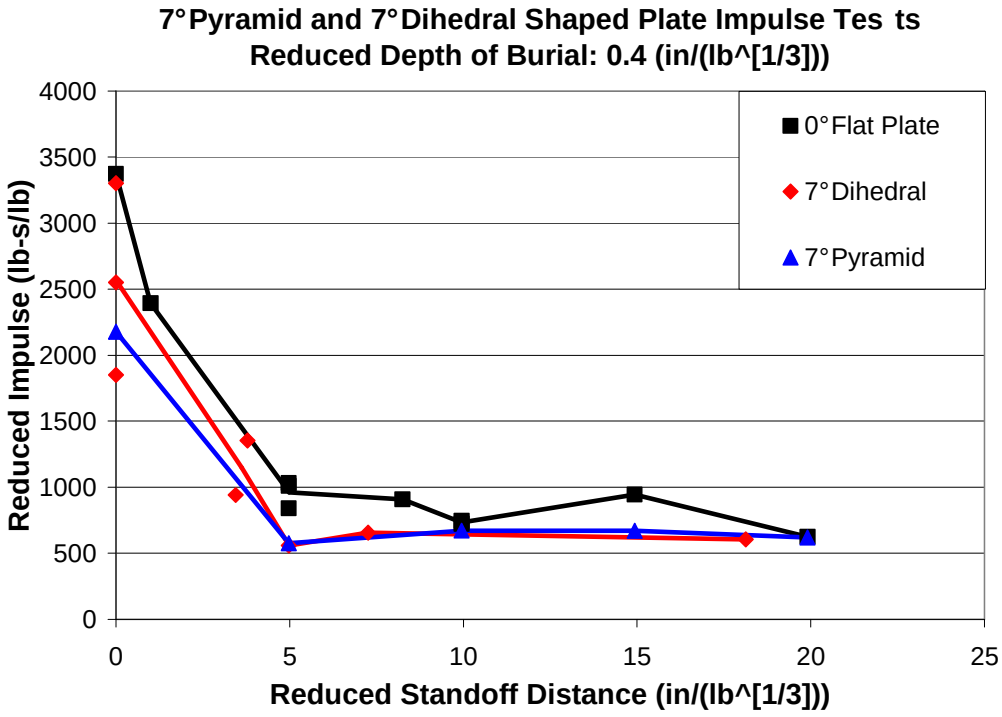

Figure B.2: 7° Pyramid and Dihedral Plate Tests

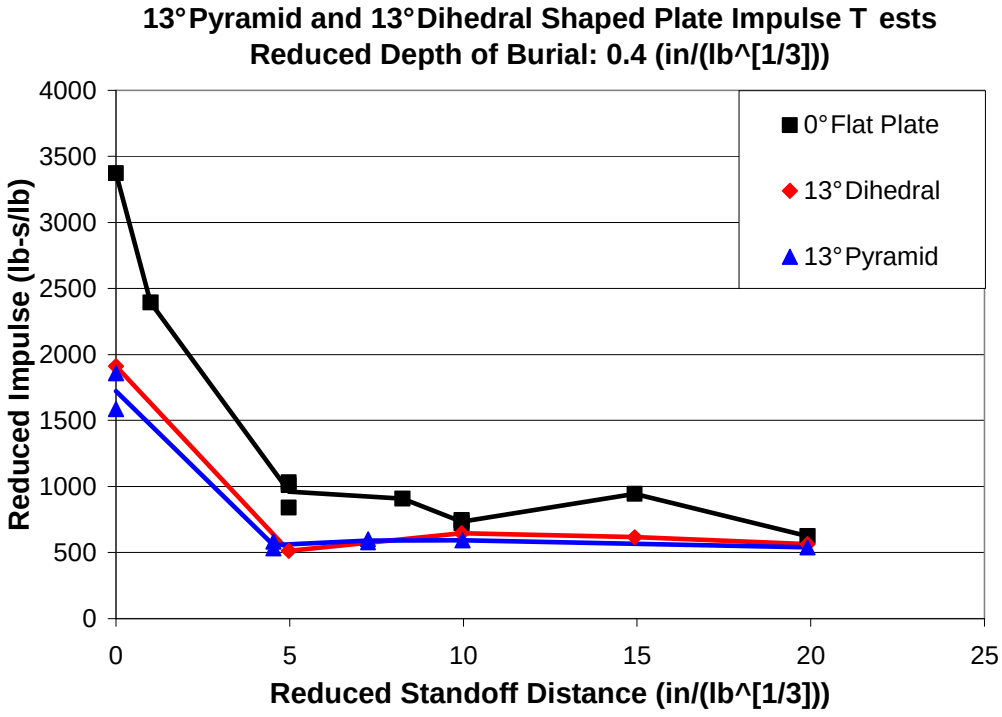

Figure B.3: 13°Pyramid and Dihedral Plate Tests

Both Figure B.2 and B.3 show impulse as a function of standoff distance for a dihedral and pyramid plate. The red lines and diamonds represent the values from dihedral shape tests, the blue lines and triangles are the pyramid shape test values, and the black line and squares are the 0° flat plate values. As discussed in Section 4.1.4 the 7° dihedral and pyramid shape differ slightly within the first range of standoff distances tested (from 0 to 4.98 $in/\sqrt[3]{lb}$), and then captured the same total impulse up to the maximum standoff distance tested. When all the values for a given standoff distance are averaged, the 7° degree dihedral target plate captures slightly more impulse than the 7° pyramid target. The 13° dihedral and pyramid target plates capture the same total impulse for the entire range of standoff distances tested.

The values for the dihedral and pyramid impulse tests support the idea that there is a maximum portion of the total impulse (the distributed load mechanism) that can be deflected by shaping the target. It is speculated that once this portion of the load is deflected, and only the impact load mechanism remains, further changes in the target geometry will have a negligible effect on total captured impulse.

B.2 Pyramid Grid Target Shapes

A second series of tests was conducted using plates machined with grid arrays of 45° pyramids of varying heights. Two target plates were tested; one with an array of pyramids 0.5” high (Figure B.1, Bottom Left, p. 115), and a second with an array of pyramids 0.25” high (Figure B.1, Bottom Right, p.115). Figure B.4 shows the results of the testing. The graph shows reduced impulse as a function of reduced standoff distance. The black squares and line represents the data for the 0° plate, the red line and diamonds are the data points of the 0.25” grid plate, and the blue line and triangles are data points for the 0.5” grid plate. Table B.2 provides the data values for the information graphed in Figure B.4.

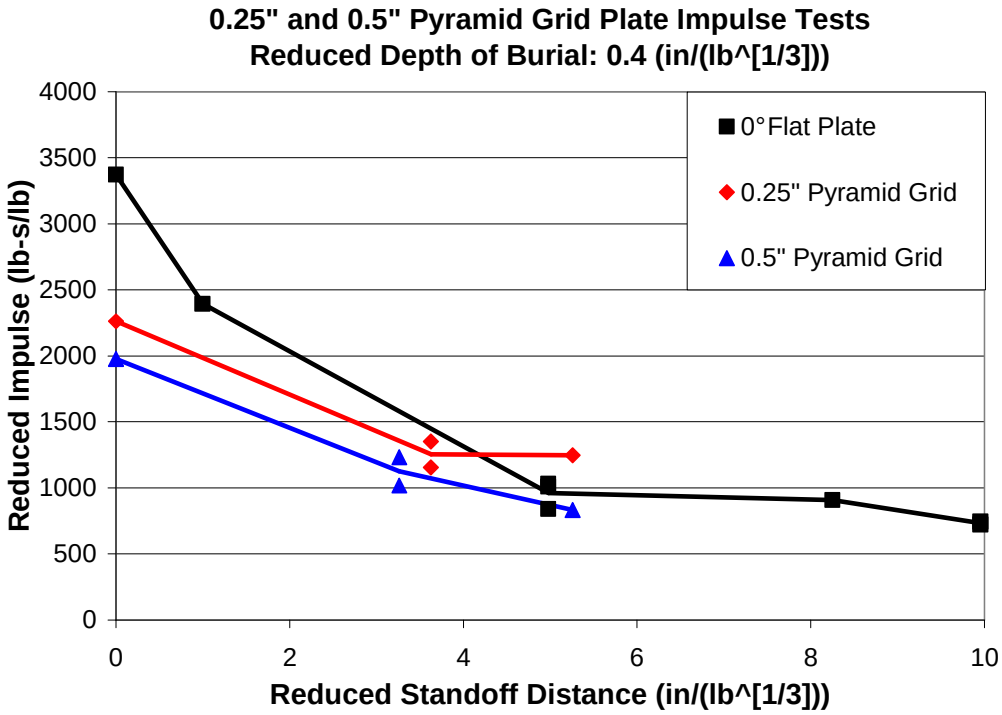

Figure B.4: 0.25” and 0.5” Pyramid Grid Plate Tests

Plate	Charge g	Reduced SOD in / (in^[1/3])	Reduced Impulse lb-s / lb
0° Flat Plate	0.460	0.00	3371.88
	0.460	4.98	840.20
	0.460	4.98	1010.90
	0.460	4.98	1030.85
	0.460	9.95	722.70
	0.460	9.95	744.87
	0.460	14.93	944.39
	0.460	19.91	625.16
	0.609	1.00	2394.53
	0.609	8.25	907.58
0.25" Pyramid Grid	0.609	0.00	2260.57
	0.609	3.63	1351.32
	0.609	3.63	1155.40
	0.609	5.26	1247.50
0.5" Pyramid Grid	0.609	0.00	1977.58
	0.609	3.26	1018.09
	0.609	3.26	1232.43
	0.609	5.26	832.22

Table B.2: 0.25” and 0.5” Pyramid Grid Plate Test Values

The graph and table shows a change in relative performance of the grid plates with respect to the 0° plate depending on the standoff distance. At the 0 $in/\sqrt[3]{lb}$ reduced standoff distance, the 0.25” and 0.5” pyramid grid plates capture roughly 60% of the total impulse that the flat plate captures. This can be explained by the influence of the shock wave loading mechanism at close standoff distances. The pyramid grid plates are stood off from the ground by some distance, and only the points of the pyramid array are touching the sand. As a result there is only limited material for the shock wave to travel through, and also gaps for the expanding gas to flow through. In contrast the flat plate completely covers the soil at the 0 $in/\sqrt[3]{lb}$ standoff distance, and captures the maximum amount of impulse.

The pyramid grid shapes capture more total impulse relative to the 0° plate as the standoff distance increases. As the standoff distance approaches 5.26 $in/\sqrt[3]{lb}$ the two pyramid grid plates capture the same total impulse as the 0° plate. In the case of

the 0.25” pyramid grid plate, the total captured impulse is actually 25% higher than the 0° plate at the 5.26 $in/\sqrt[3]{lb}$ reduced standoff distance. The increase in standoff relative to the 0° plate can be explained by the way the detonation gases and ejecta act against the pyramid grid structures. In the flat plate, the target is shaped in such a way that none of the ejecta can be captured by the geometry of the plate, and instead all of the escaping soil and gases are deflected away. ,In contrast portions of the underside of the pyramid grid plate are facing the center of the explosion. Escaping ejecta and detonation gases have to flow around these faces, and in doing so impact against the target. The surface features capture more impulse relative to a flat plate.

Figure B.5: Wear on 0.5” Pyramid Grid Plate After Testing

Figure B.5 is an expanded image of the 0.5” pyramid grid plate from Figure B.1. The majority of the wear is located in the center of the target plate, but at portions of the plate away from the center we begin to see a change in the erosion pattern. The wear is most concentrated on the sides of the pyramids that face the center of the target, and lest evident on sides facing away from the center. As the soil and gas bubble expanded, they impacted against the pyramid features facing the explosion and were then diverted around them. We can see this diversion in Figure B.6, which is a frame from a 0.5” pyramid grid plate test taken 5ms after the charge was detonated. Jets of sand and gas are projected from between the pyramid arrays, with most of the ejecta coming from the center of the pyramid plates. The results support the idea that a portion of the total impulse is heavily dependent on target geometry, and depending on the shape of the target can be increased or decreased significantly.

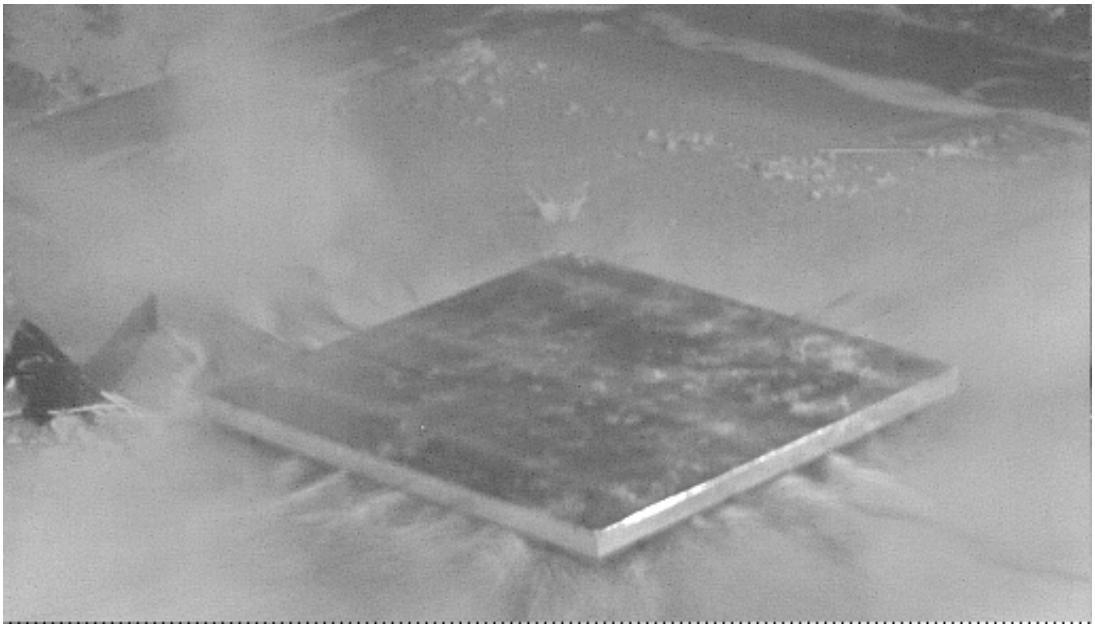

Figure B.6: 0.5” Pyramid Grid Plate, 0.04” DOB, 0.58” SOD, 5ms Elapsed Time

Appendix C: Standoff Distance Measured from Centroid

Standoff distance was found to play a significant role in the total impulse captured by a target plate from a buried charge, and where that standoff distance is measured from can greatly alter the measured values. The shape of the target plates used in this research makes choosing a reference point difficult. The decision to measure standoff distance from the surface to the lowest point on the target plate was designed to allow standoff distance to translate into the ground clearance beneath a vehicle. The disadvantage of using the lowest point on the target as the reference for standoff distance is that the average distance between the surface of the target and the ground varies with the shape of the target. In the case of dihedral and pyramid shapes, the average distance increases when the dihedral angle becomes larger.

An alternate reference point is the centroid (geometric center) of the shape on the target. Using the centroid as the reference point for standoff distance mitigates the geometry of the target, and transforms the target into a flat plate at an equivalent distance from the surface. Table C.1 contains the distance from the bottom of each target plate to centroid of the dihedral or pyramid shape. Figures C.1 through C.3, and Table C.2 through C.4, contain the graphs and values for the constant depth of burial tests using a standoff distance referencing the centroid. Regardless of whether the centroid or lowest point of the target is used as the reference for the standoff distance, the results are the same.

Plate	Distance from Bottom to Centroid (in)
13° Bent Plate	0.53
0.25" Pyramid	0.17
0.5" Pyramid	0.33
7° Pyramid	0.33
13° Pyramid	0.60
0° Flat Plate	0.00
7° Dihedral	0.32
13° Dihedral	0.60

Table C.1: Centroid Distances

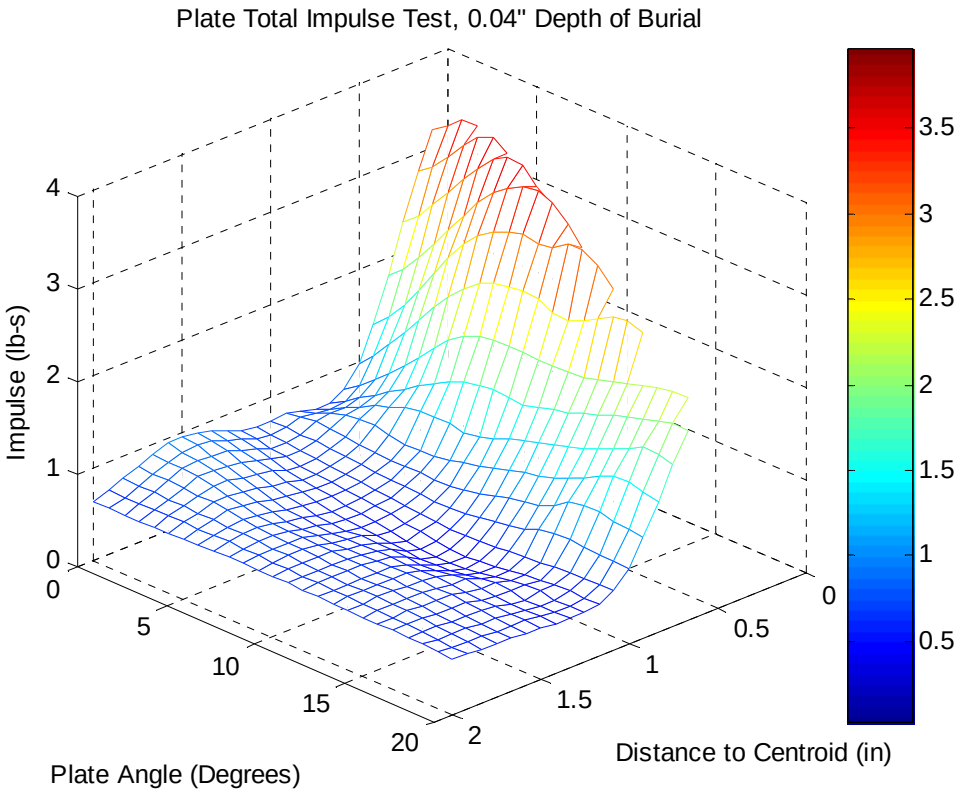

Figure C.1: Impulse Test and Centroid Standoff Distances, Constant 0.04" DOB

Plate Angle (°)	Burial Depth (in)	Centroid Standoff (in)	Total Impulse (lb-s)
0	0.04	0	3.42
0	0.04	0.5	0.97
0	0.04	1	0.75
0	0.04	1.5	0.96
0	0.04	2	0.63
7	0.04	0.32	3.39
7	0.04	0.7	1.37
7	0.04	0.82	0.88
7	0.04	1.32	0.57
7	0.04	1.82	0.71
13	0.04	0.6	1.93
13	0.04	1.1	0.52
13	0.04	1.6	0.65
13	0.04	2.1	0.63
20	0.04	0.6	2.23
20	0.04	1.1	0.61
20	0.04	1.6	0.56
20	0.04	2.1	0.60

Table C.2: Impulse Values for Figure C.1

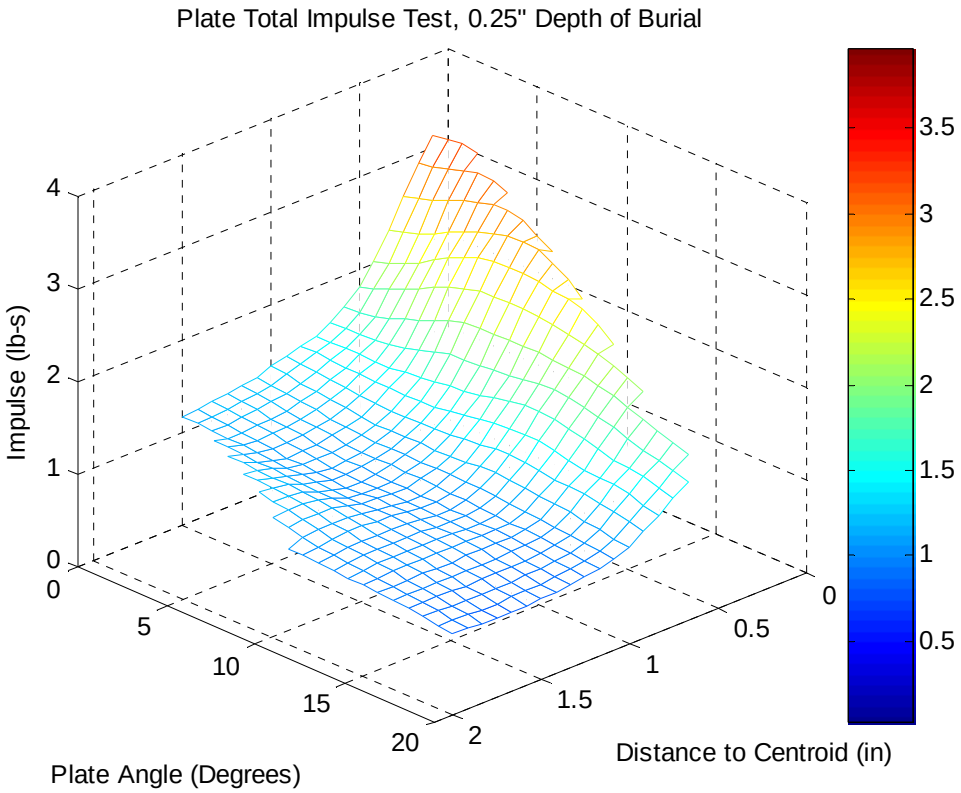

Figure C.2: Impulse Test and Centroid Standoff Distances, Constant 0.25" DOB

Plate Angle (°)	Burial Depth (in)	Centroid Standoff (in)	Total Impulse (lb-s)
0	0.25	0	3.28
0	0.25	0.5	1.80
0	0.25	1	1.33
0	0.25	1.5	1.16
7	0.25	0.32	2.81
7	0.25	0.82	1.40
7	0.25	1.32	1.05
7	0.25	1.82	1.23
13	0.25	0.6	1.99
13	0.25	1.1	1.09
13	0.25	1.6	1.05
13	0.25	2.1	0.96
20	0.25	0.6	1.57
20	0.25	1.1	0.96
20	0.25	1.6	0.85
20	0.25	2.1	0.87

Table C.3: Impulse Values for Figure C.2

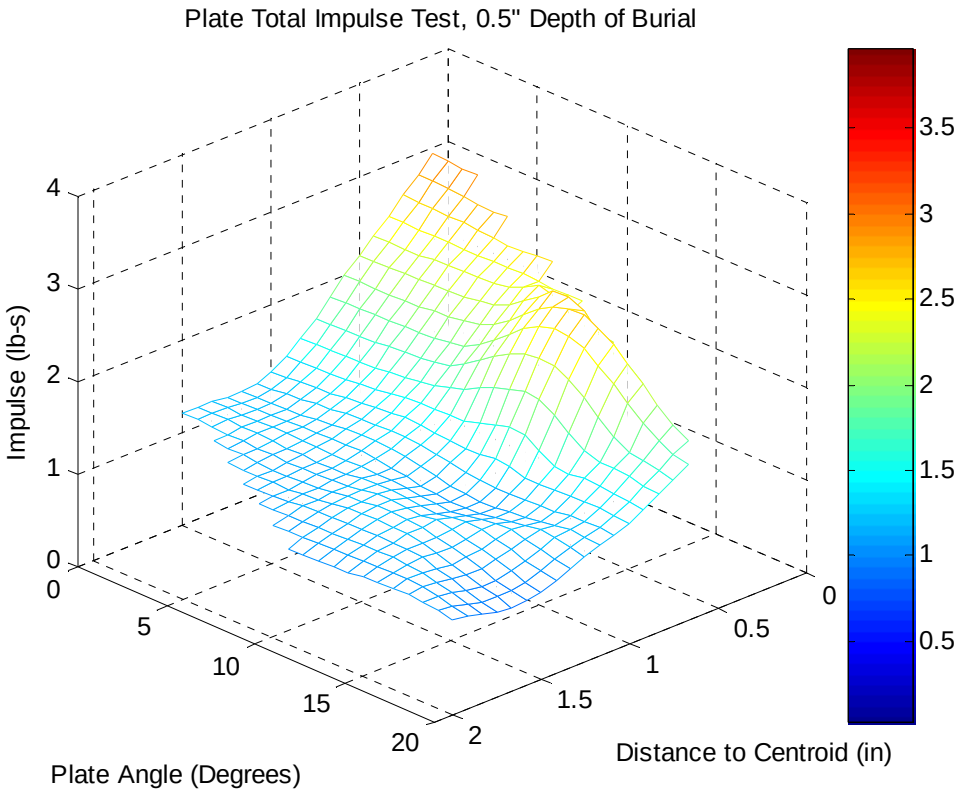

Figure C.3: Impulse Test and Centroid Standoff Distances, Constant 0.5" DOB

Plate Angle (°)	Burial Depth (in)	Centroid Standoff (in)	Total Impulse (lb-s)
0	0.5	0	3.06
0	0.5	0.5	2.14
0	0.5	1	1.27
0	0.5	1.5	1.21
7	0.5	0.32	2.45
7	0.5	0.82	1.62
7	0.5	1.32	1.20
7	0.5	1.82	1.10
13	0.5	0.6	2.66
13	0.5	1.1	1.17
13	0.5	1.6	1.23
13	0.5	2.1	0.99
20	0.5	0.6	1.74
20	0.5	1.1	1.23
20	0.5	1.6	0.90
20	0.5	2.1	1.03

Table C.4: Impulse Values for Figure C.3

Glossary

Acoustic Impedance: A material constant indicating the ability of a material to transmit sound in units of kg/s m². It is measured by multiplying the density by the speed of sound in the material. Sound travels better through materials with high acoustic impedance, such as solids or liquids.

Centroid: The geometric center of a two-dimensional shape.

Centroid Standoff Distance: The perpendicular distance from the ground to the centroid of the target shape.

Depth of Burial (DOB): The distance between the surface of the sand and the top of the charge. This measurement is taken before the sand is saturated, and is measured in inches (in.).

Dispersed Load: A component mechanism of blast loading that acts over a wide area of the target, imparting a significant amount of energy and momentum. It is composed of the gas bubble and soil annulus.

Ejecta: Soil, water, and other bits that are thrown into the air by an explosion.

Gas Bubble: An area of extremely high pressure caused by expanding gas from the detonation of an explosive charge.

Height of Target (HOT): See standoff distance. This term is primarily used when referring to reduced values ($in/\sqrt[3]{lb}$) that compare results between tests of different scales.

Impact Load: A component mechanism of blast loading that is defined by a very rapid and concentrated impact. When the charge explodes, the expanding gas acts like a piston to project the soil plug into the target like a bullet.

Impulse: The change in the momentum of a target plate as a result of loading from a buried charge, which is the integral of the applied force with respect to time. It is measured in lb-s, and was calculated by multiplying the mass of the target by the velocity.

Plate Angle: The dihedral angle of a target plate between the front face of the target (the side facing the ground) and the ground itself. It is measured in degrees.

Pyramid Height: For the pyramid grid shapes, this variable measures the height of the triangles from the base to their top point. It is measured in inches.

Reduced Value: A value that is unchanging with respect to scale, used to compare tests involving different charge sizes.

Shock Load: A component mechanism of blast loading consisting of the shock wave emitted by the detonation of an explosive charge.

Soil Annulus: A spray of ejecta that loads the plate and forms the dispersed load. It does not include the soil plug.

Soil plug: The portion of the soil directly above the charge. It is part of the impact load.

Standoff Distance (SOD): The perpendicular distance between the surface of the ground and the point of the target closest to the ground. This measurement is taken before the sand is saturated, and is measured in inches (in.).

References

[1] Tremblay, J.E., Bergeron, D.M., and Gonzalez, R., *Protection of Soft-Skinned Vehicle Occupants from Landmine Effects,* The Technical Cooperation Program, Subcommittee on Conventional Weapons Technology, Technical Panel W-1, Key Technical Activity 1-29, August 1998

[2] Bergeron, D.M., and Gonzalez, R., *Towards a Better Understanding of Land Mine Blast Loading,* The Technical Cooperation Program, Weapons Group, Conventional Weapons Technology, WPN TP-1 Terminal Effects, Key Technical Activity 1-34, June 2004

[3] Fourney, W.L., Leiste, U., Bonenberger, R., and Goodings, D., Mechanism of Loading on Plates Due to Explosive Detonation, *FRAGBLAST: International Journal for Blasting and Fragmentation*, Vol. 10, No. 3, September 2006

[4] Gupta, A.D., Skaggs, R.R, *Effect of Deflector Shapes on Mine-Blast Loading*, ARL-TR-3042, Aberdeen Research Laboratory, September 2003

[5] Baker, W.E. *Similarity Methods in Engineering Dynamics: Theory and Practice of Scale Modeling,* Rev. Ed., Elsevier, NY, 1991

[6] Chock, J.K., and Kapania, R.K., "Review of Two Methods for Calculating Explosive Air Blast," *The Shock and Vibration Digest*, Vol. 33, No. 2, March 2001, pp. 91 - 102

[7] Fu, R., Lindfors, A., Davis, J., "Scaling for Internal Blast", *AIP Conference Proceedings*, Volume 706, pp. 1440-1443, July 2004

[8] Baker, W.E., *Explosions in Air*, University of Texas Press, Austin, 1973

[9] Bergeron, D.M., and Tremblay, J.E., *Canadian Research to Characterize Mine Blast Output*, MABS 16, Oxford, UK, September 2000

[10] Sczymczak, W.G., *Simulations of Platform Loading from Explosions in Saturated Sand*, Fragblast Session of the ISEE Conference, Orlando Florida, February 6-9, 2005

[11] Leiste, U., *Visualization of Cratering and Channeling in an Underwater Environemtn*, Masters Thesis, University of Maryland, 2001

[12] *High Speed Camera.…*, http://www.visiblesolutions.com/, Vision Research Inc, Accessed July 7, 2006

[13] *Casspir*, http://www.globalsecurity.org/military/world/rsa/casspir.htm, Accessed July 7, 2006

[14] Fourney, W.L., Leiste, U., Bonenberger, R., and Goodings, D., "Explosive Impulse on Plates", *FRAGBLAST: International Journal for Blasting and Fragmentation*, Vol. 9, No. 1, March 2005, pp. 1 - 17

[15] Personal communication with Leslie C. Taylor